

Multiscale modeling and simulation of polymer nanocomposites

Q.H. Zeng^a, A.B. Yu^{a,*}, G.Q. Lu^b

^aCentre for Simulation and Modeling of Particulate Systems and School of Materials Science and Engineering,

The University of New South Wales, Sydney, NSW 2052, Australia

^bARC Centre of Excellence for Functional Nanomaterials, The University of Queensland, Brisbane, QLD 4072, Australia

Received 13 December 2006; received in revised form 5 September 2007; accepted 5 September 2007

Available online 3 December 2007

Abstract

Polymer nanocomposites offer a wide range of promising applications because of their much enhanced properties arising from the reinforcement of nanoparticles. However, further development of such nanomaterials depends on the fundamental understanding of their hierarchical structures and behaviors which requires multiscale modeling and simulation strategies to provide seamless coupling among various length and time scales. In this review, we first introduce some computational methods that have been applied to polymer nanocomposites, covering from molecular scale (e.g., molecular dynamics, Monte Carlo), microscale (e.g., Brownian dynamics, dissipative particle dynamics, lattice Boltzmann, time-dependent Ginzburg–Landau method, dynamic density functional theory method) to mesoscale and macroscale (e.g., micromechanics, equivalent-continuum and self-similar approaches, finite element method). Then, we discuss in some detail their applications to various aspects of polymer nanocomposites, including the thermodynamics and kinetics of formation, molecular structure and dynamics, morphology, processing behaviors, and mechanical properties. Finally, we address the importance of multiscale simulation strategies in the understanding and predictive capabilities of polymer nanocomposites in which few studies have been reported. The present review aims to summarize the recent advances in the fundamental understanding of polymer nanocomposites reinforced by nanofillers (e.g., spherical nanoparticles, nanotubes, clay platelets) and stimulate further research in this area.

© 2007 Elsevier Ltd. All rights reserved.

Keywords: Polymer nanocomposite; Multiscale; Modeling; Simulation; Nanostructure; Nanoparticles

Contents

1. Introduction	192
2. Modeling and simulation techniques	194
2.1. Molecular scale methods	194
2.1.1. Molecular dynamics	194
2.1.2. Monte Carlo	196

Abbreviations: BD: Brownian dynamics; BEM: boundary element method; CDM: cell dynamic method; CHC: Cahn–Hilliard–Cook; CNT: carbon nanotube; DFT: density functional theory; DPD: dissipative particle dynamics; FEM: finite element method; LB: lattice Boltzmann; MC: Monte Carlo; MD: molecular dynamics; MM: molecular mechanics; NMR: nuclear magnetic resonance; ODT: order–disorder phase transition; PCL: poly (ϵ -caprolactone); PMMA: polymethylmethacrylate; RVE: representative volume element; SCF: self-consistent field; SWCN: single-walled carbon nanotube; TDGL: time-dependent Ginsburg–Laudau

*Corresponding author. Tel.: +61 2 93854429; fax: +61 2 93855956.

E-mail address: a.yu@unsw.edu.au (A.B. Yu).

2.2.	Microscale methods	197
2.2.1.	Brownian dynamics	197
2.2.2.	Dissipative particle dynamics	197
2.2.3.	Lattice Boltzmann	198
2.2.4.	Time-dependent Ginzburg–Landau method.	199
2.2.5.	Dynamic DFT method	200
2.3.	Mesoscale and macroscale methods	200
2.3.1.	Micromechanics	201
2.3.2.	Equivalent-continuum and self-similar approaches	202
2.3.3.	Finite element method	204
3.	Modeling and simulation of polymer nanocomposites	205
3.1.	Nanocomposite thermodynamics	205
3.2.	Nanocomposite kinetics	209
3.3.	Nanocomposite molecular structure and dynamic properties	213
3.4.	Nanocomposite morphology	222
3.4.1.	Homopolymer nanocomposites	222
3.4.2.	Block copolymer nanocomposites	227
3.5.	Nanocomposite rheological and processing behaviors	233
3.6.	Nanocomposite mechanical properties	236
3.6.1.	Molecular models	237
3.6.2.	Continuum models	244
3.6.3.	Equivalent-continuum and self-similar models	251
4.	Multiscale strategies for modeling polymer nanocomposites	253
4.1.	Challenges	253
4.2.	Sequential and concurrent approaches	254
4.3.	Current research status	255
5.	Concluding remarks	260
	Acknowledgment	261
	References	261

1. Introduction

Polymer materials reinforced with nanoparticles (e.g., nanosphere, nanotube, clay platelet) have recently received tremendous attention in both scientific and industrial communities due to their extraordinary enhanced properties [1–10]. However, from the experimental point of view, it is a great challenge to characterize the structure and to manipulate the fabrication of polymer nanocomposites. The development of such materials is still largely empirical and a finer degree of control of their properties cannot be achieved so far. Therefore, computer modeling and simulation will play an ever-increasing role in predicting and designing material properties, and guiding such experimental work as synthesis and characterization. For polymer nanocomposites, computer modeling and simulation are especially useful in addressing the following fundamental issues:

1. the thermodynamics and kinetics of the formation of polymer nanocomposites;

2. the hierarchical characteristics of the structure and dynamics of polymer nanocomposites ranging from molecular scale, microscale to mesoscale and macroscale, in particular, the molecular structures and dynamics at the interface between nanoparticles and polymer matrix;
3. the dependence of polymer rheological behavior on the addition of nanoparticles, which is useful in optimizing processing conditions; and
4. the molecular origins of the reinforcement mechanisms of nanoparticles in polymer nanocomposites.

The purpose of this review is to discuss the application of modeling and simulation techniques to polymer nanocomposites. This includes a broad subject covering methodologies at various length and time scales and many aspects of polymer nanocomposites. We organize the review as follows. In Section 2, we introduce briefly the computational methods used so far for the systems of polymer nanocomposites which can be roughly divided into three types: molecular scale methods (e.g., molecular dynamics (MD), Monte Carlo

Nomenclature		
A	strain-concentration tensor of polymer composite	S average compliance of polymer composite
A_i	area of interface interaction	T temperature
a	acceleration of atom	U interaction potential
B	stress-concentration tensor of polymer composite	ΔU change of potential energy
C	stiffness tensor of polymer composite	$U_{GL}(\phi)$ Ginzburg-Landau free energy
C_f	elastic stiffness tensor of the effective fiber in polymer composite	U_{CDM} free energy calculated in cell dynamical method
E	total modulus of polymer composite	U_K kinetic energy in finite element model
E_{11}	longitudinal modulus of polymer composite	U_V Hookian potential energy in finite element model
E_{22}	transverse modulus of polymer composite	U''^m total potential energy of molecule model
E_f	modulus of filler in polymer composite	U^t total potential energy of truss model
E_m	modulus of matrix in polymer composite	U^r, U^θ, U^{vdw} energies associated with covalent bonding stretching, bond-angle bending, and van der Waals interactions, respectively
e_i	local particle velocity in lattice gas automaton method, or lattice velocity vector in lattice Boltzmann method	U^a, U^b, U^c energies associated with truss elements that represent covalent bonding stretching, bond-angle bending, and van der Waals interactions, respectively
\vec{F}_i	force acting on the i th atom or particle	\dot{u} displacement field in finite element model
F_{ij}^C	conservative force of particle j acting on particle i	$V(r)$ potential functional
F_{ij}^D	dissipative force of particle j acting on particle i	V_f volume of filler in polymer composite
F_{ij}^R	random forces of particle j acting on particle i	V_m volume of matrix in polymer composite
$f_i^\sigma(x, t)$	distribution function of the particles of component σ with velocity e_i along direction i at lattice x and time t	γ friction coefficient
$f_i^{\sigma, eq}(x, t)$	equilibrium distribution function of the particles of component σ	γ_i interface binding energy
G_{ij}	chain gyration tensor	$\bar{\varepsilon}$ volume-average strain of polymer composite
H	Hamiltonian associated with a configuration	$\bar{\varepsilon}_f$ volume-average strain of filler in polymer composite
ΔH	change of system Hamiltonian or free energy	$\bar{\varepsilon}_m$ volume-average strain of matrix in polymer composite
h, h_0	final and initial clay platelet separation	ε^f infinitesimal strain tensor of filler in polymer composite
k_B	Boltzmann constant	ε^m infinitesimal strain tensors of matrix in polymer composite
M	mobility of the order parameter field	ζ_{ij} random noise term with zero mean
M_p	particle mobility	$\zeta(r, t)$ thermal noise term with zero mean
m_i	atomic mass	η Gaussian white noise
$n_i(x, t)$	particle occupation variable with direction i at distance x and time t	λ enthalpic interaction parameter
P_2^s	average segment orientation	v_f volume fraction of filler in polymer composite
p_i	momentum of particle	v_m volume fraction of matrix in polymer composite
$p_{i \rightarrow j}$	probability of accepting a new configuration (j)	\vec{v} velocity of atom
\vec{r}_i	position of i th atom or particle	ξ random number between 0 and 1 which is to determine the acceptance or rejection of a new configuration
		ξ_f shape parameter depending on filler geometry and loading direction

ρ_{\max}	maximum stress along the tube axis	τ^σ	dimensionless collision-relaxation time constant of component σ of the fluid,
σ	noise amplitude	$\tau^\sigma = \lambda^\sigma / \Delta t$	
$\bar{\sigma}$	volume-average stress of polymer composite	ϕ	order parameter
$\bar{\sigma}_f$	volume-average stress of filler in polymer composite	ϕ_s	value of the order parameter at particle surface
$\bar{\sigma}_m$	volume-average stress of matrix in polymer composite	χ	asymmetry of diblock copolymer
σ^f	total stress of filler in polymer composite	Ω	collision operation
σ^m	total stress of matrix in polymer composite	ω_C	weight function for conservative force
		ω_D	weight function for dissipative force
		ω_R	weight function for random force

(MC)), microscale methods (e.g., Brownian dynamics (BD), dissipative particle dynamics (DPD), lattice Boltzmann (LB), time-dependent Ginzburg–Lanau method, dynamic density functional theory (DFT) method), and mesoscale and macroscale methods (e.g., micromechanics, equivalent-continuum and self-similar approaches, finite element method (FEM)). We do not aim to provide a detailed description of each method but its basic principles, strengths and weaknesses, and potential applications. Interesting readers can refer to relevant books, reviews and research articles for details. In Section 3, we discuss in detail the applications of these modeling and simulation methods in some specific aspects of polymer nanocomposites, including the thermodynamics and kinetics of the formation, molecular structure and dynamics, morphologies (i.e., phase behaviors), rheological and processing behaviors, and mechanical properties. We pay more attention to clay-based polymer nanocomposites because of their importance in polymer nanocomposites and our own research interests. Of course, we also refer to research activities in polymer systems reinforced by nanospheres and nanotubes, an area developed rapidly in the past few years. In Section 4, we highlight the importance of multiscale strategies of modeling and simulation in understanding and predicting the hierarchical structure and behaviors arising from the polymer and nanoparticle together with the properties observed at various scales. We discuss the current applications of some multiscale methods in polymer nanocomposites. Finally, we conclude the review by emphasizing the current challenges and future research directions.

2. Modeling and simulation techniques

2.1. Molecular scale methods

The modeling and simulation methods at molecular level usually employ atoms, molecules or their

clusters as the basic units considered. The most popular methods include molecular mechanics (MM), MD and MC simulation. Modeling of polymer nanocomposites at this scale is predominantly directed toward the thermodynamics and kinetics of the formation, molecular structure and interactions. The diagram in Fig. 1 describes the equation of motion for each method and the typical properties predicted from each of them [11–16]. We introduce here the two widely used molecular scale methods: MD and MC.

2.1.1. Molecular dynamics

MD is a computer simulation technique that allows one to predict the time evolution of a system of interacting particles (e.g., atoms, molecules, granules, etc.) and estimate the relevant physical properties [17,18]. Specifically, it generates such information as atomic positions, velocities and forces from which the macroscopic properties (e.g., pressure, energy, heat capacities) can be derived by means of statistical mechanics. MD simulation usually consists of three constituents: (i) a set of initial conditions (e.g., initial positions and velocities of all particles in the system); (ii) the interaction potentials to represent the forces among all the particles; (iii) the evolution of the system in time by solving a set of classical Newtonian equations of motion for all particles in the system. The equation of motion is generally given by

$$\vec{F}_i(t) = m_i \frac{d^2 \vec{r}_i}{dt^2}, \quad (1)$$

where \vec{F}_i is the force acting on the i th atom or particle at time t which is obtained as the negative gradient of the interaction potential U , m_i is the atomic mass and \vec{r}_i the atomic position. A physical simulation involves the proper selection of interaction potentials, numerical integration, periodic boundary conditions, and

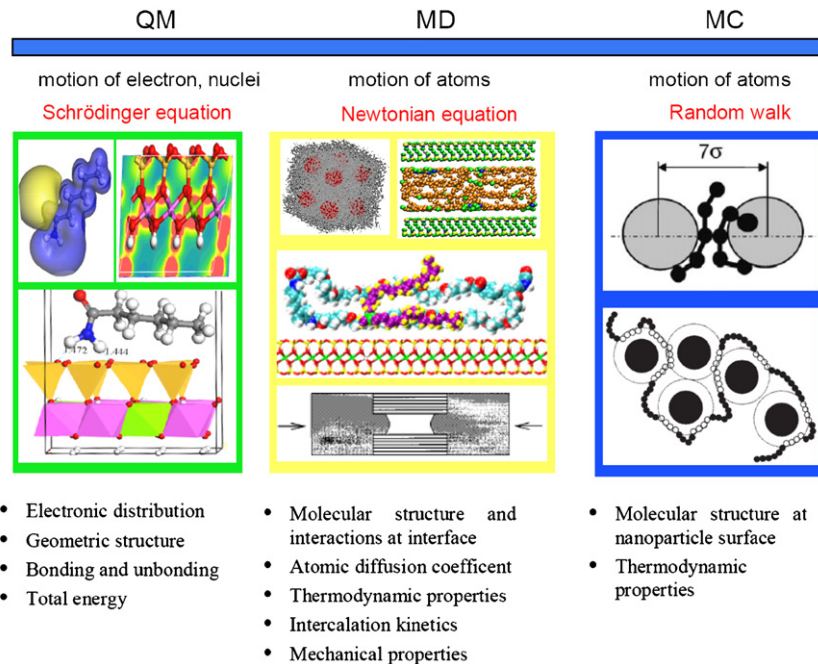


Fig. 1. Molecular modeling and simulation methods commonly used for polymer nanocomposites [11–16]. Reproduced from (i) Lee, Baljon and Loring by permission of American Institute of Physics; (ii) Smith, Bedrov, Li and Byutner by permission of American Institute of Physics; (iii) Smith, Bedrov and Smith by permission of Elsevier Science Ltd.; (iv) Zeng, Yu, Lu and Standish by permission of American Chemical Society; (v) Vacatello by permission of Wiley-VCH; and (vi) Zeng, Yu and Lu by permission of Institute of Physics.

the controls of pressure and temperature to mimic physically meaningful thermodynamic ensembles.

The interaction potentials together with their parameters, i.e., the so-called force field, describe in detail how the particles in a system interact with each other, i.e., how the potential energy of a system depends on the particle coordinates. Such a force field may be obtained by quantum method (e.g., ab initio), empirical method (e.g., Lennard-Jones, Mores, Born-Mayer) or quantum-empirical method (e.g., embedded atom model, glue model, bond-order potential). The criteria for selecting a force field include the accuracy, transferability and computational speed. A typical interaction potential U may consist of a number of bonded and non-bonded interaction terms:

$$\begin{aligned}
 U(\vec{r}_1, \vec{r}_2, \dots, \vec{r}_N) = & \sum_{i_{bond}}^{N_{bond}} U_{bond}(i_{bond}, \vec{r}_a, \vec{r}_b) \\
 & + \sum_{i_{angle}}^{N_{angle}} U_{angle}(i_{angle}, \vec{r}_a, \vec{r}_b, \vec{r}_c) \\
 & + \sum_{i_{torsion}}^{N_{torsion}} U_{torsion}(i_{torsion}, \vec{r}_a, \vec{r}_b, \vec{r}_c, \vec{r}_d)
 \end{aligned}$$

$$\begin{aligned}
 & + \sum_{i_{inversion}}^{N_{inversion}} U_{inversion}(i_{inversion}, \vec{r}_a, \vec{r}_b, \vec{r}_c, \vec{r}_d) \\
 & + \sum_{i=1}^{N-1} \sum_{j>i}^N U_{vdw}(i, j, \vec{r}_a, \vec{r}_b) \\
 & + \sum_{i=1}^{N-1} \sum_{j>i}^N U_{electrostatic}(i, j, \vec{r}_a, \vec{r}_b).
 \end{aligned} \tag{2}$$

The first four terms represent bonded interactions, i.e., bond stretching U_{bond} , bond-angle bend U_{angle} and dihedral angle torsion $U_{torsion}$ and inversion interaction $U_{inversion}$, while the last two terms are non-bonded interactions, i.e., van der Waals energy U_{vdw} and electrostatic energy $U_{electrostatic}$. In the equation, $\vec{r}_a, \vec{r}_b, \vec{r}_c$, and \vec{r}_d are the positions of the atoms or particles specifically involved in a given interaction; N_{bond} , N_{angle} , $N_{torsion}$ and $N_{inversion}$ stand for the total numbers of these respective interactions in the simulated system; i_{bond} , i_{angle} , $i_{torsion}$ and $i_{inversion}$ uniquely specify an individual interaction of each type; i and j in the van der Waals and electrostatic terms indicate the atoms involved in the interaction.

There are many algorithms for integrating the equation of motion using finite difference methods. The algorithms of verlet, velocity verlet, leap-frog and Beeman, are commonly used in MD simulations [17]. All algorithms assume that the atomic position \vec{r} , velocities \vec{v} and accelerations \vec{a} can be approximated by a Taylor series expansion:

$$\vec{r}(t + \delta t) = \vec{r}(t) + \vec{v}(t)\delta t + \frac{1}{2}\vec{a}(t)\delta t^2 + \dots, \quad (3)$$

$$\vec{v}(t + \delta t) = \vec{v}(t) + \vec{a}(t)\delta t + \frac{1}{2}\vec{b}(t)\delta t^2 + \dots, \quad (4)$$

$$\vec{a}(t + \delta t) = \vec{a}(t) + \vec{b}(t)\delta t + \dots. \quad (5)$$

Generally speaking, a good integration algorithm should conserve the total energy and momentum and be time-reversible. It should also be easy to implement and computationally efficient, and permit a relatively long time-step. The verlet algorithm is probably the most widely used method. It uses the positions $\vec{r}(t)$ and accelerations $\vec{a}(t)$ at time t , and the positions $\vec{r}(t - \delta t)$ from the previous step $t - \delta t$ to calculate the new positions $\vec{r}(t + \delta t)$ at $t + \delta t$. According to Taylor series expansion of Eq. (3), we have

$$\vec{r}(t + \delta t) = \vec{r}(t) + \vec{v}(t)\delta t + \frac{1}{2}\vec{a}(t)\delta t^2 + \dots, \quad (6)$$

$$\vec{r}(t - \delta t) = \vec{r}(t) - \vec{v}(t)\delta t + \frac{1}{2}\vec{a}(t)\delta t^2 - \dots. \quad (7)$$

Adding Eqs. (6) and (7) together gives

$$\vec{r}(t + \delta t) = 2\vec{r}(t) - \vec{r}(t - \delta t) + \vec{a}(t)\delta t^2. \quad (8)$$

The velocities at time t and $t + \frac{1}{2}\delta t$ can be respectively estimated

$$\vec{v}(t) = [\vec{r}(t + \delta t) - \vec{r}(t - \delta t)]/2\delta t, \quad (9)$$

$$\vec{v}\left(t + \frac{1}{2}\delta t\right) = [\vec{r}(t + \delta t) - \vec{r}(t)]/\delta t. \quad (10)$$

MD simulations can be performed in many different ensembles, such as grand canonical (μ VT), microcanonical (NVE), canonical (NVT) and isothermal-isobaric (NPT). The constant temperature and pressure can be controlled by adding an appropriate thermostat (e.g., Berendsen, Nose, Nose-Hoover and Nose-Poincare) and barostat (e.g., Andersen, Hoover and Berendsen), respectively. Applying MD into polymer composites allows us to investigate into the effects of fillers on polymer structure and dynamics in the vicinity of

polymer-filler interface and also to probe the effects of polymer-filler interactions on the materials properties. This will be discussed in Section 3.3.

2.1.2. Monte Carlo

MC technique, also called Metropolis method [19], is a stochastic method that uses random numbers to generate a sample population of the system from which one can calculate the properties of interest. A MC simulation usually consists of three typical steps. In the first step, the physical problem under investigation is translated into an analogous probabilistic or statistical model. In the second step, the probabilistic model is solved by a numerical stochastic sampling experiment. In the third step, the obtained data are analyzed by using statistical methods. MC provides only the information on equilibrium properties (e.g., free energy, phase equilibrium), different from MD which gives non-equilibrium as well as equilibrium properties.

In a NVT ensemble with N atoms, one hypothesizes a new configuration by arbitrarily or systematically moving one atom from position $i \rightarrow j$. Due to such atomic movement, one can compute the change in the system Hamiltonian ΔH :

$$\Delta H = H(j) - H(i), \quad (11)$$

where $H(i)$ and $H(j)$ are the Hamiltonian associated with the original and new configuration, respectively. This new configuration is then evaluated according to the following rules. If $\Delta H < 0$, then the atomic movement would bring the system to a state of lower energy. Hence, the movement is immediately accepted and the displaced atom remains in its new position. If $\Delta H \geq 0$, the move is accepted only with a certain probability $p_{i \rightarrow j}$ which is given by

$$p_{i \rightarrow j} \propto \exp\left(-\frac{\Delta H}{k_B T}\right), \quad (12)$$

where k_B is the Boltzmann constant. According to Metropolis et al. [19] one can generate a random number ξ between 0 and 1 and determine the new configuration according to the following rule:

$$\xi \leq \exp\left(-\frac{\Delta H}{k_B T}\right), \text{ the move is accepted,}$$

$$\xi > \exp\left(-\frac{\Delta H}{k_B T}\right), \text{ the move is not accepted.}$$

If the new configuration is rejected, one counts the original position as a new one and repeats the process by using other arbitrarily chosen atoms.

In a μ VT ensemble, one hypothesizes a new configuration j by arbitrarily choosing one atom and proposing that it can be exchanged by an atom of a different kind. This procedure affects the chemical composition of the system. Also, the move is accepted with a certain probability. However, one computes the energy change ΔU associated with the change in composition. The new configuration is examined according to the following rules. If $\Delta U < 0$, the move of compositional change is accepted. However, if $\Delta U \geq 0$, the move is accepted with a certain probability which is given by

$$p_{i \rightarrow j} \propto \exp\left(-\frac{\Delta U}{k_B T}\right), \quad (13)$$

where ΔU is the change in the sum of the mixing energy and the chemical potential of the mixture. If the new configuration is rejected one counts the original configuration as a new one and repeats the process by using some other arbitrarily or systematically chosen atoms. In polymer nanocomposites, MC methods have been used to investigate the molecular structure at nanoparticle surface and evaluate the effects of various factors.

2.2. Microscale methods

The modeling and simulation at microscale aim to bridge molecular methods and continuum methods and avoid their shortcomings. Specifically, in nanoparticle–polymer systems, the study of structural evolution (i.e., dynamics of phase separation) involves the description of bulk flow (i.e., hydrodynamic behavior) and the interactions between nanoparticle and polymer components. Note that hydrodynamic behavior is relatively straightforward to handle by continuum methods but is very difficult and expensive to treat by atomistic methods. In contrast, the interactions between components can be examined at an atomistic level but are usually not straightforward to incorporate at the continuum level. Therefore, various simulation methods have been evaluated and extended to study the microscopic structure and phase separation of these polymer nanocomposites, including BD, DPD, LB, time-dependent Ginsburg–Landau (TDGL) theory, and dynamic DFT. In these methods, a polymer system is usually treated with a field description or microscopic particles that incorporate molecular details implicitly. Therefore, they are able to simulate the phenomena on length

and time scales currently inaccessible by the classical MD methods.

2.2.1. Brownian dynamics

BD simulation is similar to MD simulations [20]. However, it introduces a few new approximations that allow one to perform simulations on the microsecond timescale whereas MD simulation is known up to a few nanoseconds. In BD the explicit description of solvent molecules used in MD is replaced with an implicit continuum solvent description. Besides, the internal motions of molecules are typically ignored, allowing a much larger time-step than that of MD. Therefore, BD is particularly useful for systems where there is a large gap of time scale governing the motion of different components. For example, in polymer–solvent mixture, a short time-step is required to resolve the fast motion of the solvent molecules, whereas the evolution of the slower modes of the system requires a larger time-step. However, if the detailed motion of the solvent molecules is concerned, they may be removed from the simulation and their effects on the polymer are represented by dissipative ($-\gamma p$) and random ($\sigma\zeta(t)$) force terms. Thus, the forces in the governing Eq. (1) is replaced by a Langevin equation,

$$F_i(t) = \sum_{j \neq i} F_{ij}^C - \gamma p_i + \sigma\zeta_i(t), \quad (14)$$

where F_{ij}^C is the conservative force of particle j acting on particle i , γ and σ are constants depending on the system, p_i the momentum of particle i , and $\zeta(t)$ a Gaussian random noise term. One consequence of this approximation of the fast degrees of freedom by fluctuating forces is that the energy and momentum are no longer conserved, which implies that the macroscopic behavior of the system will not be hydrodynamic. In addition, the effect of one solute molecule on another through the flow of solvent molecules is neglected. Thus, BD can only reproduce the diffusion properties but not the hydrodynamic flow properties since the simulation does not obey the Navier–Stokes equations.

2.2.2. Dissipative particle dynamics

DPD was originally developed by Hoogerbrugge and Koelman [21]. It can simulate both Newtonian and non-Newtonian fluids, including polymer melts and blends, on microscopic length and time scales. Like MD and BD, DPD is a particle-based method. However, its basic unit is not a single atom or molecule but a molecular assembly (i.e., a particle).

DPD particles are defined by their mass M_i , position r_i and momentum p_i . The interaction force between two DPD particles i and j can be described by a sum of conservative F_{ij}^C , dissipative F_{ij}^D and random forces F_{ij}^R [22–24]:

$$F_{ij} = F_{ij}^C + F_{ij}^D + F_{ij}^R, \quad (15)$$

$$F_{ij}^C = \Pi_0 \omega_C(r_{ij}) \hat{e}_{ij}, \quad (16)$$

$$F_{ij}^D = -\gamma \omega_D(r_{ij}) (\hat{e}_{ij} \cdot p_{ij}) \hat{e}_{ij}, \quad (17)$$

$$F_{ij}^R = \sigma \zeta_{ij} \omega_R(r_{ij}) \hat{e}_{ij}, \quad (18)$$

where $r_{ij} = |r_i - r_j|$, $\hat{e}_{ij} = \hat{r}_{ij}/r_{ij}$, Π_0 is a constant related to the fluid compressibility, γ is a friction coefficient, σ a noise amplitude and ζ_{ij} a random noise term with zero mean (i.e., $\langle \zeta_{ij} \rangle = 0$) and unit variance. ω_C , ω_D , and ω_R are the weight functions for each interaction force [22]. While the interaction potentials in MD are high-order polynomials of the distance r_{ij} between two particles, in DPD the potentials are softened so as to approximate the effective potential at microscopic length scales. The form of the conservative force in particular is chosen to decrease linearly with increasing r_{ij} . Beyond a certain cut-off separation r_c , the weight functions and thus the forces are all zero.

Therefore, the total force $F_i(t)$ acting on particle i at time t is

$$F_i(t) = \sum_{j \neq i} F_{ij}^C + \sum_{j \neq i} F_{ij}^D + \sum_{j \neq i} F_{ij}^R. \quad (19)$$

Because the forces are pairwise and momentum is conserved, the macroscopic behavior directly incorporates Navier–Stokes hydrodynamics. However, energy is not conserved because of the presence of the dissipative and random force terms which are similar to those of BD, but incorporate the effects of Brownian motion on larger length scales. DPD has several advantages over MD, for example, the hydrodynamic behavior is observed with far fewer particles than required in a MD simulation because of its larger particle size. Besides, its force forms allow larger time steps to be taken than those in MD.

2.2.3. Lattice Boltzmann

LB [25] is another microscale method that is suited for the efficient treatment of polymer solution dynamics. It has recently been used to investigate the phase separation of binary fluids in the presence

of solid particles. The LB method is originated from lattice gas automaton which is constructed as a simplified, fictitious molecular dynamic in which space, time and particle velocities are all discrete. A typical lattice gas automaton consists of a regular lattice with particles residing on the nodes. A set of Boolean variable $n_i(x, t)$ ($i = 1, \dots, M$) describing the particle occupation is defined, where M is the number of directions of the particle velocities at each node. The evolution equation of the lattice gas automaton is as follows:

$$\begin{aligned} n_i(x + e_i, t + 1) &= n_i(x, t) + \Omega_i(n(x, t)), \\ (i = 0, 1, \dots, M), \end{aligned} \quad (20)$$

where e_i are the local particle velocity. During the evolution, each time-step can be divided into two sub-steps: (i) streaming, in which each particle moves to the nearest node in the direction of its velocity and (ii) collision, which occurs when particles arriving at a node interact with each other and then change their velocity directions according to scattering rules.

The main feature of the LB method is to replace the particle occupation variables n_i (Boolean variables), by single-particle distribution functions (real variables) $f_i = \langle n_i \rangle$ and neglect individual particle motion and particle–particle correlations in the kinetic equation, where $\langle \rangle$ indicates an ensemble average. There are several ways to obtain the LB equation from either the discrete velocity model or the Boltzmann kinetic equation, and to derive the macroscopic Navier–Stokes equations from the LB equation. For example, based on the discrete kinetic equation, the LB equation for a multicomponent flow can be expressed as

$$\begin{aligned} f_i^\sigma(x + e_i \Delta x, t + \Delta t) - f_i^\sigma(x, t) &= \Omega_i(f_i^\sigma(x, t)), \\ (i = 0, 1, \dots, M; \sigma = 1, 2, \dots, S), \end{aligned} \quad (21)$$

where the left-hand side of the equation describes changes in the distribution function due to free particle motion and the right-hand side contains the collision operation Ω , describing changes due to pairwise collisions which are always simplified to the linear Bhatnagar–Gross–Krook form:

$$\begin{aligned} \Omega_i(f_i^\sigma(x, t)) &= \frac{1}{\tau^\sigma} (f_i^\sigma(x, t) - f_i^{\sigma, eq}(x, t)), \\ (i = 0, 1, \dots, M; \sigma = 1, 2, \dots, S), \end{aligned} \quad (22)$$

where $\tau^\sigma = \lambda^\sigma / \Delta t$ is the dimensionless collision–relaxation time constant of component σ of the fluid, e_i is the lattice velocity vector, the subscript i

represents the lattice velocity direction, $f_i^\sigma(x, t)$ is the distribution function of the particles of component σ with velocity e_i along direction i at lattice x and time t , and $f_i^{\sigma, eq}(x, t)$ is the corresponding equilibrium distribution function.

In the LB method, the thermodynamic behavior can be described by the following free-energy functional:

$$U(\phi) = U_{GL}(\phi) + \sum_{i=1}^N U_i(\phi), \quad (23)$$

where $U_{GL}(\phi)$ is the Ginzburg–Landau free energy, and $U_i(\phi)$ is a potential that describes the coupling interaction between the i th particle and the surrounding fluid,

$$U_{GL}(\phi) = \int dr \left(-\frac{\tau}{2}\phi^2 + \frac{u}{4}\phi^4 + \frac{k}{2}|\nabla\phi|^2 \right), \quad (24)$$

where the term $\frac{k}{2}|\nabla\phi|^2$ represents the free-energy cost of forming fluid–fluid interface, and $u > 0$ and $k > 0$ are phenomenological parameters. If $\tau > 0$, $U_{GL}(\phi)$ describes a single homogeneous phase, while $\tau < 0$, it yields two- or multiphases coexistence.

$$U_i(\phi) = \int dr V_0 e^{-(|r-s_i|/r_0)} (\phi(r) - \phi(s_i))^2, \quad (25)$$

where s_i is the position of i th particle and N the total number of particles. The constant $V_0 > 0$ characterizes the strength of the coupling interaction and r_0 represents its range.

An important advantage of the LB method is that microscopic physical interactions of the fluid particles can be conveniently incorporated into the numerical model. Compared with the Navier–Stokes equations, the LB method can handle the interactions among fluid particles and reproduce the microscale mechanism of hydrodynamic behavior. Therefore it belongs to the MD in nature and bridges the gap between the molecular level and macroscopic level. However, its main disadvantage is that it is typically not guaranteed to be numerically stable and may lead to physically unreasonable results, for instance, in the case of high forcing rate or high interparticle interaction strength.

2.2.4. Time-dependent Ginzburg–Landau method

TDGL is a microscale method for simulating the structural evolution of phase-separation in polymer blends and block copolymers. It is based on the Cahn–Hilliard–Cook (CHC) nonlinear diffusion equation for a binary blend and falls under the more

general phase-field and reaction-diffusion models [26–28]. In the TDGL method, a free-energy function is minimized to simulate a temperature quench from the miscible region of the phase diagram to the immiscible region. Thus, the resulting time-dependent structural evolution of the polymer blend can be investigated by solving the TDGL/CHC equation for the time dependence of the local blend concentration. Glotzer and co-workers have discussed and applied this method to polymer blends and particle-filled polymer systems [29].

For an incompressible binary polymer blend, the equation of motion can be written as follows:

$$\frac{\partial\phi(r, t)}{\partial t} = \nabla \cdot M \nabla \frac{\delta U[\phi(r, t)]}{\delta\phi(r, t)} + \zeta(r, t). \quad (26)$$

Here $\zeta(r, t)$ is a thermal noise term with zero mean, U is the free energy, and the mobility M may depend on the order parameter ϕ . For a binary polymer blend, one typically takes

$$\frac{U[\phi(r)]}{k_B T} = \int dr \left[\frac{U_{FH}[\phi(r)]}{k_B T} + k(\phi)|\nabla\phi(r)|^2 \right], \quad (27)$$

where $U_{FH}(\phi)$ is the Flory–Huggins free energy of mixing, given by

$$\frac{U_{FH}(\phi)}{k_B T} = \frac{\phi}{N_A} \ln \phi + \frac{(1-\phi)}{N_B} \ln(1-\phi) + \chi\phi(1-\phi). \quad (28)$$

Here χ is the enthalpic interaction parameter between the two polymer components. N_A and N_B are the number of segments in polymer A and polymer B, respectively. The Flory–Huggins model has a critical point at $\phi_c = N_B^{1/2}/(N_A^{1/2} + N_B^{1/2})$ and $\chi_c = (N_A^{1/2} + N_B^{1/2})^2/2N_A N_B$. If $\chi < \chi_c$ the system is miscible at the critical concentration whereas if $\chi > \chi_c$ it is immiscible.

To simplify TDGL, Oono and co-workers proposed cell dynamic method (CDM) which was derived from the discretized TDGL equation [30,31]. Here, the Laplacian term is replaced by its isotropic discretized counterpart. And, the free-energy functional in Eq. (27) is given by

$$\frac{U_{CDM}[\phi(r)]}{k_B T} = \int dr \left[-A \ln(\cosh \phi) + \frac{1}{2}\phi^2 + \frac{D}{2}|\nabla\phi(r)|^2 \right]. \quad (29)$$

This model reproduces the growth kinetics of the TDGL model, demonstrating that such quantities

are insensitive to the precise form of the double-well potential of the bulk free-energy term. The TDGL and CDM methods have recently been used to investigate the phase-separation of polymer nanocomposites and polymer blends in the presence of nanoparticles [32–36].

2.2.5. Dynamic DFT method

Dynamic DFT method is usually used to model the dynamic behavior of polymer systems and has been implemented in the software package MesodynTM from Accelrys [37]. The DFT models the behavior of polymer fluids by combining Gaussian mean-field statistics with a TDGL model for the time evolution of conserved order parameters. However, in contrast to traditional phenomenological free-energy expansion methods employed in the TDGL approach, the free energy is not truncated at a certain level, and instead retains the full polymer path integral numerically. At the expense of a more challenging computation, this allows detailed information about a specific polymer system beyond simply the Flory–Huggins parameter and mobilities to be included in the simulation. In addition, viscoelasticity, which is not included in TDGL approaches, is included at the level of the Gaussian chains. A similar DFT approach has been developed by Doi and co-workers [38,39] and forms the basis for their new software tool Simulation Utilities for Soft and Hard Interfaces (SUSHI), one of a suite of molecular and mesoscale modeling tools (called OCTA) developed for the simulation of polymer materials [40].

The essence of dynamic DFT method is that the instantaneous unique conformation distribution can be obtained from the off-equilibrium density profile by coupling a fictitious external potential to the Hamiltonian. Once such distribution is known, the free energy is then calculated by standard statistical thermodynamics. The driving force for diffusion is obtained from the spatial gradient of the first functional derivative of the free energy with respect to the density. Here, we describe briefly the equations for both polymer and particle in the diblock polymer–particle composites [35].

The dynamics of microphase separation in a melt of diblocks is described through the following equation [34]:

$$\frac{\partial \phi(r, t)}{\partial t} = M \nabla^2 \frac{\delta U[\phi(r, t)]}{\delta \phi(r, t)} - \Gamma[\phi(r, t) - \lambda] + \xi(r, t), \quad (30)$$

where ϕ is the scalar order parameter, $\phi = \rho_A - \rho_B$, i.e., the difference of the respective local densities of the A and B segments of AB diblocks. The constant M is the mobility for the order parameter field. Variable λ describes the asymmetry of the diblock. ξ is the noise field, and parameter Γ determines the thickness of the lamellar domains which is related to the length of the diblock. The free energy $U(\phi)$ is given by the local free energy U_l and polymer–particle coupling interaction term U_{cpl} :

$$U(\phi) = U_l + U_{cpl}, \quad (31)$$

$$U_l = \int dr \left[f_1(\phi(r, t)) + \frac{D}{2} (\nabla \phi(r, t))^2 \right], \quad (32)$$

$$U_{cpl} = C \int dr \sum_i V(r - R_i)(\phi(r, t) - \phi_s)^2, \quad (33)$$

where $\phi_s = 1$ is the value of the order parameter at the particle surface, and $V(r)$ is the potential functional.

The motion of particle is described by the Langevin equation

$$\dot{R}_i = M_p \left(f_i - \frac{\partial U(\phi)}{\partial R_i} \right) + \eta_i, \quad (34)$$

where M_p is the particle mobility, f_i is the force acting on the particle from other particles, and η represents a Gaussian white noise.

2.3. Mesoscale and macroscale methods

Despite the importance of understanding the molecular structure and nature of materials, their behavior can be homogenized with respect to different aspects which can be at different scales. Typically, the observed macroscopic behavior is usually explained by ignoring the discrete atomic and molecular structure and assuming that the material is continuously distributed throughout its volume. The continuum material is thus assumed to have an average density and can be subjected to body forces such as gravity and surface forces.

Generally speaking, the macroscale methods (or called continuum methods hereafter) obey the fundamental laws of: (i) continuity, derived from the conservation of mass; (ii) equilibrium, derived from momentum considerations and Newton's second law; (iii) the moment of momentum principle, based on the model that the time rate of change of angular momentum with respect to an arbitrary point is equal to the resultant moment;

(iv) conservation of energy, based on the first law of thermodynamics; and (v) conservation of entropy, based on the second law of thermodynamics. These laws provide the basis for the continuum model and must be coupled with the appropriate constitutive equations and the equations of state to provide all the equations necessary for solving a continuum problem. The continuum method relates the deformation of a continuous medium to the external forces acting on the medium and the resulting internal stress and strain. Computational approaches range from simple closed-form analytical expressions to micromechanics and complex structural mechanics calculations based on beam and shell theory. In this section, we introduce some continuum methods that have been used in polymer nanocomposites, including micromechanics models (e.g., Halpin–Tsai model, Mori–Tanaka model), equivalent-continuum model, self-consistent model and finite element analysis.

2.3.1. Micromechanics

Since the assumption of uniformity in continuum mechanics may not hold at the microscale level, micromechanics methods are used to express the continuum quantities associated with an infinitesimal material element in terms of structure and properties of the microconstituents. Thus, a central theme of micromechanics models is the development of a representative volume element (RVE) to statistically represent the local continuum properties. The RVE is constructed to ensure that the length scale is consistent with the smallest constituent that has a first-order effect on the macroscopic behavior. The RVE is then used in a repeating or periodic nature in the full-scale model. The micromechanics method can account for interfaces between constituents, discontinuities, and coupled mechanical and non-mechanical properties. Our purpose is to review the micromechanics methods used for polymer nanocomposites. Thus, we only discuss here some important concepts of micromechanics as well as the Halpin–Tsai model and Mori–Tanaka model. Interesting readers are referred to the literature [41] for details.

2.3.1.1. Basic concepts. When applied to particle-reinforced polymer composites, micromechanics models usually follow such basic assumptions as (i) linear elasticity of fillers and polymer matrix; (ii) the fillers are axisymmetric, identical in shape and size, and can be characterized by parameters

such as aspect ratio; (iii) well-bonded filler–polymer interface and the ignorance of interfacial slip, filler–polymer debonding or matrix cracking.

The first concept is the linear elasticity, i.e., the linear relationship between the total stress and infinitesimal strain tensors for the filler and matrix as expressed by the following constitutive equations:

$$\text{For filler, } \sigma^f = C^f \varepsilon^f, \quad (35)$$

$$\text{For matrix, } \sigma^m = C^m \varepsilon^m, \quad (36)$$

where C is the stiffness tensor.

The second concept is the average stress and strain. Since the pointwise stress field $\sigma(x)$ and the corresponding strain field $\varepsilon(x)$ are usually non-uniform in polymer composites, the volume-average stress $\bar{\sigma}$ and strain $\bar{\varepsilon}$ are then defined over the representative averaging volume V , respectively,

$$\bar{\sigma} = \frac{1}{V} \int_V \sigma(x) dV, \quad (37)$$

$$\bar{\varepsilon} = \frac{1}{V} \int_V \varepsilon(x) dV. \quad (38)$$

Therefore, the average filler and matrix stresses are the averages over the corresponding volumes V_f and V_m , respectively,

$$\bar{\sigma}_f = \frac{1}{V_f} \int_{V_f} \sigma(x) dV, \quad (39)$$

$$\bar{\sigma}_m = \frac{1}{V_m} \int_{V_m} \sigma(x) dV. \quad (40)$$

The average strains for the fillers and matrix are defined, respectively, as

$$\bar{\varepsilon}_f = \frac{1}{V_f} \int_{V_f} \varepsilon(x) dV, \quad (41)$$

$$\bar{\varepsilon}_m = \frac{1}{V_m} \int_{V_m} \varepsilon(x) dV. \quad (42)$$

Based on the above definitions, the relationships between the filler and matrix averages and the overall averages can be derived as follows:

$$\bar{\sigma} = v_f \bar{\sigma}_f + v_m \bar{\sigma}_m, \quad (43)$$

$$\bar{\varepsilon} = v_f \bar{\varepsilon}_f + v_m \bar{\varepsilon}_m, \quad (44)$$

where v_f , v_m are the volume fractions of the fillers and matrix, respectively.

The third concept is the average properties of composites which are actually the main goal of a

micromechanics model. The average stiffness of the composite is the tensor C that maps the uniform strain to the average stress

$$\bar{\sigma} = C\bar{\varepsilon}. \quad (45)$$

The average compliance S is defined in the same way:

$$\bar{\varepsilon} = S\bar{\sigma}. \quad (46)$$

Another important concept is the strain-concentration and stress-concentration tensors A and B which are basically the ratios between the average filler strain (or stress) and the corresponding average of the composites.

$$\bar{\varepsilon}_f = A\bar{\varepsilon}, \quad (47)$$

$$\bar{\sigma}_f = B\bar{\sigma}. \quad (48)$$

Using the above concepts and equations, the average composite stiffness can be obtained from the strain-concentration tensor A and the filler and matrix properties:

$$C = C_m + v_f(C_f - C_m)A. \quad (49)$$

2.3.1.2. Halpin-Tsai model. The Halpin-Tsai model is a well-known composite theory to predict the stiffness of unidirectional composites as a functional of aspect ratio. In this model, the longitudinal E_{11} and transverse E_{22} engineering moduli are expressed in the following general form:

$$\frac{E}{E_m} = \frac{1 + \xi\eta v_f}{1 - \eta v_f}, \quad (50)$$

where E and E_m represent the Young's modulus of the composite and matrix, respectively, v_f is the volume fraction of filler, and η is given by

$$\eta = \frac{E/E_m - 1}{E_f/E_m + \xi_f}, \quad (51)$$

where E_f represents the Young's modulus of the filler and ξ_f the shape parameter depending on the filler geometry and loading direction. When calculating longitudinal modulus E_{11} , ξ_f is equal to $1/t$, and when calculating transverse modulus E_{22} , ξ_f is equal to w/t . Here, the parameters of l , w and t are the length, width and thickness of the dispersed fillers, respectively. If $\xi_f \rightarrow 0$, the Halpin-Tsai theory converges to the inverse rule of mixture

(lower bound),

$$\frac{1}{E} = \frac{v_f}{E_f} + \frac{1 - v_f}{E_m}. \quad (52)$$

Conversely, if $\xi \rightarrow \infty$, the theory reduces to the rule of mixtures (upper bound),

$$E = v_f E_f + (1 - v_f) E_m. \quad (53)$$

2.3.1.3. Mori-Tanaka model. The Mori-Tanaka model is derived based on the principles of Eshelby's inclusion model for predicting an elastic stress field in and around an ellipsoidal filler in an infinite matrix. The complete analytical solutions for longitudinal E_{11} and transverse E_{22} elastic moduli of an isotropic matrix filled with aligned spherical inclusion are [42,43]:

$$\frac{E_{11}}{E_m} = \frac{A_0}{A_0 + v_f(A_1 + 2v_0 A_2)}, \quad (54)$$

$$\frac{E_{22}}{E_m} = \frac{2A_0}{2A_0 + v_f(-2A_3 + (1 - v_0)A_4 + (1 + v_0)A_5 A_0)}, \quad (55)$$

where E_m represents the Young's modulus of the matrix, v_f the volume fraction of filler, v_0 the Poisson's ratio of the matrix, parameters, A_0, A_1, \dots, A_5 are functions of the Eshelby's tensor and the properties of the filler and the matrix, including Young's modulus, Poisson's ratio, filler concentration and filler aspect ratio [42].

2.3.2. Equivalent-continuum and self-similar approaches

Numerous micromechanical models have been successfully used to predict the macroscopic behavior of fiber-reinforced composites. However, the direct use of these models for nanotube-reinforced composites is doubtful due to the significant scale difference between nanotube and typical carbon fiber. Recently, two methods have been proposed for modeling the mechanical behavior of single-walled carbon nanotube (SWCN) composites: equivalent-continuum approach and self-similar approach [44].

The equivalent-continuum approach was proposed by Odegard et al. [45]. In this approach, MD was used to model the molecular interactions between SWCN-polymer and a homogeneous equivalent-continuum reinforcing element (e.g., a SWCN surrounded by a cylindrical volume of

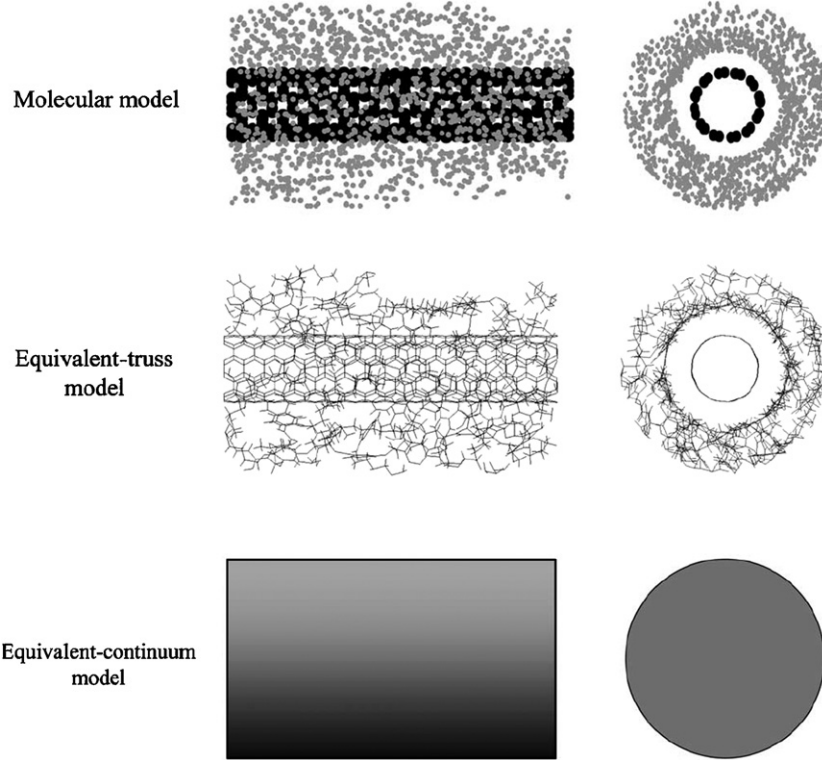


Fig. 2. Representative volume elements of molecular, equivalent-truss and equivalent-continuum models [44]. Reproduced from Odegard, Ripes and Hubert by permission of Elsevier Science Ltd.

polymer) was constructed as shown in Fig. 2. Then, micromechanics are used to determine the effective bulk properties of the equivalent-continuum reinforcing element embedded in a continuous polymer. The equivalent-continuum approach consists of four major steps, as briefly described below.

Step 1: MD simulation is used to generate the equilibrium structure of a SWCN–polymer composite and then to establish the RVE of the molecular model and the equivalent-continuum model.

Step 2: The potential energies of deformation for the molecular model and effective fiber are derived and equated for identical loading conditions. The bonded and non-bonded interactions within a polymer molecule are quantitatively described by MM. For the SWCN/polymer system, the total potential energy U^m of the molecular model is

$$U^m = \sum U^r(k_r) + \sum U^\theta(k_\theta) + \sum U^{vdw}(k_{vdw}), \quad (56)$$

where U^r , U^θ and U^{vdw} are the energies associated with covalent bond stretching, bond-angle bending, and van der Waals interactions, respectively. An

equivalent-truss model of the RVE is used as an intermediate step to link the molecular and equivalent-continuum models. Each atom in the molecular model is represented by a pin-joint, and each truss element represents an atomic bonded or non-bonded interaction. The potential energy of the truss model is

$$U^t = \sum U^a(E^a) + \sum U^b(E^b) + \sum U^c(E^c), \quad (57)$$

where U^a , U^b and U^c are the energies associated with truss elements that represent covalent bond stretching, bond-angle bending, and van der Waals interactions, respectively. The energies of each truss element are a function of the Young's modulus, E . The potential energy (or strain energy) of the homogeneous, linear-elastic, effective fiber is

$$U^f = U^f(C^f), \quad (58)$$

where C^f is the elastic stiffness tensor of the effective fiber. Equating Eqs. (56)–(58) yields

$$U^f = U^t = U^m. \quad (59)$$

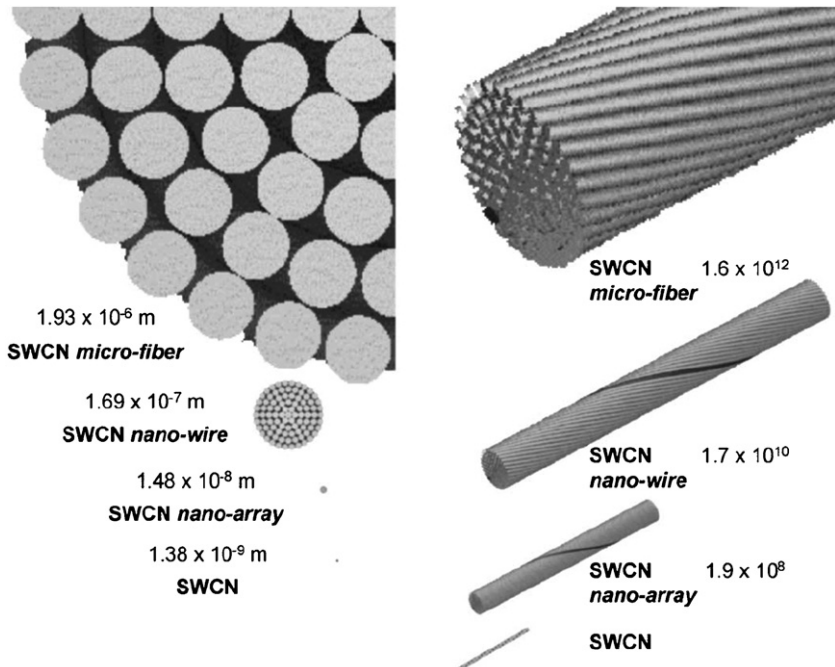


Fig. 3. Self-similar scales (left) and number of single-walled carbon nanotube per meter length [44]. Reproduced from Odegard, Ripes and Hubert by permission of Elsevier Science Ltd.

Eq. (59) relates the elastic stiffness tensor of the effective fiber to the force constants of the molecular model.

Step 3: A constitutive equation for the effective fiber is established. Since the values of the elastic stiffness tensor components are not known a priori, a set of loading conditions are chosen such that each component is uniquely determined from Eq. (59).

Step 4: Overall constitutive properties of the dilute and unidirectional SWCN/polymer composite are determined with Mori-Tanaka model with the mechanical properties of the effective fiber and the bulk polymer. The layer of polymer molecules that are near the polymer/nanotube interface (Fig. 2) is included in the effective fiber, and it is assumed that the matrix polymer surrounding the effective fiber has mechanical properties equal to those of the bulk polymer.

The self-similar approach was proposed by Pipes and Hubert [46] which consists of three major steps. First, a helical array of SWCNs is assembled. This array is termed as the SWCN nanoarray where 91 SWCNs make up the cross-section of the helical nanoarray. Then, the SWCN nanoarrays are surrounded by a polymer matrix and assembled into a second twisted array, termed as the SWCN nano-

wire. Finally, the SWCN nanowires are further impregnated with a polymer matrix and assembled into the final helical array—the SWCN microfiber. The self-similar geometries described in the nanoarray, nanowire and microfiber (Fig. 3) allow the use of the same mathematical and geometric model for all three geometries [46].

2.3.3. Finite element method

FEM is a general numerical method for obtaining approximate solutions in space to initial-value and boundary-value problems including time-dependent processes. It employs preprocessed mesh generation, which enables the model to fully capture the spatial discontinuities of highly inhomogeneous materials. It also allows complex, nonlinear tensile relationships to be incorporated into the analysis. Thus, it has been widely used in mechanical, biological and geological systems.

In FEM, the entire domain of interest is spatially discretized into an assembly of simply shaped subdomains (e.g., hexahedra or tetrahedral in three dimensions, and rectangles or triangles in two dimensions) without gaps and without overlaps. The subdomains are interconnected at joints (i.e., nodes). The implementation of FEM includes the important steps shown in Fig. 4.

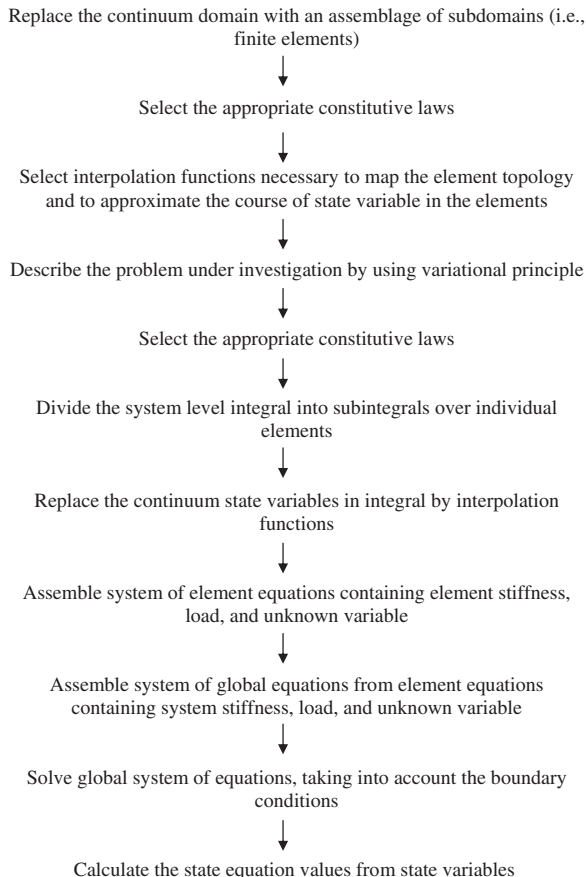


Fig. 4. Important steps in the finite element method.

The energy in FEM is taken from the theory of linear elasticity and thus the input parameters are simply the elastic moduli and the density of the material. Since these parameters are in agreement with the values computed by MD, the simulation is consistent across the scales. More specifically, the total elastic energy in the absence of tractions and body forces within the continuum model is given by [47]

$$U = U_V + U_K, \quad (60)$$

$$U_V = \frac{1}{2} \int dr \sum_{\mu, v, \lambda, \sigma=1}^3 \varepsilon_{\mu\nu}(r) C_{\mu\nu\lambda\sigma} \varepsilon_{\lambda\sigma}(r), \quad (61)$$

$$U_K = \frac{1}{2} \int dr \rho(r) |\dot{u}(r)|^2, \quad (62)$$

where U_V is the Hookian potential energy term which is quadratic in the symmetric strain tensor ε , contracted with the elastic constant tensor C . The

Greek indices (i.e., μ , v , λ , σ) denote Cartesian directions. The kinetic energy U_K involves the time rate of change of the displacement field \dot{u} , and the mass density ρ . The strains are related to the displacements according to

$$\varepsilon_{\mu\nu} = \frac{\partial u_\mu}{\partial r_\nu} + \frac{\partial u_\nu}{\partial r_\mu}. \quad (63)$$

These are fields defined throughout space in the continuum theory. Thus, the total energy of the system is an integral of these quantities over the volume of the sample dv . The FEM has been incorporated in some commercial software packages and open source codes (e.g., ABAQUS, ANSYS, Palmyra and OOF) and widely used to evaluate the mechanical properties of polymer composites. Some attempts have recently been made to apply the FEM to nanoparticle-reinforced polymer nanocomposites. In order to capture the multiscale material behaviors, efforts are also underway to combine the multiscale models spanning from molecular to macroscopic levels [48,49].

3. Modeling and simulation of polymer nanocomposites

3.1. Nanocomposite thermodynamics

The formation of stable nanocomposites depends on the thermodynamics of the multicomponent mixture concerned. In the case of polymer–nanoparticle mixtures, their final structures are strongly influenced by the characteristics of nanoparticles (e.g., size, shape, aspect ratio), polymer (e.g., molecular weight, structure, polarity and its compatibility with the particle), and surfactant if employed. The remarkably improved properties are usually observed from the structure in which nanoparticles are uniformly dispersed in polymer matrix. Therefore, in order to achieve such polymer nanocomposites and the maximal property improvement, it is very important to determine thoroughly the effects of various factors on the final structure and then isolate the thermodynamic conditions for the stable and uniform dispersion of nanoparticles. Experimentally, it is very difficult to ascertain these issues at a nanoscale.

Computer modeling and simulations have shown great success in colloid–polymer solutions. However, the colloid particles in such systems are much larger than the gyration radius of a polymer. These methods may not directly be extendable to

nano particle–polymer systems in which particle size is equivalent to the gyration radius. Therefore, in order to elucidate the formation of nanoparticle–polymer nanocomposites at a molecular level, some theoretical and simulation efforts have been made recently, especially on polymer nanocomposites. The simulation methods used include mean-field model [50,51], combined model of DFT and self-consistent field (SCF) [52], and molecular dynamic model [53,54]. Table 1 presents a brief description of the theoretical studies on the thermodynamics of polymer nanocomposites.

It is well recognized that the dispersion of layered clays or silicates in polymer matrix may lead to three kinds of structures, i.e., conventional immiscible microstructure, intercalated nanostructure and exfoliated/delaminated nanostructure. The formation of these equilibrium structures is believed to be determined by the interplay of entropic (i.e., intermolecular interactions) and enthalpic (i.e., configurational changes in the components) factors. Based on this consideration, Vaia and Giannelis [50,51] developed a modified mean-field model to predict the above three possible structures. Fig. 5 shows the free-energy change of polymer–organoclay mixtures as a function of clay platelet separation. In their mean-field model, the free-energy

change ΔH associated with the platelet separation and polymer incorporation is divided into two terms: one is the internal energy change ΔU associated with the establishment of new intermolecular interactions, and the other is the combinatorial entropy change ΔS associated with configuration changes of the various components. This is

$$\Delta H = H(h) - H(h_0) = \Delta U - T\Delta S, \quad (64)$$

where h and h_0 are the final and initial clay platelet separations and T is the temperature. Thus, $\Delta H < 0$ indicates the intercalation process is favorable while $\Delta H > 0$ indicates the initial unintercalated state is favorable. Based on their calculated results, three kinds of equilibrium structures have been isolated as shown in Fig. 5.

It has been shown that the entropy loss associated with polymer confinement in the clay gallery is approximately compensated by the entropy gain associated with the increased conformational freedom of the surfactants as the gallery distance increases due to the polymer intercalation. Thus, the enthalpy determines whether or not polymer intercalation will take place. From this point of view, it is possible to select potentially compatible polymer and organoclays systems to produce materials

Table 1
Simulation studies on the thermodynamics of polymer nanocomposites

Material system and references	Simulation method	Key features and findings
Clay–polymer [50,51]	Mean-field	Evaluation of the effects of various aspects of polymer and clay/organoclay on nanocomposite formation; and Limitation of assumption, i.e., separation of configurational terms and intermolecular interaction and separation of the entropy of various components.
Clay–polymer [52]	Density functional theory and self-consistent field	Addressing the thermodynamic and architectural requirement for intercalated and exfoliated nanostructures; Relating the particle–polymer interaction to free energy: increasing the interaction strength decreases free energy; and Coupling the conformation of polymer and that of surfactants in organoclay.
Clay–nylon 6 Clay–nylon 66 [53,54]	Molecular dynamics	Binding energy between various components (i.e., polymer, surfactant and clay surface).
Nanoparticle–polymer [13]	Coarse-grained molecular dynamics	Weak attractive particle–polymer interaction leads to nanoparticle aggregation; Strong attractive interaction promotes the dispersion of nanoparticles; and Repulsive nanoparticle–polymer interaction leads to an energetic contribution that dominates the interactions between two nanoparticles while the entropic is less pronounced.

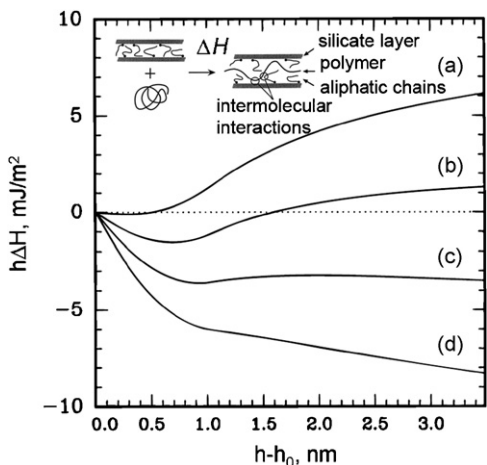


Fig. 5. The free-energy change (ΔH) of polymer–organoclay mixtures as a function of clay gallery separation under different intercalation strength (ε) between polymer–organoclay: (a) $\varepsilon = 0$; (b) $\varepsilon = -4$; (c) $\varepsilon = -8$; and (d) $\varepsilon = -12 \text{ mJ/m}^2$. The inset shows the intercalation process of polymer in organoclay [51]. Reproduced from Vaia and Giannelis by permission of American Chemical Society.

with desirable structures. The greatest advantage of mean-field model is that it is able to explore the effect of various aspects of the polymer and organoclay on nanocomposite formation. However, the assumptions, such as the separation of configurational terms and intermolecular interactions and the further separation of the entropic behavior of the components, somewhat limit the usefulness of the model.

To overcome some of the limitations in the above mean-field model, Balazs and co-workers have recently developed a series of models based on the theories of Scheutjens and Fleer [55,56], and Carignano and Szleifer [57] in which the conformations of polymer and tethered surfactants are no longer decoupled, but instead, the equilibrium conformation of one component is intimately influenced by the configuration of the other. For example, they used the SCF calculation to address the thermodynamic and architectural requirements necessary to achieve polymer intercalation and ultimately the exfoliated nanostructures [52,58]. Their results shown in Fig. 6 are qualitatively similar to the findings based on the above mean-field model [51], i.e., with the increase of polymer–clay/organoclay interaction (χ), the free-energy change decreases from positive (curves a and b) to negative (curves d and e). This means that the final equilibrium structure of the mixtures changes from immiscible (curves a and b) to intercalated (curve c)

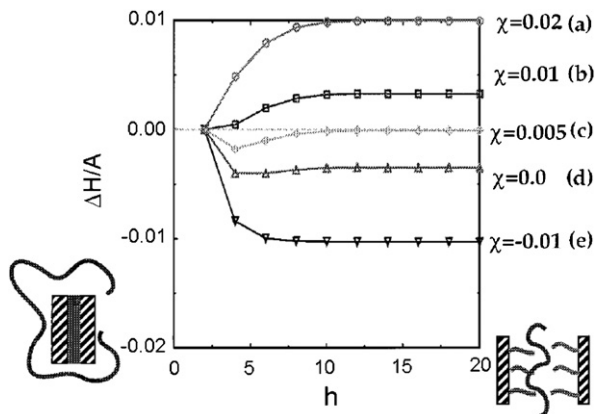


Fig. 6. Free-energy change per unit area ($\Delta H/A$) as a function of surface separation (h) for various interaction parameter values (χ), the left diagram shows the reference state where the grafted chains form a melt between the surfaces, and the right diagram shows the surfaces are separated by the intercalated polymers [58]. Reproduced from Balazs, Singh, Zhulina and Lyatskaya by permission of American Chemical Society.

and exfoliated (curves d and e). By using an integrated DFT–SCF model, they [59–62] investigated further the effects of various factors (e.g., surfactant-coated clay surface, end-functionalization of polymer, block copolymer) on the equilibrium structures of polymer–clay mixtures.

Moreover, Balazs and co-workers found that adding polymers with one reactive end group to a melt of chemically identical non-functionalized polymers can lead to the formation of exfoliated nanostructures while adding polymers with two reactive end groups (the so-called telechelic polymers) can promote the formation of thermodynamically stable intercalated nanostructures but not the more desirable exfoliated nanostructures [52,59]. The chain length ratio of functionalized polymer and non-functionalized polymer shows a significant influence on the location of the phase boundaries between the immiscible, intercalated, and exfoliated states. More recently, Groenewold and Fredrickson [63] carried out the theoretical calculation to explore the thermodynamic behavior of block copolymer–clay mixture in which the grafted clay particle is embedded in a lamellar block copolymer matrix as shown in Fig. 7. They found that the high aspect ratio of the clay platelets implies a long range of interaction.

Kudryavtsev et al. [64] studied theoretically the thermodynamic equilibrium of a mixture of homopolymer and clay modified with a diblock

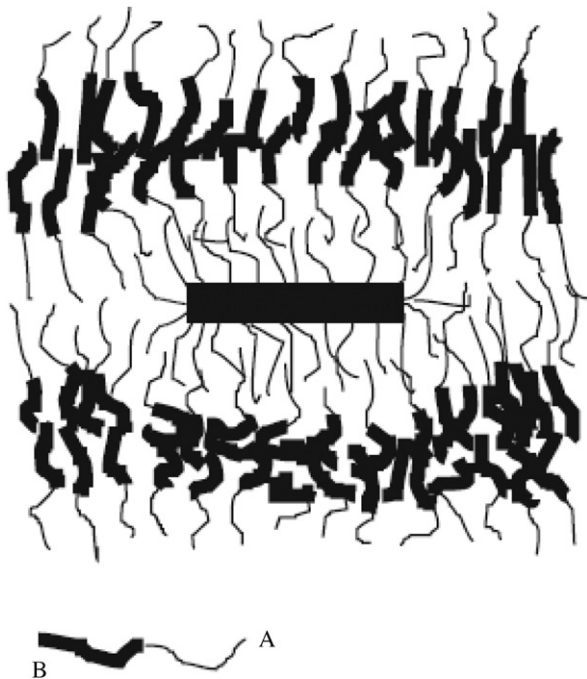


Fig. 7. Visualization of a clay platelet grafted with chains of type A, embedded in a lamellar matrix composed of AB block copolymers [63]. Reproduced from Groenewold and Fredrickson by permission of Springer.

copolymer to seek strategies for polymer melt intercalation. They concluded that a co-modification by both diblocks and surfactants is probably the best means for facilitating the intercalation. Reister and Fredrickson [65] investigated the potential of mean force between two nanoparticles surrounded by a diblock copolymer matrix. By using the SCF theory, they analyzed the energy change of the system. Above the order-disorder transition, attractive potential of the particles for one kind of monomers leads to a lamellar structure around the particles. Below the transition, they inserted particles in such a way that the axis connecting them is either perpendicular or parallel to the lamellar polymer structure. They then used the SCF theory to investigate the energy and structural change of the system with the particle distance. More recently, Kim and White [66] studied the formation of polymer-clay intercalation and nanocomposites by using statistical thermodynamical equilibrium principles. They proposed that the exothermic heat of mixing between polymer chains and organic amine on organically modified clay surface is the key to the intercalation of the polymer melt and hence the formation of polymer nanocomposites.

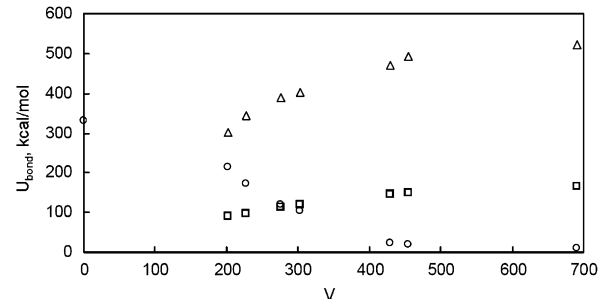


Fig. 8. Predicted binding energies (U_{bond}) as a function of surfactant molecular volume (V): $U_{\text{clay}-\text{nylon}_6}$ (circle), $U_{\text{nylon}_6-\text{surfactant}}$ (square) and $U_{\text{clay}-\text{surfactant}}$ (triangle) [54]. Reproduced from Fermeglia, Ferrone and Pril by permission of Elsevier Science Ltd.

MD simulations have also been used to investigate the thermodynamic behavior of polymer nanocomposites. For example, the binding energies between the components (i.e., polymer, surfactant and clay platelet) of nylon 6,6-clay nanocomposite and nylon 6-clay nanocomposites were calculated by Tanaka and Goettler [53] and Fermeglia et al. [54], respectively. Interestingly, both simulation studies draw the exact conclusions: (i) the binding energy between the polymer matrix and clay platelet decreases with the increase of surfactant volume while the binding energy between polymer and surfactant and that between surfactant and clay increase with the increase of surfactant volume (Fig. 8); (ii) the use of surfactant whose hydrogen atoms are substituted with polar groups (i.e., $-\text{OH}$, $-\text{COOH}$) generally results in a stronger interaction between polymer and surfactant. By using MD simulation, Toth et al. [67] studied the structure and energetic of different biocompatible polymer nanocomposites made up of two biodegradable polymers (poly (β -hydroxybutyrate) and poly (vinyl alcohol)), hydrotalcite (either in an anhydrous or in a solvated environment), and seven non-steroidal anti-inflammatory drugs. Their results showed that nanoconfined conformations of smaller and polar drug molecules are more easily affected by the presence of water molecules in the clay gallery with respect to their larger and less polar counterparts. The binding energy between a drug and hydrotalcite layers can be increased by intercalating polymers in the gallery of the drug-pretreated hydrotalcite. In particular, the simulation results indicated that for hydrophobic drugs, the best results for a solvated environment could be obtained via intercalation with poly (vinyl alcohol) while for acidic drugs poly

(β -hydroxybutyrate) could be the polymer of choice for intercalation.

Smith et al. [13] used the coarse-grained MD simulation to study the interactions between two spherical nanoparticles immersed in a polymer matrix, where the nanoparticle radius, the gyration radius and statistical segment length of polymer are comparable. They found that the polymer-induced interaction is greater than the direct nanoparticle–nanoparticle interaction in all systems with a range of polymer–nanoparticle interactions and polymer molecular weights. The nanoparticle–nanoparticle radial distribution functions in Fig. 9 show that a relatively weak interaction ($\epsilon_{np} = 1$) between polymer and nanoparticle promotes nanoparticle aggregation indicated from the sharp peak, while increased attractive nanoparticle–polymer interaction can lead to strong adsorption of the polymer chains on the surface of nanoparticles and thus promote dispersion of nanoparticles. In a further study, Bedrov et al. [68] found that in systems with repulsive nanoparticle–polymer interactions the energetic contribution dominates the interactions between two nanoparticles while the entropic contribution is less pronounced but not negligible. The dependence of the thermodynamic properties as a function of nanoparticle separation is strongly correlated with the overall polymer density, and the polymer structure at the interface and between particles. In addition, as nanoparticles approach to each other, systems gain entropy due to destabilization of the homogeneous polymers in

the nanoconfined interparticle region. Further approach resulted in the overlap of the interfacial shells and the reduction of the number of the polymer beads at the nanoparticle interface.

3.2. Nanocomposite kinetics

Another important issue of polymer nanocomposites is the formation kinetics, that is, how fast and in what way such nanocomposites are formed. The formation kinetics of polymer nanocomposites is much less understood than that of formation thermodynamics. For example, in the case of layered clays, it is still unclear how the surfactant or polymer get into clay gallery and form the intercalated or exfoliated structure since the gallery is initially separated by less than 1 nm and thus hinders the infusion of external species. However, the formation process must be well understood before the material design, controllable manufacturing and long-term usage of clay-based polymer nanocomposites become possible. As an initial stage, we should address such intercalation kinetics as: (i) how do the galleries open for the accommodation of intercalating chains (i.e., surfactant or polymer)? (ii) by what mechanisms do the chains enter the galleries? (iii) what are the natures of clay structure and polymer, and how do clay–clay and polymer–clay interactions affect the penetration of polymers into the galleries? (iv) how does the diffusivity of the intercalated chains compare to that of bulk chains? In the past few years, some simulation work has been done (as listed in Table 2) on such kinetics issues for polymer nanocomposites [11,69–73].

Loring and co-workers [11,69] first investigated the intercalation process of clay-based polymer nanocomposites. They employed the coarse-grained MD simulations to examine the flow of a polymer melt into an initially evacuated rectangular slit as shown in Fig. 10. They found that as the polymer–surface affinity increases, the flow of polymer into the slit is slowed down (Fig. 11), which is in agreement with the experimental observation for clay-based polymer nanocomposites. However, the effective diffusion coefficient in the simulation demonstrated a weaker dependence on molecular weight rather than an inverse dependence observed experimentally [74]. This model, however, ignores two major features of the experimental systems: the presence of surfactants grafted to the clay surface and the swelling of the slit during

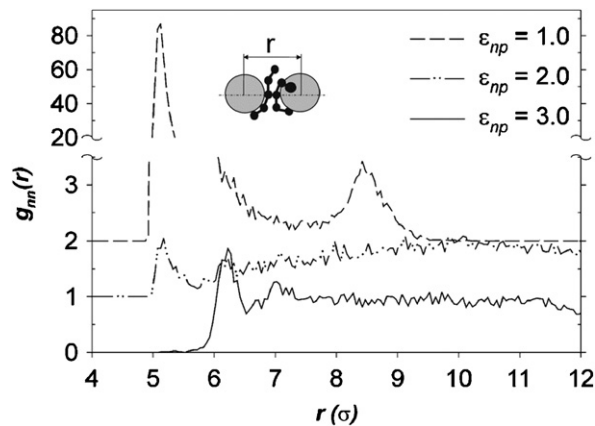


Fig. 9. The nanoparticle–nanoparticle radial distribution functions under different interaction parameter values (ϵ_{np}), data are offset vertically by 2.0 and 1.0 for $\epsilon_{np} = 1.0$ and $\epsilon_{np} = 2.0$, respectively [13]. Reproduced from Smith, Bedrov and Smith by permission of Elsevier Science Ltd.

Table 2

Simulation studies on the formation kinetics of polymer nanocomposites

Material system and references	Simulation method	Key features and findings
Clay–polymer [11,69]	Coarse-grained molecular dynamics	The intercalation process and interlayer swelling of clay require a moderate polymer–surface affinity; Increasing polymer–surface affinity slows down the flow of polymer into the interlayer space; and Increasing polymer molecular length leads to the decrease of flow rate.
Nanoparticle–binary polymer blend [70,71]	Multiscale method (coarse-grained Cahn–Hilliard approach and Brownian dynamics)	Effect of shear: the domains grow initially in an isotropic manner, and in the later stage grow faster along the shear direction; Addition of solid particles significantly changes both the speed and the morphology of the phase separation; and High density of particle will destroy the shear-induced anisotropic growth.
Clay–polymer [72,73]	Semiphenomenological model	External stress and bending of clay platelets affect clay intercalation; Strong external force is necessary to induce clay intercalation; and Intercalation kinetics is solely governed by the initial stage.

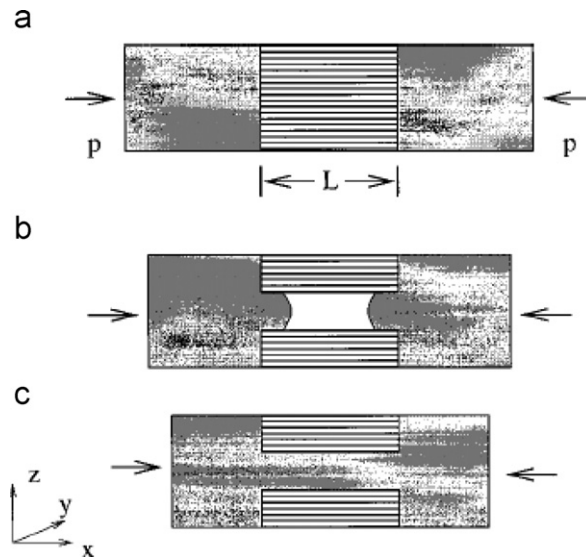


Fig. 10. MD simulation scheme of intercalation process. Gray regions represent the polymer melt and striped regions represent the silicate particle: (a) reservoirs are equilibrated under constant pressure with slit closed, (b) slit is opened, and intercalation proceeds and (c) intercalation is complete [11]. Reproduced from Lee, Baljon and Loring by permission of American Institute of Physics.

the intercalation process. The surfactants undoubtedly play an important role since the intercalation process for relatively non-polar polymers does not take place in their absence. Therefore, in a more recent study [75], they introduced the two features in their simulation. The results (Figs. 12 and 13)

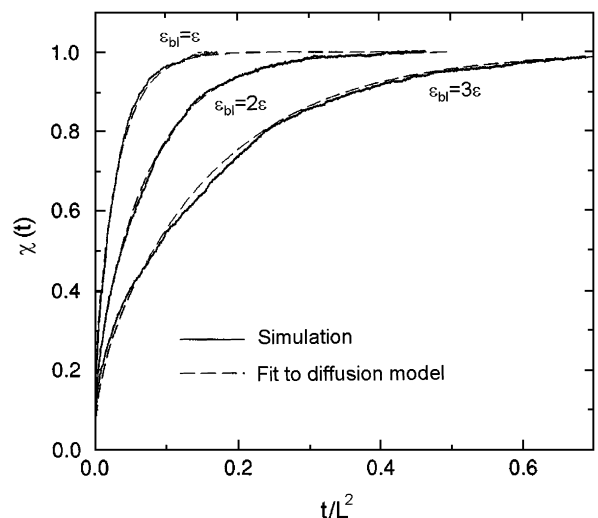


Fig. 11. The effect of the bead–lattice interaction on intercalation dynamics, $\chi(t)$ is the number of beads at time t in the slit, normalized by its value at the equilibrium after the slit is filled, L is slit length, ε_{bl} is the bead–lattice interactions [11]. Reproduced from Lee, Baljon and Loring by permission of American Institute of Physics.

indicated that the spontaneous intercalation and swelling of clay need a moderate polymer–clay affinity. More specifically, increasing the polymer–clay affinity would induce spontaneous intercalation and clay swelling. However, for a relatively higher polymer–clay affinity, the amount of intercalated

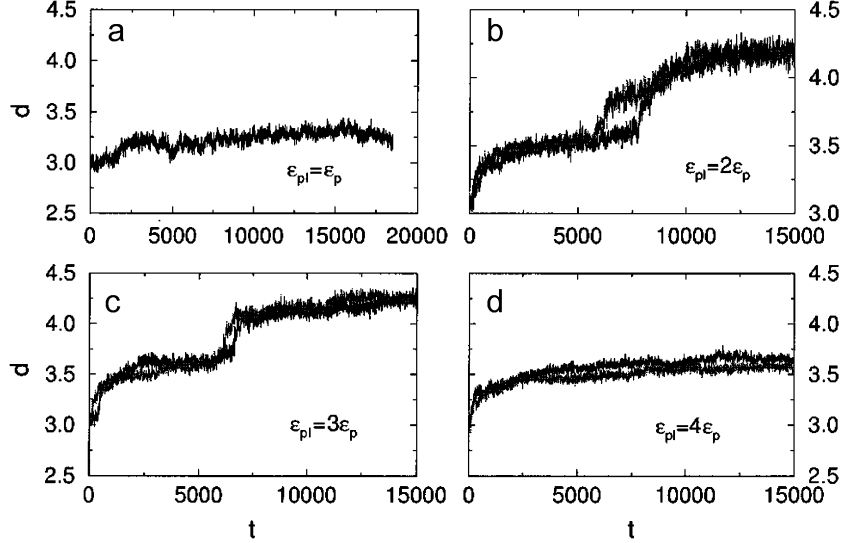


Fig. 12. Slit spacing (d) as a function of simulation time in units of τ_p under four different polymer–silicate interaction strengths, i.e., $\varepsilon_{pl} = 1, 2, 3$ and $4\varepsilon_p$, respectively, where ε_p is polymer–polymer interaction strength [75]. Reproduced from Lee, Baljon and Loring by permission of American Institute of Physics.

material at a given time is reduced. In addition, their results, unlike the cases with fixed slit volume, indicated that the flow rate decreases when the polymer molecular length increases. This is probably attributed to the relaxation of polymer bridges that connect the two clay surfaces since the number of these bridges is controlled by chain length. A further study has been done on the flow of a symmetric diblock copolymer from a bulk melt into a slit whose walls are grafted with surfactants. The result indicates that the use of diblock copolymer can produce structures containing material that would not spontaneously intercalate as a homopolymer [76].

The above simulations, however, have not considered the flow fields which are commonly used during the processing of polymer composite to promote greater intermixing of the different components. Such processing conditions are believed to play a critical role in the morphology formation and final properties of the materials. Balazs and co-workers [70,71] developed a multiscale model to represent particle-filled polymers. This model contains a phase-separating binary mixture or diblock copolymer and mobile, solid particles. By combining a mesoscopic, coarse-grained description of the fluids with a discrete model for particles, they found that the addition of solid particles significantly changes both the speed and morphology of the phase separation (Fig. 14). By using a mean-field

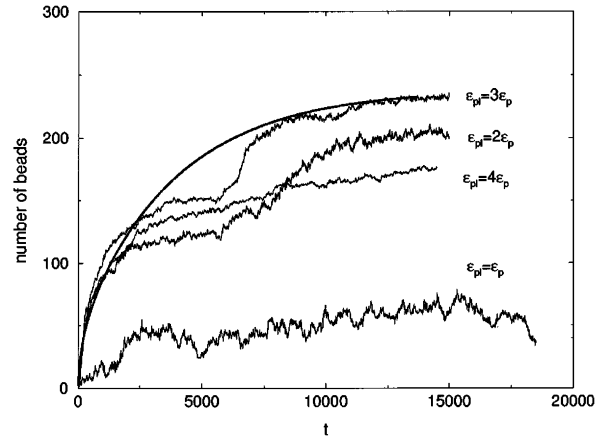


Fig. 13. The time dependence of the number of intercalated polymer beads for the trajectories of Fig. 12. The thick line shows a fit of the $\varepsilon_{pl} = 3\varepsilon_p$ case to the solution of the diffusion equation for material filling a rectangular slit [75]. Reproduced from Lee, Baljon and Loring by permission of American Institute of Physics.

rate-equation model for the kinetics of phase separation, they found that the phase separation is captured in the later stage if particles are preferentially wet by one of the fluids. The steady-state domain size depends strongly on the particle concentration and diffusion constant. In addition, when the binary fluid–particle mixture is under shear, it was found that initially the domains grow in an isotropic manner while later the domains

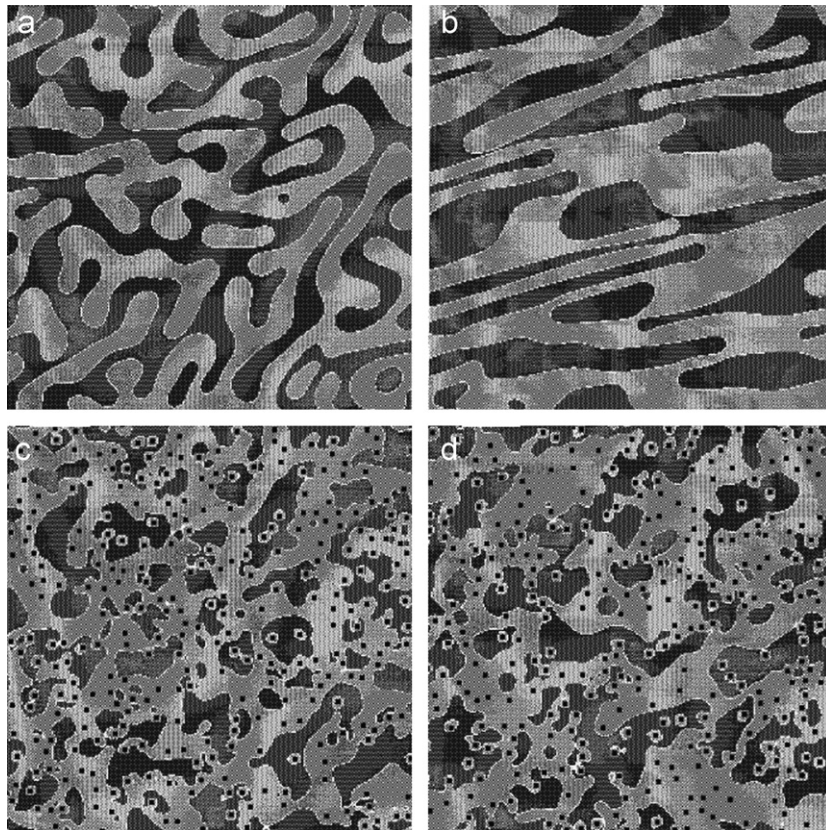


Fig. 14. Morphology of the mixture under the shear rate $S = 1 \times 10^{-4}$: (a) $N = 0$, $\gamma = 1$; (b) $N = 0$, $\gamma = 5$; (c) $N = 300$, $\gamma = 1$; and (d) $N = 300$, $\gamma = 5$, where N is the particle number and γ is the shear strain. Black circles represent particles, light gray regions are the A-phase domains, dark gray regions are the B-phase domains, and white points are interfaces [70]. Reproduced from Balazs, Ginzburg, Qiu, Peng and Jasnow by permission of American Chemical Society.

grow faster along the shear direction and ultimately stop growing or grow extremely slowly in the perpendicular direction (Fig. 15). However, for sufficiently high particle density, the shear-induced anisotropic growth is destroyed by the randomly moving, coated particles, and thus isotropic morphology can be observed even at large shear strains.

Cheng et al. [77] also developed a multiscale computational approach to study the reactive compatibilization in an immiscible binary AB blend with interacting particles. Their simulation results, consistent with the theoretical analyses, showed that the reaction kinetics is first order in the initial density of reactants. The simulation also showed that a competition among three effects (i.e., Brownian motion, the coupling interaction and A–B reaction) induces interfacial motion. Thus, their work provided some insight into the factors that affect the structural evolution at the interface of incompatible A and B domains.

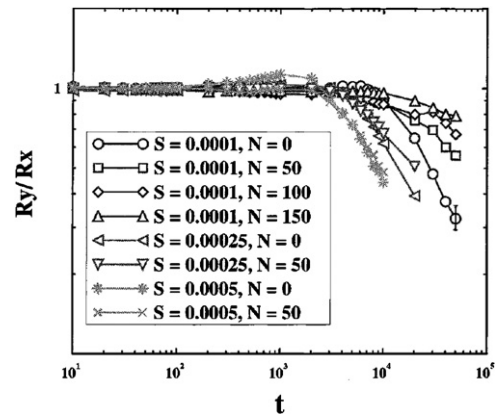


Fig. 15. Anisotropic growth (R_y/R_x) as a function of time for different particle number N and shear rates S [70]. Reproduced from Balazs, Ginzburg, Qiu, Peng and Jasnow by permission of American Chemical Society.

Although nanofillers are usually regarded as rigid particles, some of them may show a certain level of flexibility, for example, the bending of nanotubes or

clay platelets. Unlike the assumption of rigid particle model used in the previous simulation, Ginzburg et al. [73] recently proposed a simple analytical model to take the bending of clay platelets and external shear into account, which allows one to construct analytical solutions for the intercalation process (Fig. 16). They found that the intercalation process could be carried out by the novel type of soliton-like excitations—kinks which result from the balance between the bending elasticity of the clay platelets, the polymer-induced interaction between the platelets and the external elongational shear force. They showed that a strong external force is necessary to induce kink formation and hence clay intercalation. Gendelman et al. [72] improved such a model by taking into account the initial opening of the clay galleries as well as kinetic features of the process. Their study showed that the activation of the intercalation process by the external force is sufficient for further propagation of the kink with finite velocity. Therefore, the kinetics of the intercalation is solely governed by the initiation stage.

In a recently study, Anderson et al. [78] used coarse-grained MD simulations to investigate the behavior of a system consisting of a mixture of binary fluids and a stack of silicate platelets and then how the interactions between the components affect the ability of the monomers to open and

infuse the clay galleries. The fluids consist of a certain ratio of type A beads (i.e., highly self-attractive molecules) and type B beads (i.e., marginally self-attractive molecules), specifically, A75, A25 and A01 represent the mixtures of fluids containing 75%, 25% and 1% of type A beads. The clay platelets are treated as flexible sheets other than rigid plates. Fig. 17 shows the platelet configuration obtained from A25-clay system in the course of the simulation. In all cases the two outermost galleries are first to begin filling with fluid beads (Fig. 18). For A25-clay system, there are three distinguishable regimes of infusion: simultaneously initial intercalation, two outermost gallery intercalated and finally innermost galleries intercalated. For A75-clay system, the intercalation occurs almost simultaneously. For A01-clay system, only the outermost galleries are intercalated due to the lack of highly attractive fluid A type beads.

3.3. Nanocomposite molecular structure and dynamic properties

It is generally accepted that the structure of polymer–nanoparticle mixtures has an important influence on the properties of the ultimate materials. Experimentally, the structural information on these materials, in particular, polymer–clay nanocomposites, can only be inferred based on the measurement of X-ray diffraction, transaction electronic microscopy, small-angle neutron scattering, nuclear magnetic resonance (NMR) spectroscopy [4,8,79]. However, it is quite difficult to ascertain by direct experiments the details about molecular structure and dynamics in the clay gallery or at the interface. Further progress in this field thus suffers badly from the limited ability of experimental characterization and the lack of a profound understanding of molecular interactions among various components that control the structural evolution and final morphology of the materials, e.g., intercalated or exfoliated structures of clays. This is probably the main reason why there is an increasing need for computer modeling and simulation of such materials using different techniques, including MC, MD and lattice energy minimization.

The structure of molecular chains in the vicinity of solid surface is believed to be significantly different from that of bulk chains due to the restriction of surface impact on the chains. Generally, the polymer chains in the immediate vicinity of the surface are preferentially aligned in the

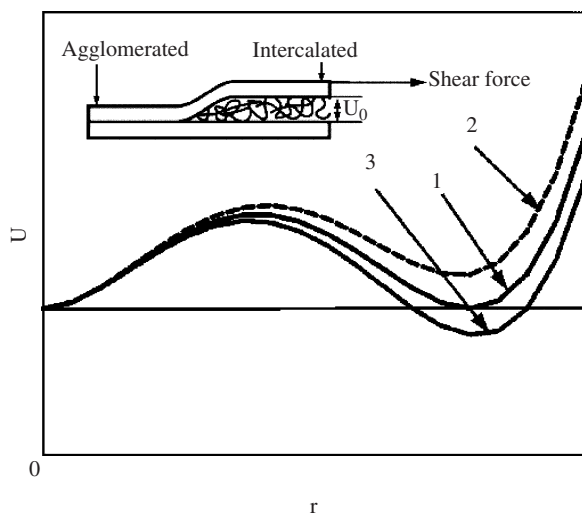


Fig. 16. Sketch of the plate-plate interaction potential $U(r)$. Curve 1 corresponds to a symmetric case $U(r) = U(r_0)$, curves 2 and 3 depict asymmetric cases $U(r) > U(r_0)$ and $U(r) < U(r_0)$, respectively, where, r_0 is the plate separation in this state [73]. Reproduced from Ginzburg, Gendelman and Manevitch by permission of American Physical Society.

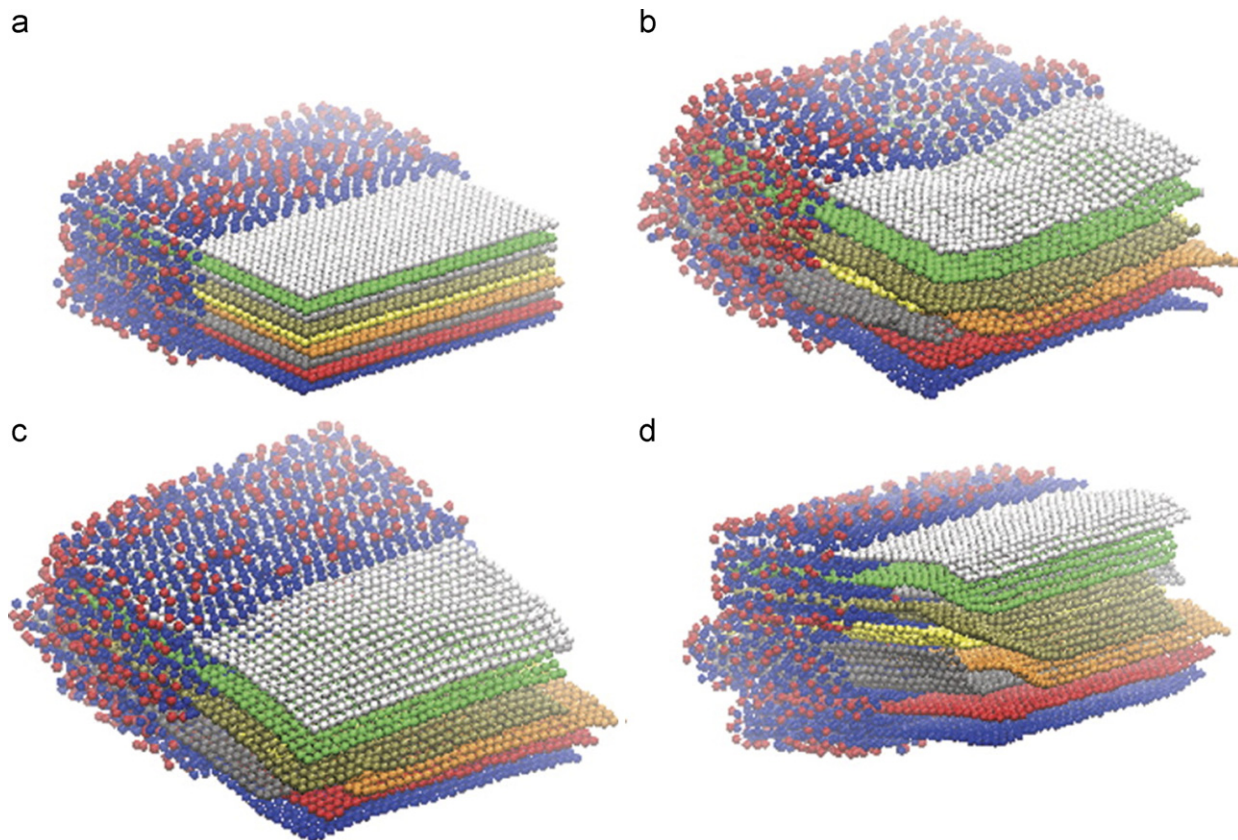


Fig. 17. Snapshots of A25-clay taken (a) initially, (b) after 10,000 MD steps, (c) after 100,000 MD steps and (d) after 1,000,000 MD steps. Each silicate plate is colored differently. Type A (attractive) fluid beads are blue, and type B (non-attractive) fluid beads are red. Only fluid within 2σ of one-half of the tactoid is shown for clarity. All the fluid beads have been removed from the front half of the pictures to show the changes that occur in the sheets [78]. Reproduced from Anderson, Sinswat, Vaia and Farmer by permission of Wiley Periodicals, Inc.

direction parallel to the surface and have reduced mobility. The degree of alignment depends on the interaction strength of the chains with the surface. However, the structure of polymers confined between two spherical particles is still a subject of debate and has recently stimulated research activities. Such systems, in particular nanoconfined systems, represent the recently developed polymer nanocomposites reinforced with spherical nanoparticle. So far, some theoretical efforts have been made to investigate the structural changes of polymer chains due to the addition of spherical nanoparticles. The properties studied include chain dimension (i.e., end-to-end distance), atomic/segment density profile, chain orientation/alignment and chain conformations. Besides, the variables like particle size/curvature, particle loading, chain length and particle–polymer interaction strength have also been examined. For example, Mark and co-workers [80–82] investigated the effect of sphe-

rical nanoparticle inclusion on chain deformation (i.e., end-to-end chain distance). They found that the volume fraction and/or the size of nanoparticles as well as their spatial arrangement in a polymer matrix significantly affect the end-to-end chain distance. Specifically, their theory predicts that the chain dimension in the presence of nanoparticles with equivalent size as polymer chains is smaller than that of bulk polymer chains and such dimension increases for longer chains.

More recently, MC [83] and MD [84,85] simulations were employed to study the molecular structure at the surface of nanoparticle embedded in polymer matrix. Fig. 19 represents some of these models employed [15,84,86,87]. The simulations indicated that chain dimensions of systems with high and moderate filler volume fractions are always smaller than those of corresponding bulk systems. Vacatello [88], however, questioned the assumption of non-interacting chains in both studies [81,82] for

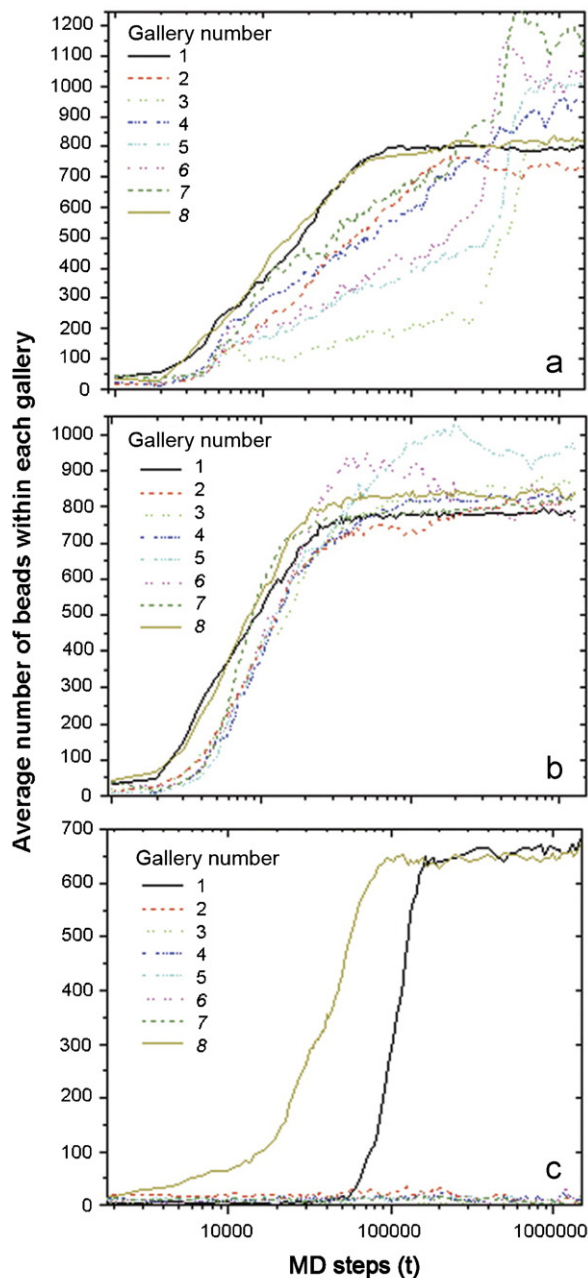


Fig. 18. Number of beads in each gallery of (a) A25-caly, (b) A75-clay, and (c) A01-clay. Galleries 1 and 8 represent the spacing between the top two and bottom two sheets, respectively [78]. Reproduced from Anderson, Sinsawat, Vaia and Farmer by permission of Wiley Periodicals Inc.

filled systems and noted that the chains simulated are too short to be directly compared with real systems. In a further study, by using bead–spring model and MC method, Ozmusul and Pico [89] studied the polymer structure in the vicinity of the

spherical surface. It was observed that the bead number density is lower at the surface than that in the bulk. Besides, the surface induces preferential bond and chain segment orientation in the tangential direction. The degree of preferential orientation does not depend on chain length but surface curvature. Fillers having radii larger than the root mean square gyration radius of the molecular chain lead to similar structure on the scale of the chain, while smaller fillers leave both the size and the orientation of the chain coils unperturbed.

Picu and Ozmusul [90] used MC simulation to investigate the bond-scale and chain-scale structure of linear polymers confined between spherical nanofillers. They examined the dependence of polymer structure on the various types of interactions, chain length, polymer density, surface curvature and the size of nanofillers. On the bond scale, the chain ends segregate to the nanofiller surface and are essentially independent of surface curvature. On the chain scale, the ellipsoidal chains undergo a docking transition to the spherical nanofillers. The ellipsoids do not deform, but rotate with their large semiaxis in the direction tangential to the nanofiller as their centers of mass approach the nanofiller surface. In addition, the chain dimension decreases in the direction of its large semiaxis when the distance between nanofillers is less than two bulk gyration radii, an effect essentially independent of the energetic interactions in the system. In the above analysis, polymer structures in bond-scale and chain-scale are represented by average segment orientation P_2^s and chain gyration tensor G_{ij} , calculated by the following equations:

$$P_2^s(x) = \frac{1}{4\pi} \int_0^{2\pi} \int_0^\xi \frac{1}{2} (3 \cos^2 \theta - 1) \sin \theta d\theta d\varphi \quad (\text{in bond-scale}) \quad (65)$$

$$G_{ij} = \frac{1}{N} \sum_{k=1}^N (X_i^k - X_i^{\text{c.m.}})(X_j^k - X_j^{\text{c.m.}}) \quad (\text{in chain-scale}) \quad (66)$$

where x and ξ are defined in Fig. 20, $X^k = (X_1^k, X_2^k, X_3^k)$ is the position vector of bead k , c.m. represents the center of mass of the current chain, and N is the number of beads in each chain.

In a recent study, Ozmusul and Picu [91] further investigated the static structure of polymer chains filled with nanoparticles by means of MC lattice simulation. The overall conformation of the chains

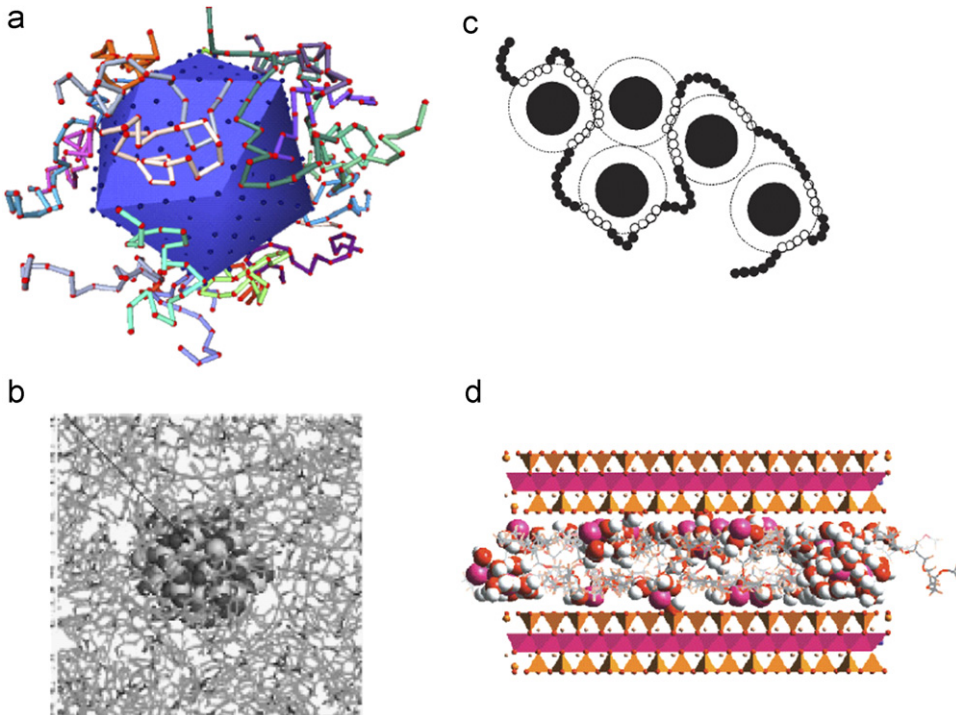


Fig. 19. Representative models of nanoparticle-reinforced polymer systems: (a) one spherical nanoparticle in polymer [84]. Reproduced from Starr, Schroder and Glotzer by permission of American Chemical Society; (b) one silica nanoparticle in polyimide [86]. Reproduced from Odegard, Clancy and Gates by permission of Elsevier Science Ltd.; (c) multiple nanoparticles in polymer [15]. Reproduced from Vacatello by permission of Wiley-VCH; and (d) polymer intercalated nanocomposite [87]. Reproduced from Hackett, Manias and Giannelis by permission of American Chemical Society.

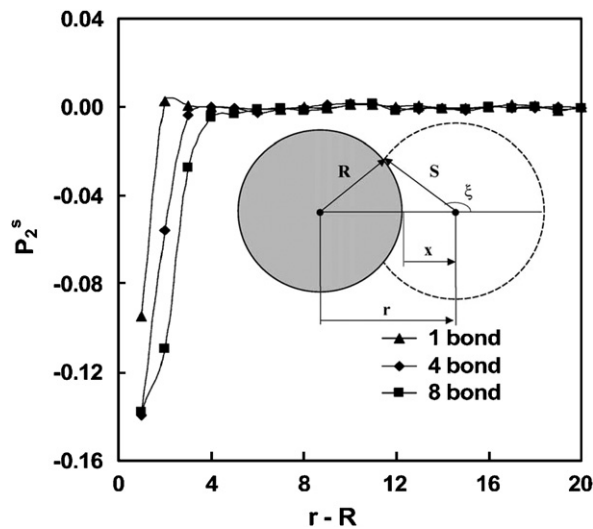


Fig. 20. Average segment orientation P_2^s as a function of the distance $(r-R)$ from the surface of particle. Inset shows the schematics of allowable directions for the segment end-to-end vector in the vicinity of a curved wall. Here R is the radius of curvature and S represents the bulk length of the end-to-end vector considered [89]. Reproduced from Ozmusul and Picu by permission of Elsevier Science Ltd.

is expressed statistically with the subchain segments as defined in Fig. 21: bridges, dangling segments (tails), loops and trains. Their results supported the notion that the mechanical reinforcement of fillers is due to the polymer-mediated transient network created among the fillers. In addition, it was shown that increasing filler loading leads to a larger fraction of bridges, probably due to the decrease in mean distance between fillers.

Vacatello [83] found that the polymer chains at the nanofiller surface are arranged in densely packed and ordered shells similar to the layered structures found for the same model polymer near planar solid surfaces [92] and for shorter coarse-grained chains near the surface of a nanoparticle [84]. Accordingly, the polymer chains are divided into different conformations, i.e., interface segments (totally running in the interface shell of a given particle), bridge segments (non-interface units with the two adjoining units in the interface shells of two different particles) and loop segments (similar to bridge segments, but starting and ending in the interface shell of the same particle). The relative

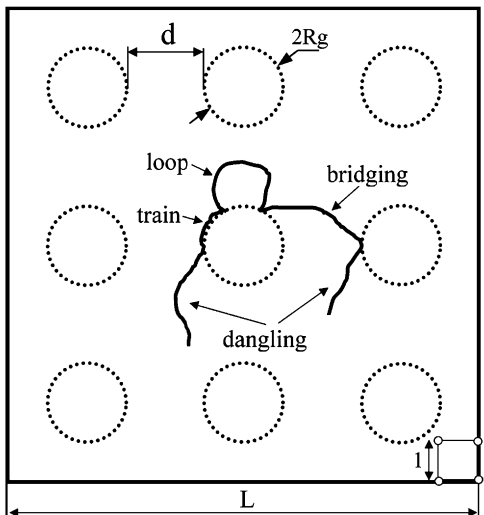


Fig. 21. Schematic 2D representation of the 3D polymer nanocomposite model with a unit cell of the lattice being sketched in the right lower corner [91]. Reproduced from Ozmusul, Picu, Sternstein and Kumar by permission of American Chemical Society.

abundance and average lengths of these conformations usually depend on the composition of the systems (i.e., the size and volume fraction of the nanofillers). Thus, such simulation results can be used as a guide in experimental work and as a basis for theoretical studies.

Further simulations [15] for systems with a fixed content of particles but various particle diameters have led to the establishments of a few simple rules to predict the molecular arrangements in polymer–nanofiller systems. However, MC simulations of polymers filled with randomly distributed solid nanoparticles are limited to systems with short chains and small particles and are not feasible for systems with long chains. One reason is that there are no suitable methods for equilibrating and sampling such systems. Another reason is that systems of large particles and small filling density contain a large proportion of free chains and very long terminal segments. Therefore, the results obtained with these systems are of little use for predicting the behavior of longer chains. In order to overcome such problem, Vacatello [93,94] carried out phantom chain simulations to study the molecular arrangements in systems of chain molecules filled with randomly distributed nanoparticles. The results showed that proper modification of interaction energy between chain units and fillers can lead to an excellent agreement of phantom chain

properties with those obtained for dense systems having the same composition [15]. For the nanocomposites with long chains and a random distribution of large nanoparticles, some fundamental parameters, such as fraction of interface units, length of interface segments, number of different particles in contact with a given chain, number of different chains in contact with a given particle, and fraction of free chains, can be predicted on the basis of simple considerations. However, other parameters, such as average length of the bridge and loop segments, and the segment number per chain, depend on the exact composition of the systems in a much less predictable way.

Theoretical studies have also been done on polymer nanocomposites reinforced with disk-like nanoparticles, e.g., clay platelets. The objective is to seek the best synthetic strategies for such polymer nanocomposites. Thus, it is essential to obtain an atomic scale description of intercalated clays with species, like surfactants, monomers or polymers. Also, the structural changes of intercalated species induced from the nanoconfinement should be examined. As an initial effort, Breu et al. [95] used lattice energy minimization techniques to investigate the molecular arrangement of intercalated organometallic complexes in layered clay. By examining the different arrangements as shown in Fig. 21, they concluded that the structure of intercalated guest species is controlled by the complex interplay of long range and short range clay–guest and guest–guest interactions.

Manias and co-workers [87,96] used MC and MD simulations to explore the atomic scale structure of intercalated PEO–montmorillonite nanocomposites. The simulated atomic density profile shown in Fig. 22 indicates that intercalated PEO chains are arranged in a disordered, liquid-like bilayer parallel to the clay platelets, in contrast to the all-trans or helical extended interlayer structures traditionally suggested but in agreement with more recent small-angle neutron scattering experiments. These disordered PEO arrangements are attributed to the confinement-induced effects on the chain–chain packing and to the oxygen–Li coordination in the interlayer galleries. Moreover, in the dry nanocomposites, the cations (Li^+) reside primarily in the immediate vicinity of the silicate surface rather than being coordinated with PEO. In contrast, in the hydrated nanocomposites, more than half of the cations exist in the layers near the clay surfaces, partly inserted in the clay surface cavities. In

another study, Manias et al. [97] investigated the structure of polystyrene confined in 2 nm slit, representing the experimentally intercalated polystyrene nanocomposites, using MD simulations. Their simulations shown in Fig. 23 suggest that the confined polymer chains adopt a layered structure normal to the solid surfaces, with the polar phenyls dominating the organic material adsorbed on the walls, and the aliphatic groups predominately in the center of the slit. Interesting,

the MD simulations on poly (ethylene glycol)-clay nanocomposites by Boulet et al. [98] showed that Li^+ cations are able to diffuse into the tetrahedral cavities of the clay and the middle of the clay galleries, which agrees with the experimental observation [99] and the previous simulations [87].

Lazzaroni and co-workers [100,101] used MD method to reveal the structure of intercalated and exfoliated poly (ϵ -caprolactone) (PCL) in clay. In the case of exfoliated nanocomposites, the density profile indicates that PCL chains are arranged in a successive five-layer structure (Fig. 24). The maximum density of the first five peaks is higher than the density of amorphous PCL (i.e., 1.04 g cm^{-3}) and the first three peaks is higher than the density of crystalline PCL (i.e., 1.21 g cm^{-3}). Meanwhile, the highest density peak for the layer at the interface contributes to the strong affinity between the polymer and clay surface while the descending density peaks observed for the layers from the interface to bulk are believed to be due to the shielding effect of the inner layer to the outer layer. Moreover, the calculated order parameters indicate that PCL chains in the first three layers adopt a preferential parallel alignment with respect to the clay surface. In the case of intercalated nanocomposites, the PCL chains can form bridging structures across the galleries that hinder the exfoliation process while such bridging are not expected in situ

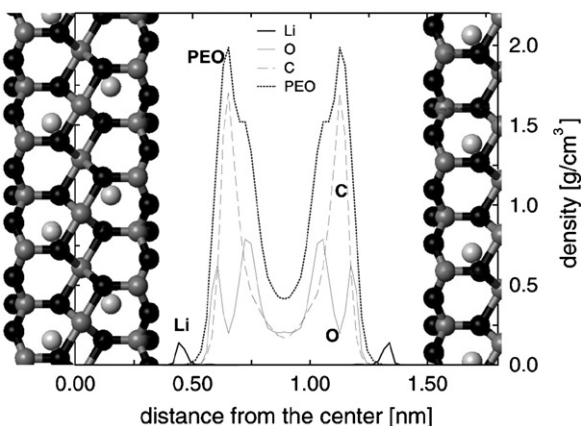


Fig. 22. One dimensional mass density profiles across the silicate gallery of Li-montmorillonite/PEO nanocomposite [96]. Reproduced from Kuppa, Menakanit, Krishnamoorti and Manias by permission of Wiley Periodicals Inc.

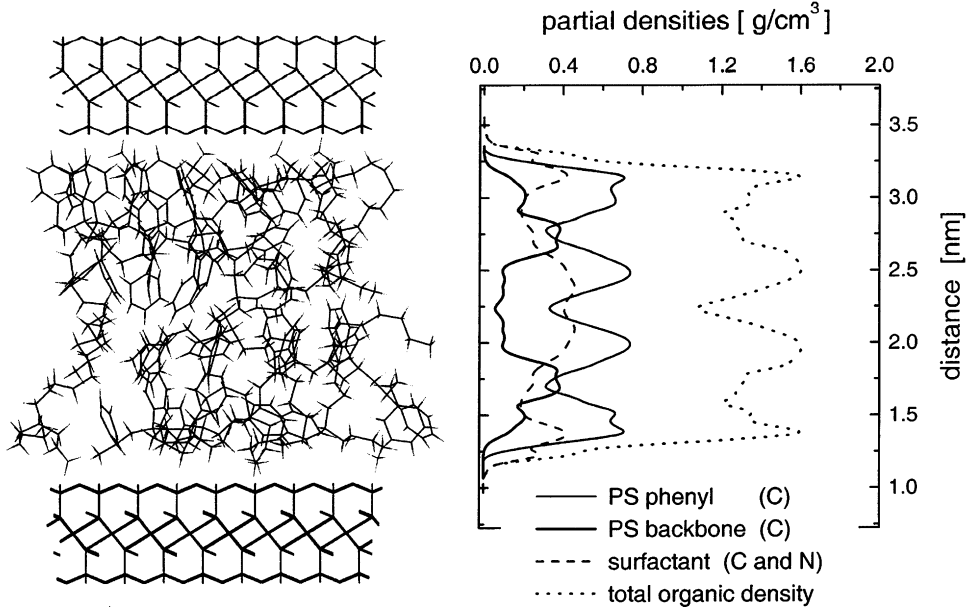


Fig. 23. Density profiles versus distance normal to the confining surfaces in PS intercalated nanocomposites [97]. Reproduced from Manias, Kuppa, Yang and Zax by permission of Elsevier Science Ltd.

polymerization of ϵ -caprolactone monomers. Katti and co-workers [102,103] recently modeled clay-based polymer nanocomposites by a combined MD simulation and experimental (FTIR and XRD)

approach. They investigated the organic modifier orientation and surface coverage, its interaction with nylon 6 chain and clay surface, chain conformation and atom density profiles by MD simulation.

By using MD method, Zeng and co-workers [14,104,105] investigated the molecular packing and chain orientation of intercalated quaternary alkyl ammoniums in organoclays in terms of atomic density distribution, chain tilt angle, order parameter and conformation. They observed various layered structure for the intercalated alkyl ammoniums, from monolayer, bilayer, pseudo-trilayer to pseudo-quadrilayer structure (Fig. 25). These layering structures are closely related to the alkyl chain length and cationic exchange capacity of clays, and the long alkyl chains, for example, octadecyltrimethyl ammoniums, do not lie flat within a single layer but interlace (Fig. 26). Moreover, the intercalated long alkyl chains demonstrate a predominant trans conformation although there is also extensive gauche conformation. In the case of polyurethane nanocomposites, both the hard and soft segments demonstrate layered structure in clay

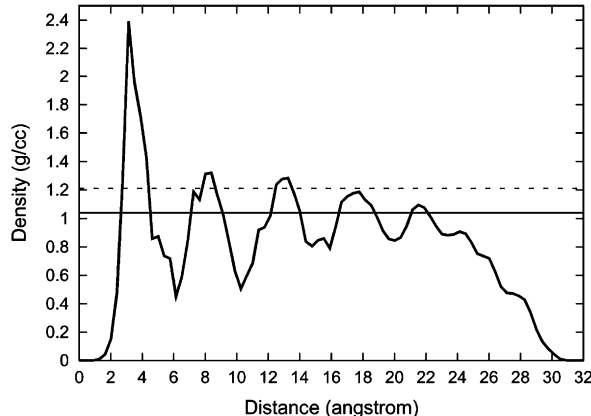


Fig. 24. Density profile in the direction normal to the clay layers for the exfoliated poly (ϵ -caprolactone) nanocomposite model (thick line). Amorphous and crystalline densities for the bulk PCL are also reported (thin and dashed lines, respectively) [101]. Reproduced from Gardebein, Bredas and Lazzaroni by permission of American Chemical Society.

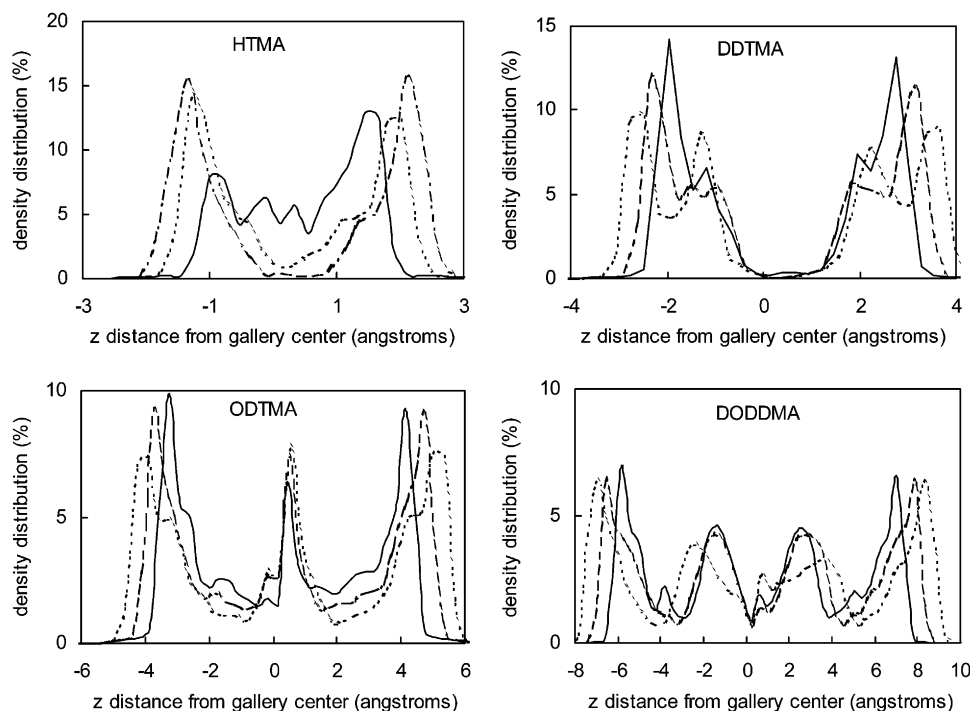


Fig. 25. Methylen group density distributions of organoclays with different alkyl chain lengths and CEC as a function of z distance from gallery center: solid curve, CEC 85 meq/100 g; dashed curve, CEC 102 meq/100 g; dotted curve, CEC 119 meq/100 g. Here the surfactants include hexyltrimethyl (HTMA), dodecyltrimethyl (DDTMA), octadecyltrimethyl (ODTMA) and dioctadecyldimethyl (DODDMA) [14]. Reproduced from Zeng, Yu, Lu and Standish by permission of American Chemical Society.

gallery [16,106]. More importantly, phase-separation, a common phenomenon in bulk polyurethane, has not been observed in such intercalated polyurethane. The absence of phase-separation is attributed to the nanoconfinement and the competitive interactions among clay surface, surfactant and polyurethane. Recently, Greenwell et al. [107] presented large-scale MD simulations for the systems of primary amine intercalated clays. They found that the interlayer spacing depends on the number of intercalated ammonium groups, which agrees well with the results of Paul et al. [105] on

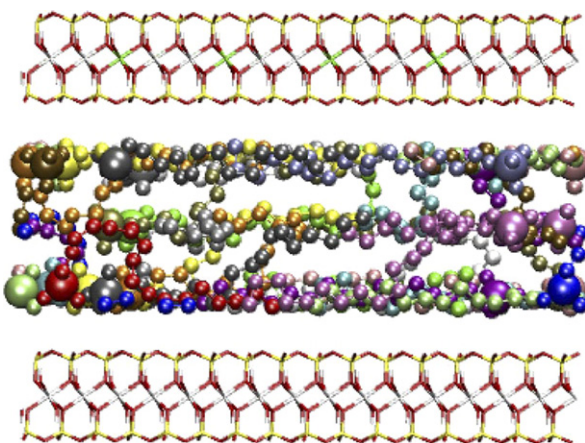


Fig. 26. Snapshot at 1000 ps of octadecyltrimethyl-clay. Clay platelets are represented by a stick model and each surfactant chain is represented by a ball model with a different color for better visualization and includes nitrogen (large ball), united carbon (small ball) of hydrocarbon chain, and oxygen (medium ball) [105]. Reproduced from Paul, Zeng, Yu and Lu by permission of Elsevier Science Ltd.

organoclays modified with quaternary alkyl ammoniums. Their results showed that amine functional groups do not interact strongly with clay platelets whereas ammonium groups do. In addition, they observed the long wavelength undulations (Fig. 27) in the clay platelets which they believed to be related to the exceptionally large supercell considered. The undulation phenomenon perhaps supports the notion of flexible other than rigid clay platelets [73,78]. Recently, Heinz et al. [108] investigated the structure and dynamics of alkylammonium-modified montmorillonite by means of MD simulation and experimental study. They examined the effects of monomorillonite cation exchangeable capacity, ammonium head groups and chain length.

In addition to the structural properties, it is also very important to investigate the MD of small molecules and polymer in the vicinity of nanoparticles or confined between two nanoparticles. Understanding the changes in the dynamics due to this extreme confinement would provide complementary information to those obtained from traditional surface force apparatus (SFA) measurements. Experimentally, Krishnamoorti et al. [109] found that mass transport of the polymer intercalated into the clay gallery is unhindered and exhibits mobility similar to that of the pure polymer. However, both the local and global dynamics of the polymer in the hybrids are dramatically different from those in the bulk. On a local scale, intercalated polymer chains exhibit higher flexibility along their backbone and a marked suppression or even absence of cooperative dynamics. On a global scale, the relaxation behavior of the polymer chains in the nanocomposites is

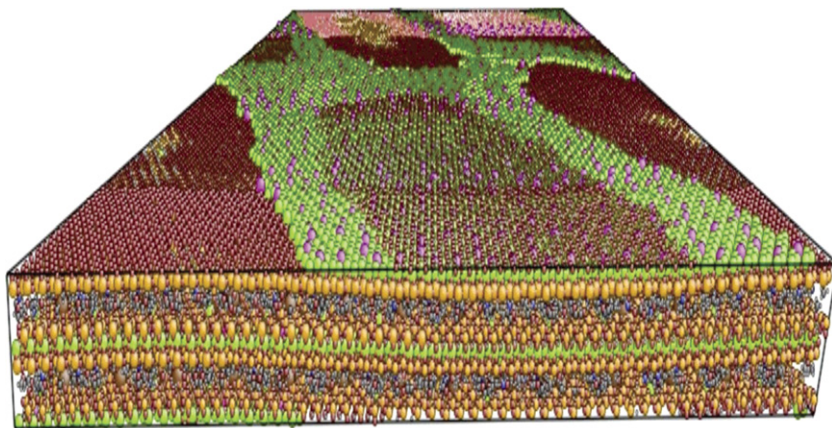


Fig. 27. Snapshot of the 350,840-atom supercell after 0.5 ns of MD simulation showing a perspective view of the rectilinear supercell, the clay sheets exhibiting gentle undulations. The color scheme is C gray, H white, O red, N blue, Si orange, Al green, Mg magenta and Na brown [107]. Reproduced from Greenwell, Harvey, Boulet, Bowden, Coveney and Whiting by permission of American Chemical Society.

dramatically altered when they are tethered to or are in close proximity to the silicate surface. Theoretically, by using MD simulations, Manias et al. [110] demonstrated a dramatic increase in the relaxation times of nanoconfined oligomers and a corresponding dramatic reduction of the mobility as compared to the simulated results of bulk oligomers [111].

More recently, non-equilibrium MD [112] has been used to probe the dynamics of nanoscopically confined fluid films with an emphasis on the inhomogeneities across the films. Manias et al. [97] revealed a coexistence of extremely faster and much slower segmental motions in intercalated polystyrene, different from the corresponding bulk polymer at the same temperature. The origins of these dynamical inhomogeneities are attributed to the confinement induced density inhomogeneities inside the 2 nm slits. Fast relaxing phenyl and backbone moieties are found in low density regions across the film, and preferentially in the center, whereas slow relaxing moieties are concentrated in denser regions in the immediate vicinity of the confining surfaces. Similar results have also been reported in MC and MD simulations of intercalated PEO/montmorillonite nanocomposites in which Hackett et al. [87] observed that ions near the silicate surface move much more slowly than those in the center of the gallery. In addition, the ion hydration environment was observed to change most rapidly in the center of the gallery, which is related to the mobility of the ions in this region.

The recent MD simulations by Zeng et al. [104] on quaternary alkyl modified clays showed that the nitrogen atoms are relatively immobile at the clay surface, whereas the mobility of methylene increases along the chain from the head groups (i.e., nitrogen-end) to the tail groups (Fig. 28). In another study, He et al. [113] found the mobility of the confined alkyl chain in organoclay decreases from monolayer to bilayer with the increase of the intercalated surfactant. In the case of nanosphere-polymer nanocomposites, Ozmusul and Picu [89] by using lattice MC simulations found that the bead mobility in the direction tangential to the particle surface is similar to that in the bulk whereas the bead mobility normal to the spherical filler is lower in the immediate neighborhood of the surface and, at larger distance, equivalent to that of the bulk value. In another study, Picu and Rakshit [114] investigated the dynamics of free chains in polymer nanocomposites filled with ungrafted and grafted nanoparticles by MD simulation. They found that

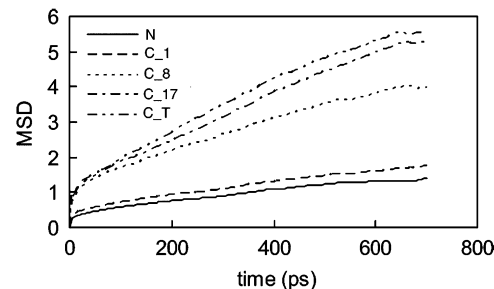


Fig. 28. Mean squared displacement of atoms along the chains as a function of time at 300 K [104]. Reproduced from Zeng, Yu, Lu and Standish by permission of American Chemical Society.

the dynamics of free polymer chains at a distance larger than twice of polymer gyration radius ($2R_g$) is indirectly modified by the presence of nanoparticles. Their mobility is slower than that of chains in the neat melt but significantly faster than that of chains directly contacting with the nanoparticle surface. Moreover, they concluded that the reduced dynamics of free chains in the ungrafted systems is due to the energetic polymer-nanoparticle interaction while that in the grafted systems is due to the interaction between free polymer and grafted polymer. On the other hand, Desai et al. [115] investigated the effect of spherical nanoparticles on chain diffusion by using coarse-grained based MD simulation. For single nanoparticle embedded in polymer matrix, they found that the chain diffusion coefficient near the nanoparticle surface is enhanced by about 20% for repulsive polymer-particle interactions while there is a reduction of about 40% for strongly polymer-particle interactions. They also examined the effect of particle concentration on the overall chain diffusion coefficient (Fig. 29). In the case of repulsive particles, the diffusion coefficient initially increases with particle concentration up to a maximum and then decreases with further increase in particle concentration. In contrast, in the case of strongly attractive particles, the overall chain diffusion coefficient decreases linearly with the increase of particle concentration, which is similar to the results from dynamic MC simulation reported by Huang et al [116]. More interestingly, the particle self-diffusion coefficient is found to depend on the particle mass, which disagrees with the Stokes equation where particle diffusion coefficient is mass-independent. The reason is probably due to the equivalent mass between particles and polymer chains and hence the comparable diffusion coefficients.

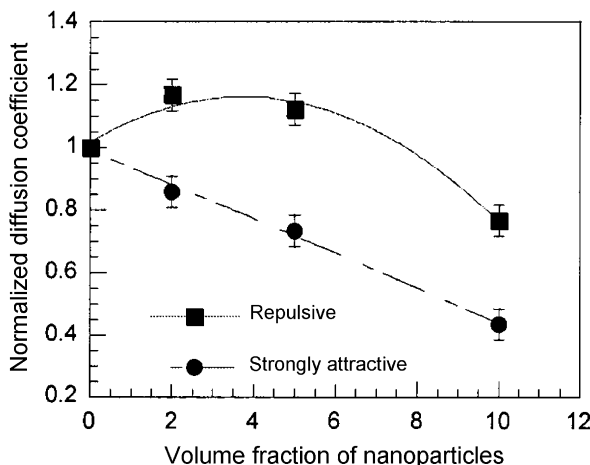


Fig. 29. The normalized overall diffusion coefficient as a function of volume fraction of nanoparticles for the repulsive and the strongly attractive system [115]. Reproduced from Desai, Kebinski and Kumar by permission of American Institute of Physics.

3.4. Nanocomposite morphology

The material properties of polymer nanocomposites are highly related to their overall morphologies. For example, in clay-based polymer nanocomposites, the optimal performance (e.g., strength, heat resistance, barrier properties) is generally obtained from exfoliated structure other than intercalated structure. The morphology of polymer nanocomposites depends on not only the nature of the components (i.e., polymer, nanofiller and surfactant) and the interactions among the components but also the volume fraction of nanofiller and processing conditions. It is very important to understand the effects of various factors on the macroscopic morphology of the materials, such as the size and shape of nanofiller, the clustering of nanofiller, polymer architecture (e.g., homopolymer vs. copolymer), hydrodynamic interaction (e.g., shear field), and eventually establish the correlations between the morphology of the resulting composites and their properties, for instance, mechanical properties [117–121], gas permeability [122–125] and electrical conductivity [126].

Theoretically, the major challenge in developing models for the phase behavior of clay-based polymer mixtures is how to correctly treat the strong structural anisotropy of the clay platelets and properly characterize all possible mesophases of the mixture. Although polymer–colloid mixture has been the subject of numerous theoretical and computational studies [127–132], the colloidal particles were mostly

assumed to be spherical in shape in most of these investigations. The few studies on the mixtures containing anisotropic colloidal particles were focused on rod-like colloids rather than disk-like particles [133–135]. In order to describe the morphologies of clay–polymer mixtures, we should address at least two issues at different length scales. The first is to determine polymer-mediated interactions between the clay layers (i.e., nanoscale), which deals with the properties of polymers confined between the clay surfaces. The second is to calculate the phase diagram (i.e., macroscale) which concerns the thermodynamics of anisotropic particles in a polymer melt. The behavior of polymer melts in confined geometries (i.e., between two parallel plates) has been discussed at the molecular level in Section 3.1. Thus, this Section focuses on the morphologies of nanoparticle–polymer composites and their dependence on various factors.

3.4.1. Homopolymer nanocomposites

We have discussed in Section 3.1 the thermodynamic aspects of polymer–nanoparticle mixtures, and showed that the final structure of a given mixture can be predicted by means of the mean-field model, SCF theory or combined SCF–DFT method. For example, by using a mean-field model, it is possible to predict what kind of equilibrium structures (i.e., immiscible phase-separation, intercalated or exfoliated nanostructure) would be for a given polymer–clay mixture. By using an integrated DFT–SCF model, Ginzburg et al. [136] predicted a complete phase diagram of a polymer–rigid disk mixture which includes phases such as isotropic, nematic, smectic, crystal, columnar phase and house-of-cards plastic solid as shown in Fig. 30. Recently, Lyatskaya and Balazs [137] reported an Onsager-type DFT [138] to analyze the phase behavior of polymer–clay mixtures. They found that the final structure of polymer–disk mixtures can be controlled by tuning chain length and/or Flory–Huggins interaction strength, which provides useful guidelines for tailoring the polymer molecular weight and the volume fraction of the different components to fabricate desired structures. By extending the above Onsager-type theory, Ginzburg and Balazs [139] calculated the complete phase diagram (i.e., liquid, crystal, and liquid crystal) of a polymer–particle mixture. Such a phase diagram (Fig. 31) was shown to strongly depend on the shape anisotropy (i.e., aspect ratio) of the particles, the polymer chain length, and the strength of the

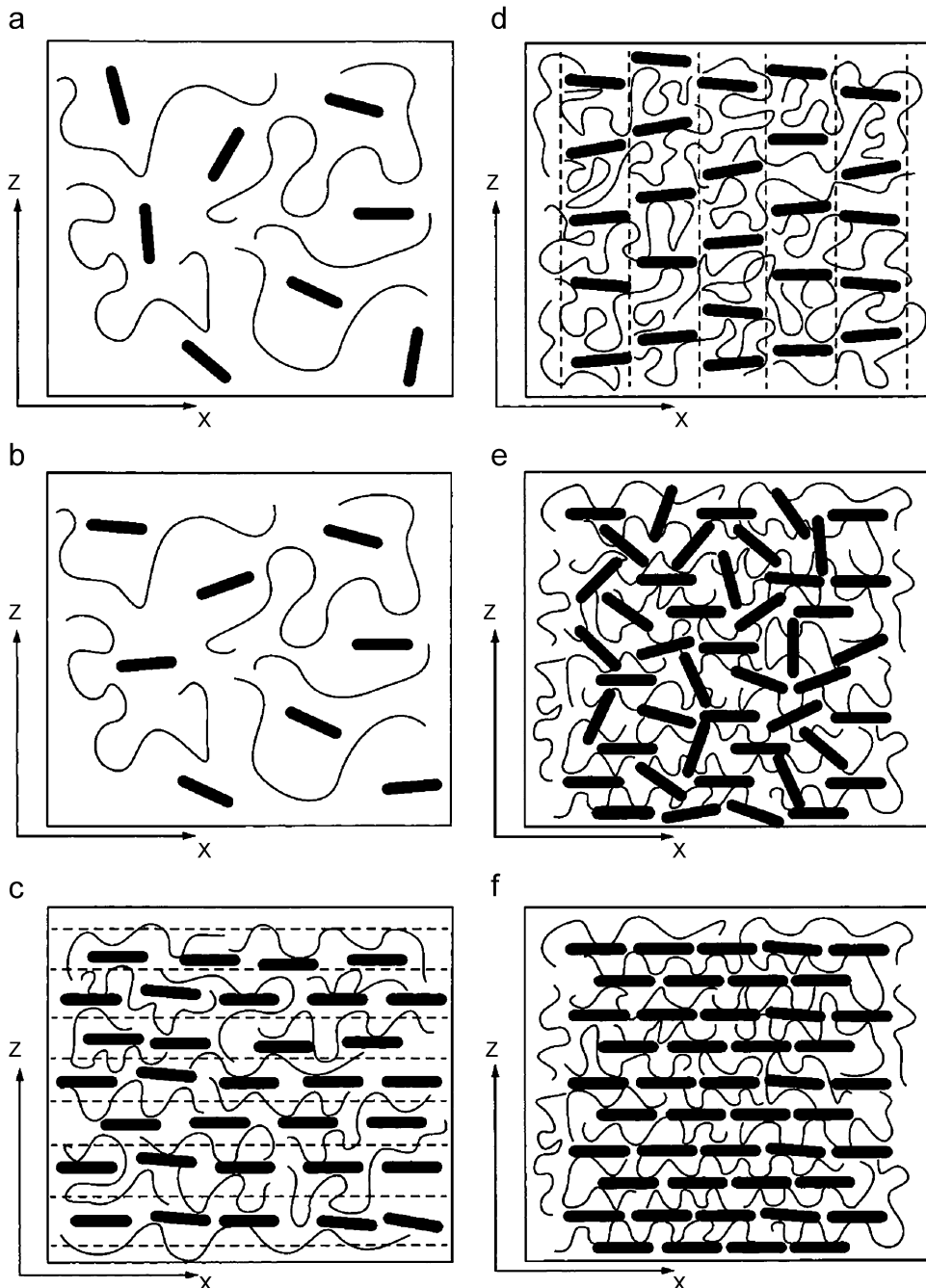


Fig. 30. Mesophases of oblate uniaxial particles dispersed in a polymer: (a) isotropic, (b) nematic, (c) smectic A, (d) columnar, (e) plastic solid and (f) crystal [136]. Reproduced from Ginzburg, Singh and Balazs by permission of American Chemical Society.

interparticle interaction. In particular, an increase in the shape anisotropy for oblate ellipsoidal particles leads to the broadening of the nematic phase at the expense of the isotropic region. The increase in the polymer chain length leads to the formation of the crystalline and/or liquid crystalline mesophases

and promotes segregation between polymer-rich regions and particles (Fig. 32). Finally, an increase in the strength of the interparticle potential leads to the complete elimination of the nematic phase and the coexistence between isotropic and crystal or columnar phases (Fig. 32). Thus, this method allows

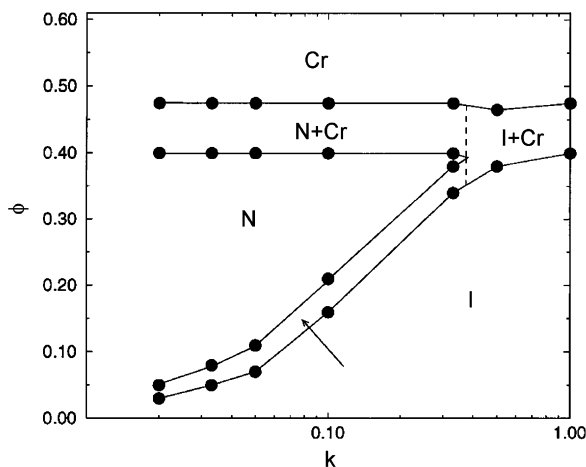


Fig. 31. Phase diagram of hard oblate ellipsoids dispersed in a polymer as a function of the shape anisotropy κ . Dashed line represents the three-phase coexistence. Phases: I, isotropic; N, nematic; Cr, crystal [139]. Reproduced from Ginzburg and Balazs by permission of American Chemical Society.

one to establish a correlation between the phase diagram and the architecture of grafted chains.

Ginzberg et al. [136] used the combined SCF–DFT method to calculate the phase behavior of clay-based polymer nanocomposites. Using the SCF model, the interaction information among clay layers (treated as infinite, planar surfaces), organic surfactants and polymer chains is obtained, which serves as an input to a DFT. Using the DFT, they calculated phase diagrams for finite-sized, rigid clay disks that are dispersed in an incompressible fluid and interact via excluded-volume and effective long-range potentials. Depending on the values of these critical parameters and the clay volume fraction, the system can form an isotropic or nematic phase (which corresponds to an exfoliated nanocomposite) as well as other phases, including smectic, crystal, columnar phase, house-of-cards plastic solid, phase-separating (i.e., immiscible) mixture. In a further study [140], they adopted this integrated multiscale approach to study mixtures of organo-clay, non-functionalized polymers, and end-functionalized polymers containing an end group (sticker). It was showed that the addition of the end-functionalized polymers promotes the formation of thermodynamically stable, exfoliated nanocomposites. Moreover, as the sticker–clay interaction increases, the system exhibited morphological changes from phase-separating (i.e., immiscible) to isotropic and nematic (i.e., exfoliated nanostructures), and finally plastic solid (at low clay volume

fraction) and columnar phase (at very high clay volume fraction).

Schweizer and co-workers [141–144] employed the polymer reference interaction site model (PRISM) integral equation theory, a method initially proposed for calculating the equilibrium properties of dense polymer solutions and melts, to investigate the equilibrium miscibility, particle dispersion and phase separation of polymer–particle mixtures and polymer nanocomposites. They examined the influence of particle size, polymerization degree of polymer and melt density on the structure, effective forces and thermodynamics of entropy-controlled athermal mixtures, and found that the ratio of particle diameter to monomer diameter is a key geometric variable. In addition, for hard sphere-filled polymer they believed that there are four kinds of polymer-mediated organization including contact aggregation, segment level tight particle bridging, and steric stabilization and tele-bridging. They predicted further two distinct phase separation behaviors. One occurs at lower monomer–filler attraction strength and corresponds to a very abrupt transition from an entropic depletion attraction-induced phase separated state to an enthalpically stabilized miscible fluid. The other occurs at a higher monomer–filler adsorption energy and involves the formation of an equilibrium physical network phase with local bridging of fillers by polymers. Zhao et al. [145–147] have also used the PRISM integral equation theory to study the structure and effective interaction of polymer nanocomposites. In particular, they investigated the mixtures of star polymer (i.e., branched polymers) and nanoparticles, and the influences of various parameters (e.g., nanoparticle–monomer attraction strength, particle volume fraction, arm length, and nanoparticle–monomer size ratio). They found that the star architecture can suppress the organization states of direct contact and bridging structure for moderate nanoparticle–monomer attraction, and promote the bridging-type organization for larger nanoparticle–monomer attraction.

Other equations and algorithm have also been developed to investigate the effects of mobile other than immobile nanoparticles, imposed shear and hydrodynamics. Ginzburg et al. [32] developed a combined model which integrates a coarse-grained mesoscopic TDGL description of the mixture with a BD (i.e., Langevin equation) description for particles. This model was used to simulate the behavior of mobile particles in a phase-separating binary

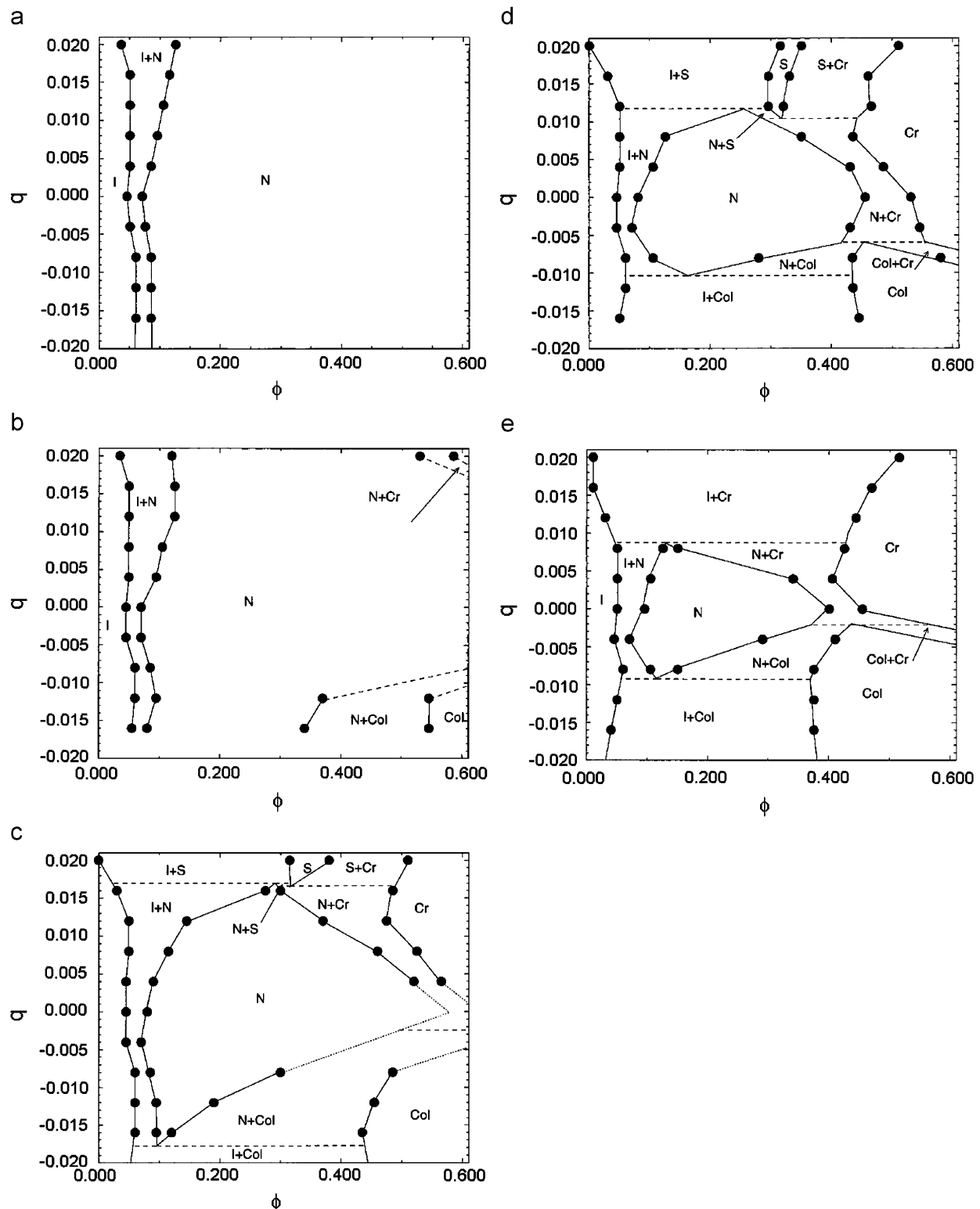


Fig. 32. Phase diagram of the mixture of ellipsoidal particles with an ideal polymer and its dependence on chain length (N). Phases: I, isotropic; N, nematic; S, smectic A (lamellar); Col, columnar; Cr, crystal. Chain length is 10 (a), 20 (b), 50 (c), 100 (d) and 1000 (e) [139]. Reproduced from Ginzburg and Balazs by permission of American Chemical Society.

fluid mixture where one fluid preferentially wets particle surface. Their results showed that the addition of hard particles significantly changes both the speed and the morphology of phase separation. At the later stage, particle addition significantly slows down the domain growth, which is in qualitative agreement with the experimental observation [148]. The original model was later extended to investigate the effect of shear on an immiscible binary mixture that contains mobile particles [33,70]. It was found that these particles can play a dominant role in shaping the structure of a system. The domain evolution is initially isotropic and obeys the Lifshitz–Slyozov law. Then, the domain grows faster in the shear direction than in the perpendicular direction, and ultimately stops growing in the perpendicular direction. If particle density is high enough, this anisotropic growth is destroyed by the randomly moving coated particles, and hence an isotropic morphology is observed even at large shear strain. For immobile particles, the domains always remain anisotropic under any shear rate. For mobile particles, their results suggested that increasing the particle loading to a critical value promotes greater intermixing between phase A and B. Overall, these models make it possible to probe the effects of various features, such as the wetting interactions between the particles and the fluids, long-range interparticle forces (i.e., van der Waals or electrostatic), particle size, particle shape and mixture composition. Moreover, they can be used to isolate the factors that control the growth of fluid domains, the dispersion of particles, and the structure of solid–liquid and liquid–liquid interfaces. By applying shear and other imposed flows, these models can also reveal how processing affects the morphology of the mixture and macroscopic properties of polymer composites.

In another work, Ginzburg et al. [71] developed a mean-field kinetic rate-equation model to characterize the effect of particles on the structure of fluid mixture which provides additional insight into the late stage behavior of the system. Balazs and co-workers [149,150] introduced the Navier–Stokes equation to incorporate hydrodynamic effects of the fluid. Suppa et al. [150] developed a LB algorithm to investigate the phase separation process of a binary fluid in the presence of immobile penetrable particles which are preferentially wetted by one of the fluid components. They found that at early stages the hydrodynamic flow promotes growth of the fluid domains and at later stages the

domains are pinned to a finite size if there is a sufficiently strong interaction between particles and compatible fluid. The pinning of the domains agrees with the experimental studies on phase-separation in thin films containing immobile particles that are preferentially wetted by one of the binary fluids [148,151]. Their results (Fig. 33) also showed that the final size of the domains can be tailored by varying the strength of the coupling interaction between particles and compatible fluid, which can be achieved by altering the coating on filler particles or by using chemically different species.

Paul and co-workers [152–154] recently examined the effects of polymer rheology and processing conditions on the formation of polymer nanocomposites via melt intercalation processing. They found that when organoclays and polymer are marginally compatible, the processing (i.e., extrusion) condition must be optimized with regard to both shear intensity and residence time to achieve high levels of clay platelet exfoliation [152]. Moreover, the use of high molecular weight nylon 6 leads to much better exfoliation owing to the high shear stresses in the extruder that result from its high melt viscosity [153,154]. By using MC simulations Dijkstra et al. [155] analyzed specifically the phase behavior of clay particles (i.e., modeled as infinitely thin disks with quadrupolar potentials), in the absence of solvent or polymer.

Recently, Maiti et al. [156] attempted to determine the equilibrium morphology of carbon

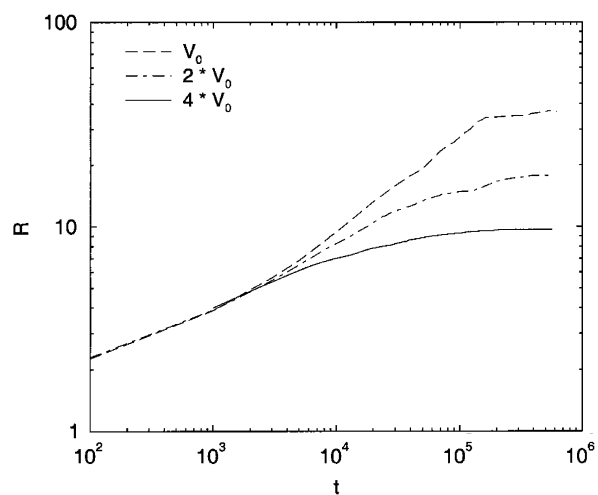


Fig. 33. Evolution of the characteristic domain size for three different values of the coupling constant [150]. Reproduced from Suppa, Kuksenok, Balazs and Yeomans by permission of American Institute of Physics.

nanotube (CNT) polymer composites through the mesoscale DPD method. Fig. 34 displays the results of (15,15) nanotube–polymethylmethacrylate (PMMA) systems. It shows that unfunctionalized nanotubes segregate and bundle together and thus is immiscible with PMMA matrix. When functionalized with 30% of acrylate groups, the nanotubes are dispersed well into the PMMA matrix.

3.4.2. Block copolymer nanocomposites

The mixtures of block copolymers and nanoparticles are another class of promising systems that have attracted numerous research activities. Such a mixture provides an efficient self-assembly route to create highly ordered nanostructured composites with dramatically improved properties. For example, the composite of a diblock polyelectrolyte and

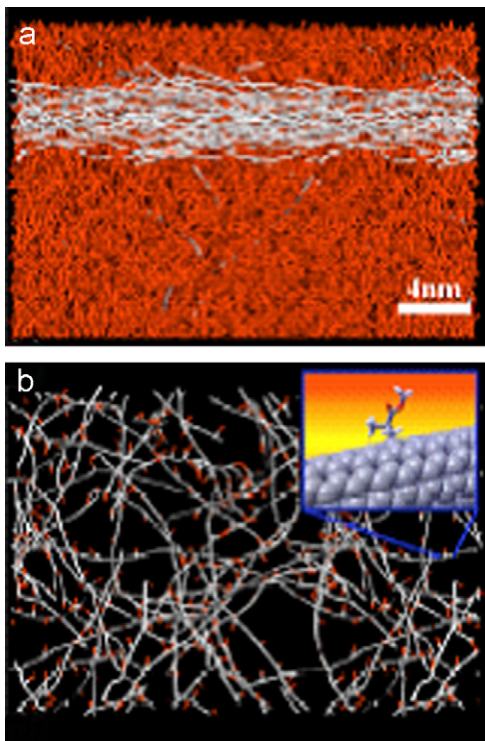


Fig. 34. Equilibrium morphologies of (15,15) CNT-PMMA composites at ambient temperature and pressure as modeled by DPD: (a) unfunctionalized (15,15) CNTs which quickly segregate and align, and (b) dispersion of (15,15) CNTs functionalized with 30% acrylate groups attached at regular intervals (shown in red). Inset in (b) is an atomistic representation of one of the acrylate groups attached to a CNT. CNTs are shown in white in both images. In (a) the PMMA chains are shown in red while in (b) they are hidden for clarity [156]. Reproduced from Maiti, Wescott and Kung by permission of Taylor & Francis Group Ltd.

carbon black nanoparticles exhibits improved electric conductivity and mechanical stability, making it an optimal material for solid-state rechargeable batteries [157]. As another example, a mixture of diblock copolymer with clay nanoparticles yields new polymer nanocomposites with increased mechanical strength and toughness [158]. In spite of some success in experimental studies of fabricating nanoparticle-based diblock composites [159–163], there have been few theoretical investigations into the factors that control the formation and behavior of these composites. Theoretically, it is a great challenge to predict properly the morphology of such systems because the theories must capture both the formation of mesophases of block copolymers and interactions among the various components. Besides, the morphologies and final properties of the resulting nanocomposites are closely related to a great number of variables, including the composition and architecture of block copolymers, the size and shape of nanoparticles, the volume fraction of nanoparticles, the mobility of nanoparticles and chemical modification of nanoparticle surface. Several numerical methods were recently used to study the morphology and properties of such systems, including free-energy expansion method (CHC model) [29], dynamic DFT [164], CDM [34,70], MC [165,166], MD [167], and the combined SCF-DFT method [35,168–172]. These approaches made it possible to study the effects of the above variables, the interplay between the diblock microphase separation and the self-assembly, and the clustering of nanoparticles.

We discuss here the theoretical work on the systems of block copolymers filled with monosized nanoparticles of different sizes, either immobile or mobile. Lee et al. [29] investigated the influence of immobile fillers on polymer-blend phase separation by using CHC model. Their simulation showed that the selective affinity of one of the polymers for the filler surface leads to the development of concentration waves about the fillers at an early stage of phase separation (Fig. 35). In the late stage, however, these phase separation patterns are changed by a growing background spinodal pattern characteristic of blends without fillers. Sevink et al. [164] simulated the microphase ordering in diblock copolymers filled with immobile particles using dynamic DFT [173–175] which was initially developed for investigating the dynamic formation of mesostructures. They showed that the lamellar structure in the vicinity of the fillers is modified by

the presence of fillers. In particular, the introduction of small fillers (i.e., rods) has a dramatic effect on the morphology of polymer melts whereas the mesostructures in the presence of large fillers (i.e., plates) are totally governed by the geometry of fillers. Furthermore, the filler in a diblock copolymer melt induces ordering in the system and speeds up mesophase separation enormously. Their

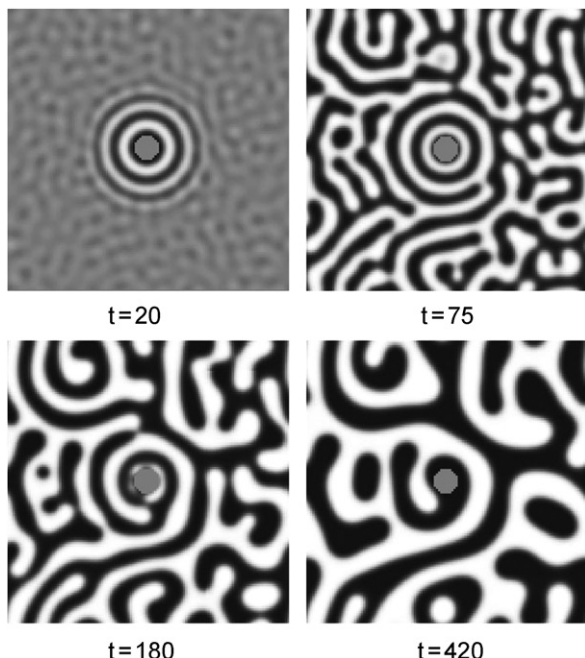


Fig. 35. CHC simulation of the influence of filler particles on polymer-blend phase separation in a critical composition blend [29]. Reproduced from Lee, Douglas and Glotzer by permission of American Physical Society.

calculated results are similar to those of particle-filled phase-separating polymer blends by Lee et al. [29].

These studies improved our understanding of the influence of individual filler on the phase separation in blends or copolymers. However, they did not take into account the dependence of the morphology of the composite on the volume fraction or mobility of fillers. To overcome this problem, Ginzburg et al. [34] developed a hybrid CDM which combines a coarse-grained description for the copolymer with the Langevin dynamics for particles. They investigated in detail the dependence of microphase separation of AB-diblock copolymers mixed with spherical nanoparticles on the variables like interaction strength, particle number density and particle mobility. They showed that mobile particles destroy bicontinuous structure observed typically for symmetric diblocks (Fig. 36). In particular, if the interactions between A-block and particle are weak, the A-blocks form the continuous phase and the B-blocks form isolated domains. In contrast, if the interactions are strong, the B phase is continuous and the A blocks self-assemble into distinct islands. Such results are in qualitative agreement with the recent experiments [161].

The above studies [34,164] provide some significant insights into the kinetic behavior of the mixtures of diblock copolymers and spherical nanoparticles. However, they have not addressed the structural stability of the phase behavior of such a system, which is complicated by the involvement of several length scales (i.e., monomer size, particle size, and the gyration radius of the polymer chain).

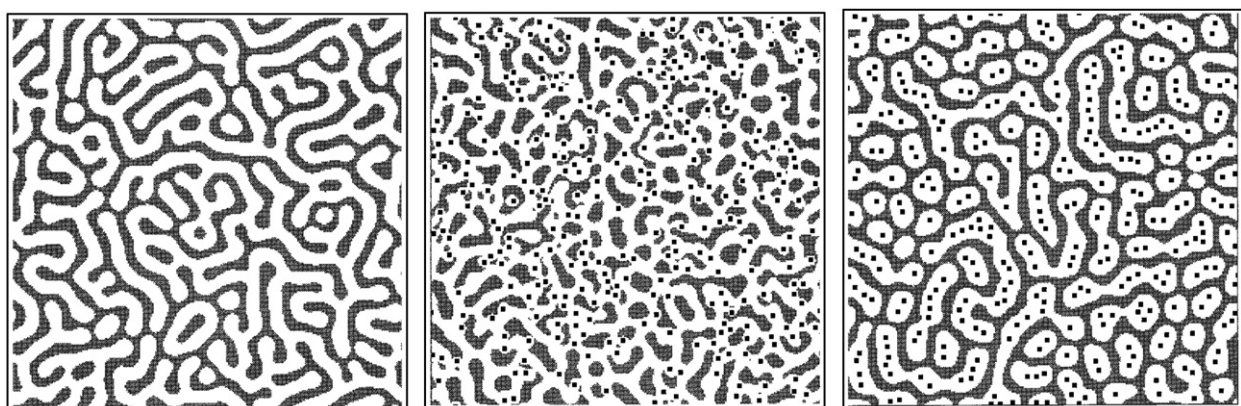


Fig. 36. Late-stage morphology ($t = 30,000$ time steps) of symmetric diblock copolymer containing: no particle (left), mobile particles of weak interactions with A-block (middle) and mobile particles of strong interactions with A-block [34]. Reproduced from Ginzburg, Qiu, Peng and Balazs by permission of American Chemical Society.

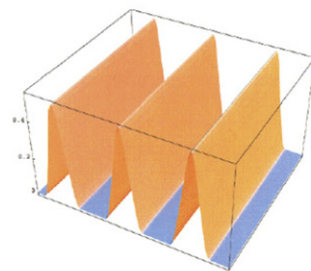
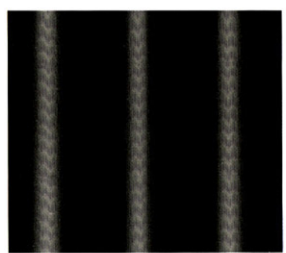
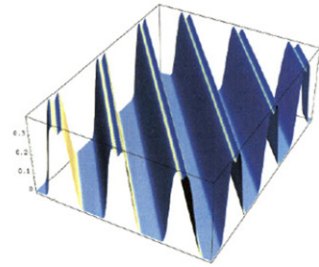
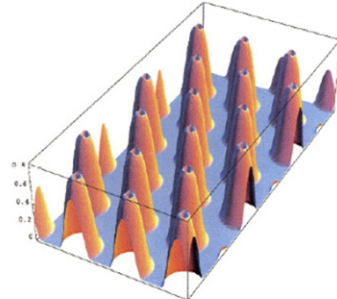
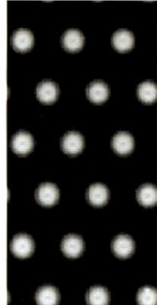
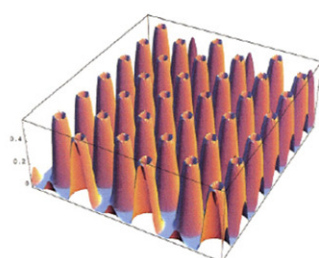
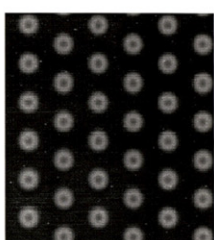
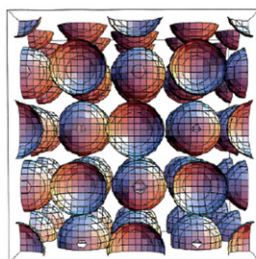
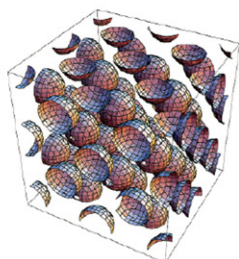
In typical experiments, nanoparticles are larger than monomer units yet smaller than the gyration radius of the chain [161,163,176]. Thus, in a further study, Huh et al. [165] studied the phase behavior of the mixtures by using MC simulations and a scaling theory. It was found that phase diagram strongly depends on particle size. When particle size is comparable to the gyration radius of the minority A-block and particles have a strong preferential attraction to this A-block, a new microphase ordering takes place in a narrow range of particle volume fractions and diblock compositions. The new ordered phases are made of three-layer micelles, with each micelle consisting of a particle-rich inner layer, an A-block central layer, and a B-block outer layer.

In order to calculate the morphology and thermodynamic behavior of copolymer–particle mixtures, Thompson et al. [177] employed a combined SCF–DFT approach which can examine the contributions of enthalpic and entropic energies in multiphase media to the observed morphologies and the role of copolymer architecture (e.g., tri-blocks, multiblocks, combs, stars), particle shape, and the mixture composition. They [168] used this approach to isolate a variety of one-, two-, and three-dimensional morphologies for particles. They showed that if particles are preferentially localized in the minority phase, particles can form not only nanosheets, nanowires and nanodots but also continuous nanoarrays in the hexagonally perforated lamellar or gyroid structures (Fig. 37). On the other hand, if particles are preferentially located in the majority phase of the system, different morphologies can be obtained in which particles segregate into a matrix instead of the hexagonally packed cylinders.

In another study, Lee et al. [171] investigated the effect of particle size and its interaction with diblock copolymer on the morphologies of various polymer–particle mixtures. They showed that the morphologies of these systems can be tailored by adding particles of specific sizes and chemistry. Such understanding of the interactions in copolymer–particle mixtures is helpful in facilitating the fabrication of nanostructured composites with desired morphologies and properties. In a more recently work, Buxton et al. [178] observed that the changes in the chemical natures (i.e., selective vs. non-selective) result in different spatial distribution of the nanoparticles and hence significantly different optical properties of the resultant nanocomposites.

Furthermore, Ginzburg et al. [35] extended their hybrid cell dynamic model [34] from two to three dimensions and studied the coupling between the microphase separation of the diblocks and the cluster formation for particles. They showed that the use of diblocks instead of homopolymers could decrease the effective percolation threshold by roughly a factor of two, which was qualitatively in agreement with the double percolation model proposed earlier for the behavior of carbon black particle in binary polymer blends [179–181]. Wescott et al. [182] used DPD simulation to seek better methods of controlling the assembly of percolating networks of CNTs in thin films of block copolymer melts. They found that under a suitable choice of polymers the CNTs can spontaneously self-assemble into topologically interesting patterns. Once such mesoscale morphology is projected onto a finite element grid, the electrical conductivity of the films can be calculated as shown in Fig. 38.

The SCF–DFT model has also been modified to examine the systems of bidisperse (i.e., binary particles) and microphase separating AB diblock copolymer [169,170]. In the first case, spherical particles are chemically identical but different in sizes, namely, large and small particles have the same preferential attraction to one of the blocks (i.e., A-block) of the copolymer. It was found that large and small particles are not homogeneously distributed, instead, large particles are concentrated in the preferred, compatible phase and small particles spread out in the interfacial regions and in the incompatible phase of the diblock copolymer [169]. The rich phase behavior of such nanostructured composites is attributed to a number of entropic effects, including entropic interactions between the A-blocks and larger particles, excluded volume effects between different particles, and the translational entropy of small particles gained from their delocalizing and migrating into the unfavorable B-phase. By integrating the SCF–DFT model with a scaling theory, Lee et al. [183] also calculated the phase diagrams for the mixtures as a function of the ratio of particles sizes. They found that other morphology can also be obtained by changing the volume fraction of the small or large particles. For example, a transition from a cylindrical structure to a lamellar film can be created by altering the volume fraction (Fig. 39). In the second case [170], spherical particles have the same size but different chemical nature, in particular, half of the particles favor A-rich regions and the other half favor B-rich

a**b****c****d****e**

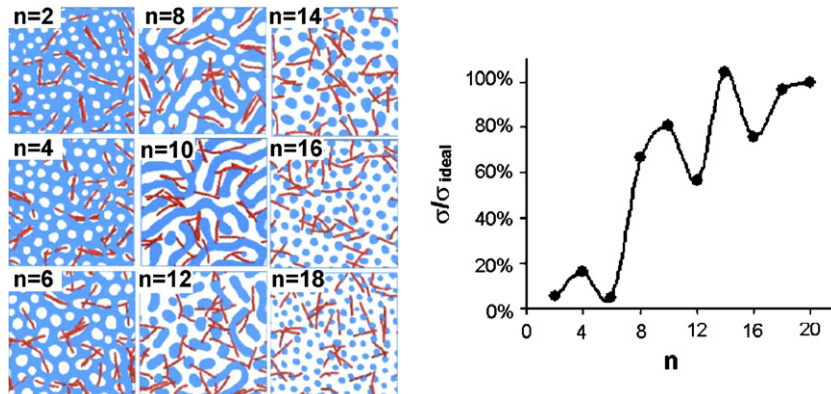


Fig. 38. Left pane shows representative configurations from the simulations for 0.75 vol% CNTs in $A_nB_{(20-n)}$ block copolymers. Polymer density fields are shown in white (A material) and blue (B material). CNTs beads are shown in red. The right curve plots the electrical conductivity of these structures averaged over the whole trajectory as a function of n [182]. Reproduced from Wescott, Kung and Maiti by permission of American Institute of Physics.

regions. In the presence of the AB diblocks, a spatially ordered nanocomposite was observed in which one species of particles forms a hexagonal matrix while the other particles form nanowires that weave through the first. Therefore, the introduction of physically or chemically distinct particles can be exploited to control the self-assembly and the equilibrium morphology of organic-inorganic composites. However, the first case shows an entropic separation of particles in the diblock copolymer whereas the second one shows an enthalpic separation. This integrated approach can provide guidelines for controlling structural formation in a variety of block copolymer–sphere mixtures and designing hybrid materials with the desired morphology for novel optoelectronic devices, separation membranes and catalysts. Liu and Zhong [184] used DPD simulation to investigate the self-assembly of binary nanoparticle mixture in lamellar diblock copolymers. They found that there is a cooperative assembly which is affected by various factors, including interactions between nanoparticle and block, interactions between the blocks, and nanoparticle size and shape. Various ordered microstructures can be formed by tailoring the

characteristics of the components, which provides useful information for the design of polymer nanocomposites with target properties.

The above models initially developed for spheres have been modified to describe the more complex mixtures consisting of anisotropic particles, such as rod-like particles, plate-like particles or the mixtures of particles of different shapes. Peng et al. [185] probed insight into the interactions in binary fluids with nanorods through a two-dimensional simulation which combined a coarse-grained description of the binary fluids with a discrete model for solid additives [32,33,70,71]. Their results showed that adding low-volume fractions of nanorods in a binary, phase-separating blend leads to the self-assembly of nanorods into needlelike, percolating networks. Such interconnected network arises through the dynamic interplay of phase-separation between the fluids, through preferential adsorption of the minority component onto the mobile rods, and through rod-rod repulsion. The cooperative effect can be exploited to drive the self-assembly of nanorods into supramolecular networks.

By using a combination of a CHC theory for binary mixtures and a BD for nanorods, Buxton

Fig. 37. Nanophase structures obtained from diblock-nanoparticle systems if particles are preferentially located in the minority phase. Density plots (left) and surface plots (right) are given for the particle distribution, where R is the radius of each spherical particle, R_0 the natural size of polymer, N number of segments in the chain, χ the interaction strength, ϕ_p the particle volume fraction and f the fraction of the diblock that is of the A chemical species. From top to bottom: (a) center-filled lamellar phase ($R = 0.3R_0$, $N = 1000$, $\chi = 20$, $\phi_p = 0.15$, and $f = 0.35$); (b) edge-filled lamellar phase ($R = 0.2R_0$, $N = 1000$, $\chi = 20$, $\phi_p = 0.15$, and $f = 0.35$); (c) center-filled cylindrical phase ($R = 0.3R_0$, $N = 1000$, $\chi = 20$, $\phi_p = 0.15$, and $f = 0.2$); (d) edge-filled cylindrical phase ($R = 0.2R_0$, $N = 1000$, $\chi = 20$, $\phi_p = 0.15$, and $f = 0.2$); and (e) spherical nanodot phase ($R = 0.2R_0$, $N = 1000$, $\chi = 20$, $\phi_p = 0.05$, and $f = 0.21$) [168]. Reproduced from Thompson, Ginzburg, Matsen and Balazs by permission of American Chemical Society.

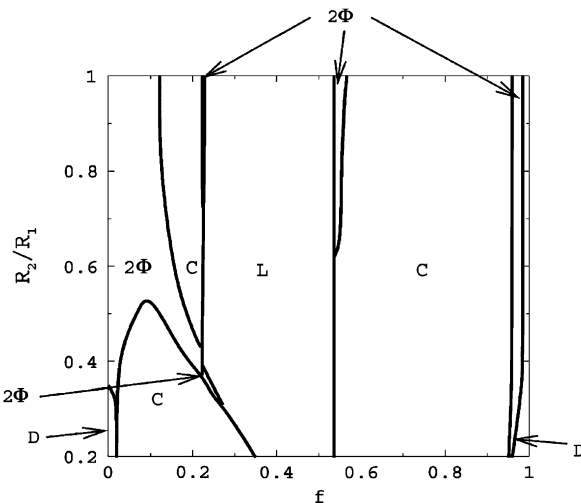


Fig. 39. Phase diagram for mixtures of bidisperse spheres and diblocks calculated using strong segregation theory. R_2/R_1 is the ratio of the smaller to larger particle radii and f is the fraction of A units in the diblock. Letters L and C designate lamellar and cylindrical morphologies, respectively. The regions marked D delineate the location of the disordered phases and the area labeled 2Φ marks the two-phase coexistence region. The total volume fraction of particles is fixed at 20%, of which 3% are the larger and 17% are the smaller spheres. Here, $N = 300$ and $\chi_{p1A} = \chi_{p2A} = 0$, and $\chi_{AB} = \chi_{p1B} = \chi_{p2B} = 1$ [183]. Reproduced from Lee, Thompson, Jasnow and Balazs by permission of the Royal Society of Chemistry.

and Balazs [186] investigated the self-assembly and macroscopic properties of nanocomposites composed of nanorods and a binary polymer blend. They found that the incorporation of nanorods into the minority phase of the phase-separating blend yields a bicontinuous morphology, where the nanorods form a percolating network within the continuous minority phase (Fig. 40). Recently, He et al. [187] determined the phase behavior of nanoparticle-filled binary blends by introducing a free-energy expression for these systems. They used independent parameters for the interaction between different species. Using this expression, they identified the conditions under which the mixture forms a stable, single-phase material. They also examined the effects of system variables, such as polymer composition, particle volume fraction and size, interaction energies on the phase diagrams. Shou et al. [120] investigated the effects of particle aspect ratio on the self-assembled morphology of mixtures of diblock copolymers and rod-like nanoparticles. They found that the distribution of particles within the polymers is dependent on not only the relative interaction energies between particles and different

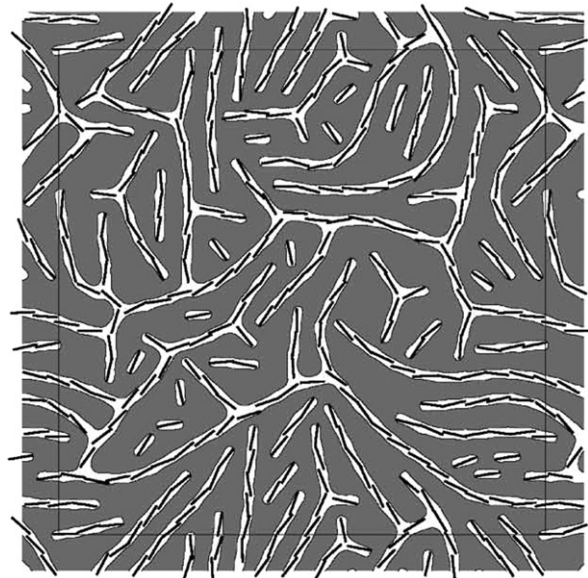


Fig. 40. Morphology of nanorod/polymer blend system for 6% volume fraction of nanorods. White regions are the minority phase A, gray regions are the majority phase B, a contour line separates them at $\psi(r) = 0$ and the rods are shown as black rectangles [186]. Reproduced from Buxton and Balazs by permission of Taylor & Francis Group Ltd.

blocks, but also on aspect ratio of the rod-like particles. Chervanyov and Balazs [188] investigated the effect of particle size and shape on the order-disorder phase transition (ODT) of a symmetric diblock copolymer melt. In the case of spherical particles, they found that a small volume fraction of particles leads to a significant suppression of the ODT and the magnitude of the ODT temperature shift is strictly dependent on particle size. For a constant volume fraction of particles, smaller particles produce a larger effect on the ODT. The effect of particle shape on the ODT was investigated by adding the spherocylindrical particles into the diblock copolymer matrix. It was found that the spherocylinders with a smaller aspect ratio produce more significant effect on the ODT (Fig. 41). The results are qualitatively in agreement with the experimental results [189].

Composite films with alternating layers of polymers and inorganic particles can make advantage of the unique optical, electrical, and magnetic properties of semiconductor or metal nanoparticles, and the flexibility and processibility of polymers [190, 191]. Previous studies indicated that the morphology of confined copolymer films can be controlled by tailoring the interactions between polymer and

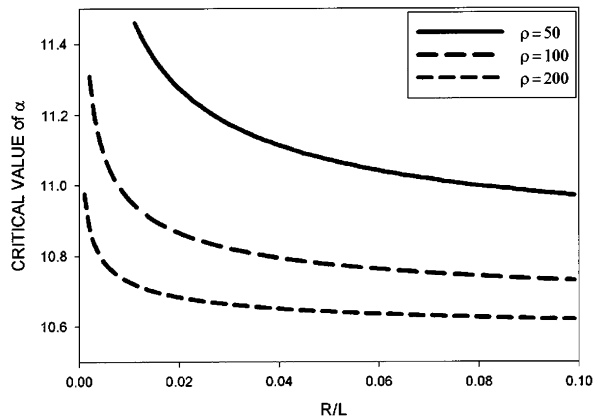


Fig. 41. Critical value of the segregation factor α_c plotted against the aspect ratio R/L for several values of the effective radius ρ of the spherocylindrical particle [188]. Reproduced from Chervayov and Balazs by permission of American Institute of Physics.

confining surface [192]. However, few studies have been done regarding the self-assembly and equilibrium structure of confined films consisting of particle-copolymer mixtures. Lee et al. [193] reported the first morphological study of mixtures of AB diblocks and nanoparticles that are confined between two hard walls by using a SCF-DFT model [168–171,183]. They showed that the complex interplay of entropic and enthalpic interactions drives the non-selective particles to localize at the hard walls and A/B interfaces, causing the mixture to spontaneously self-assemble into particle-decorated lamellae that are oriented perpendicular to solid wall surfaces. Meanwhile, a scaling theory is also developed to determine the effect of the particles on the behavior of the confined diblock copolymers [194]. It is reported that in such restricted geometries a polymer-induced depletion attraction (i.e., entropic effect) drives particles to the wall surfaces. If particles are chemically distinct from the walls, they will effectively modify the chemical nature of these walls. This change in chemistry, in turn, affects the polymer–wall interactions and consequently the structure of the film. Therefore, such confining walls can be exploited to promote the self-assembly of the system into particle nanowires that extend throughout the films and are separated by nanoscale stripes of polymer domains. This provides an alternative technique for modifying the chemical nature of coatings and films, and fabricating nanostructured materials by means of self-assembly.

In addition to the SCF-DFT method, Sides et al. [172] recently developed a new methodology (i.e.,

the so-called hybrid particle-field simulation) to investigate the equilibrium structure and properties of polymeric fluids with embedded particles. In their method, the polymeric fluids are also described by a field theory as in the SCF-DFT method. However, it is not restricted to the mean-field approximation implied by the SCF theory. Particles are described using a discrete particle-based simulation other than a DFT approximation, which makes it possible to trace individual particles during a simulation. This method has been successfully applied to a poly(styrene-*b*-2-vinylpyridine) diblock copolymer with embedded polystyrene-functionalized gold nanoparticles. It is believed that such a method can be applied to systems containing polymers and copolymers of arbitrary chemical architecture and particles with a variety of shapes, interactions and surface treatments.

3.5. Nanocomposite rheological and processing behaviors

It is very important to understand the rheological properties of polymer nanocomposites for material processing. Generally, the influence of microparticles on the viscoelastic properties (e.g., shear modulus and viscosity) of polymer composites can be quantified in terms of the volume fraction of particles. However, the influence of nanoparticles in polymer nanocomposites is complicated by the dramatical increase in interfacial area between nanoparticle and polymer matrix. In addition, the applications of these polymer nanocomposites depend to a large extent upon the viscoelastic properties that determine their processibility and mechanical integrity. However, our understanding of the viscoelastic properties of polymer nanocomposites and the influence of nanoparticle–polymer interactions on the viscoelastic properties of the polymer matrix is quite immature. In the case of clay-based polymer nanocomposites, the manufacturing processing can be optimized if the rheological properties of nanoconfined polymers are well understood. Computer simulation also plays a useful role in this area.

Some studies on nanoconfined homopolymers indicated that the shear stress increases linearly with shear rate up to a certain point and then the shear stress scales with shear rate to the power α whose value depends on the strength of homopolymer–surface interaction [195–203]. In one study, non-equilibrium MD simulation has been used to probe

the dynamics and the rheology of the nanoscopically confined fluid films, specifically the inhomogeneities across the films [112]. It was found that when these films are subjected to strong shear flows, slip appears at the confining surfaces, depending on the wall interactions. For strong wall affinities, the inhomogeneity in structure and dynamics of nano-confined films are observed, which is attributed to the interlayer slip between the surface adsorbed chain layer and the free chains. In another study, Boek et al. [204] demonstrated that the mesoscopic simulation DPD can be successfully applied to study the rheology of particle dispersed dense suspensions of spheres, rods, and disks. Recently, Huh and Balazs [60] used a coarse-grained MC simulation to investigate the rheological behavior of end functionalized chains (i.e., telechelic chains) confined between two surfaces. They showed that the shear response of the associated structure is significantly changed when there are more than one end-functional groups in the chains, which is qualitatively in agreement with the recent experimental studies on the shear response of telechelic polymers [205,206].

The response of intercalated and/or exfoliated nanocomposites to external flow is vital in terms of processing optimization. Krishnamoorti et al. [207] recently studied experimentally a series of intercalated nanocomposites in order to elucidate the role of highly anisotropic nanometer platelets in altering the materials flow properties (i.e., viscoelastic properties). It was found that both viscosity and elasticity of these intercalated nanocomposites are surprisingly independent of the clay loading and equivalent to those of unfilled polymers, respectively, which is attributed to the ability of highly-antisotropic clay platelets to be oriented in the flow direction. Theoretically, Havet and Isayev [208,209] simulated the rheological behavior of highly interactive filler–polymer mixtures using a double network, that is, the entangled polymer network and the surface adsorbed polymer network. The relative contribution of both networks is computed through the energy balance consistent with the thermodynamics of filler–polymer interactions and fluid mechanics. This approach makes it possible to predict the dependence dynamic properties on strain under oscillatory flow and the dependence of shear stress on shear rate under steady simple shear flow.

Smith et al. [12] utilized MD simulations to gain insight into the viscoelastic of model nanoparticle–

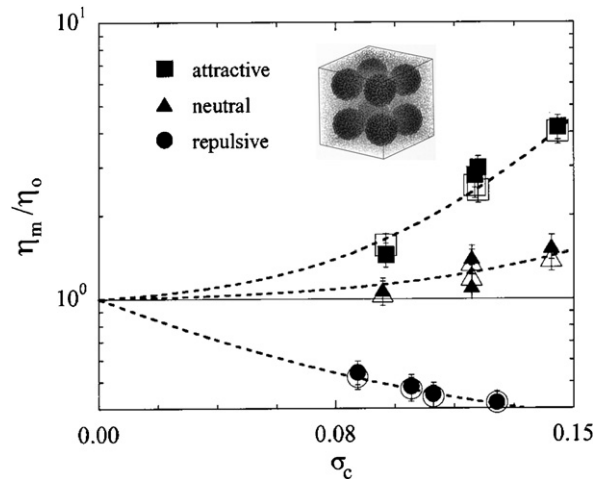


Fig. 42. Normalized polymer matrix viscosity as a function of specific interfacial area. Open and filled symbols are for $N_b = 10$ and 520 chains, respectively. The solid line is the expected behavior for conventional composites. Inset is a representative periodic nanoparticle–polymer nanocomposite [12]. Reproduced from Smith, Bedrov, Li and Bytner by permission of American Institute of Physics.

polymer composites (Fig. 42). In the simulation, the shear stress relaxation modulus $G(t)$ for each composite was calculated using the time autocorrelation function of the stress tensor and the viscosity η of each composite was calculated based on the Einstein relations:

$$G(t) = \frac{V}{k_B T} \langle P_{\alpha\beta}(t)P_{\alpha\beta}(0) \rangle, \quad (67)$$

$$\eta = \lim_{t \rightarrow \infty} \frac{V}{12k_B T t} \left\langle \sum_{\alpha} \sum_{\beta \neq \alpha} [A_{\alpha\beta}(t) - A_{\alpha\beta}(0)]^2 \right\rangle, \quad (68)$$

$$A_{\alpha\beta}(t) - A_{\alpha\beta}(0) = \int_0^t P_{\alpha\beta}(t') dt', \quad (69)$$

where $P_{\alpha\beta}(t)$ is an instantaneous value of the off-diagonal element ($\alpha\beta$) of the stress tensor at time t , V is the volume of the system, k_B the Boltzmann constant, T the temperature, and the brackets denote averaging over the whole trajectory and all six off-diagonal elements of the stress tensor. The dependence of dynamic shear modulus and viscosity of nanoparticle–polymer composites on the variables, such as nanoparticle volume fraction, specific nanoparticle–polymer interfacial area, and the nature of nanoparticle–polymer interaction, was determined. In contrast to many conventional composites, the viscoelastic properties of the polymer

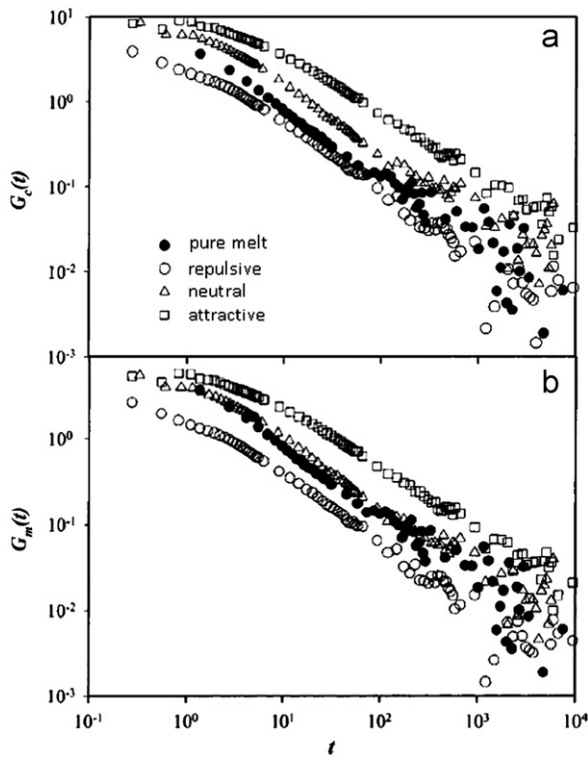


Fig. 43. The dynamic shear modulus for the systems of composites (a) and polymer matrix (b) with attractive, neutral, repulsive particles [12]. Reproduced from Smith, Bedrov, Li and Byutner by permission of American Institute of Physics.

matrix are strongly perturbed by the nanoparticles and depend upon the nature of the nanoparticle–polymer interactions. The viscosity (Fig. 42) and dynamic shear modulus (Fig. 43) can be dramatically increased for nanoparticle–polymer composites with attractive nanoparticle–polymer interactions relative to the pure melt, less dramatically increased with neutral nanoparticle–polymer interactions, and reduced with repulsive nanoparticle–polymer interactions. Thus, it provides an additional design parameter in the engineering of nanoparticle–polymer composites and the possibility to achieve desired properties at a much lower filler volume fraction than that necessary in conventional microparticle filled polymers.

In another MD study, Starr et al. [210] investigated the mechanisms of nanoparticle clustering and the dependence of the clustering on various parameters (e.g., particle loading, shear rate and temperature) in a simple model polymer nanocomposite (Fig. 44). They found that, as shown in Fig. 45, the shear viscosity for dispersed configurations is larger than that for clustered configurations,

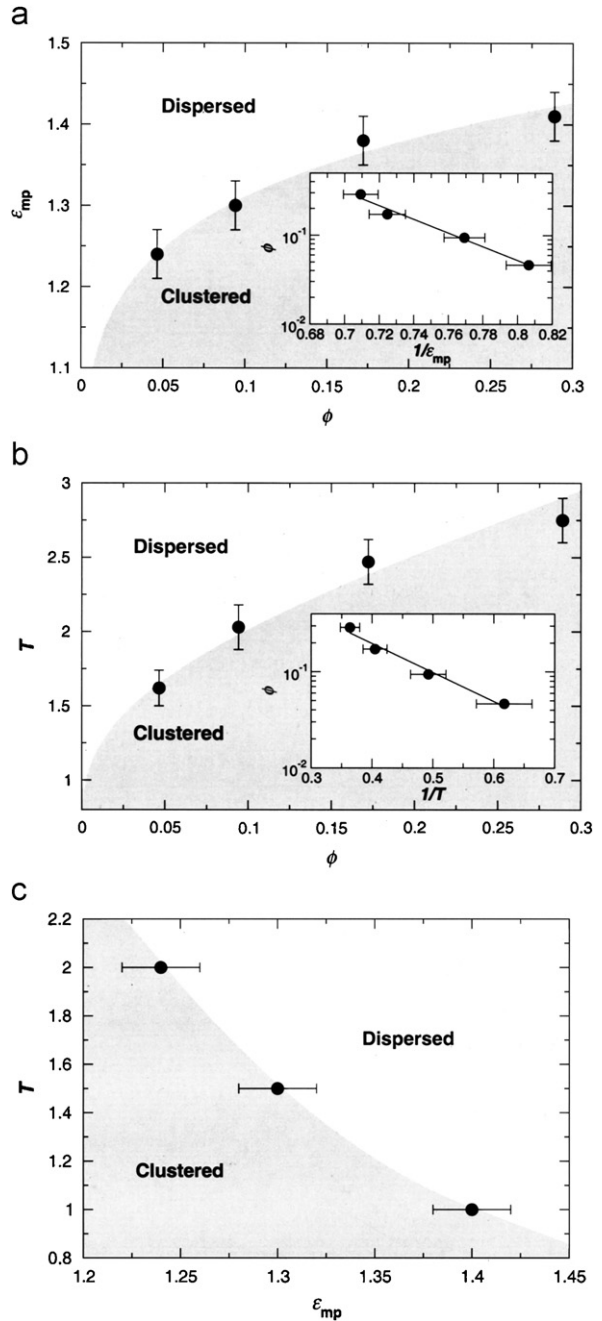


Fig. 44. The clustering diagrams of the nanoparticles as a function of: (a) polymer–nanoparticle interaction strength ϵ_{np} , and particle loading ϕ , (b) temperature T and particle loading, (c) temperature T and polymer–nanoparticle interaction strength ϵ_{np} [210]. Reproduced from Starr, Douglas and Glotzer by permission of American Institute of Physics.

in contrast to expectations based on macroscopic colloidal dispersions, which is attributed to the alteration of the polymer matrix properties in the

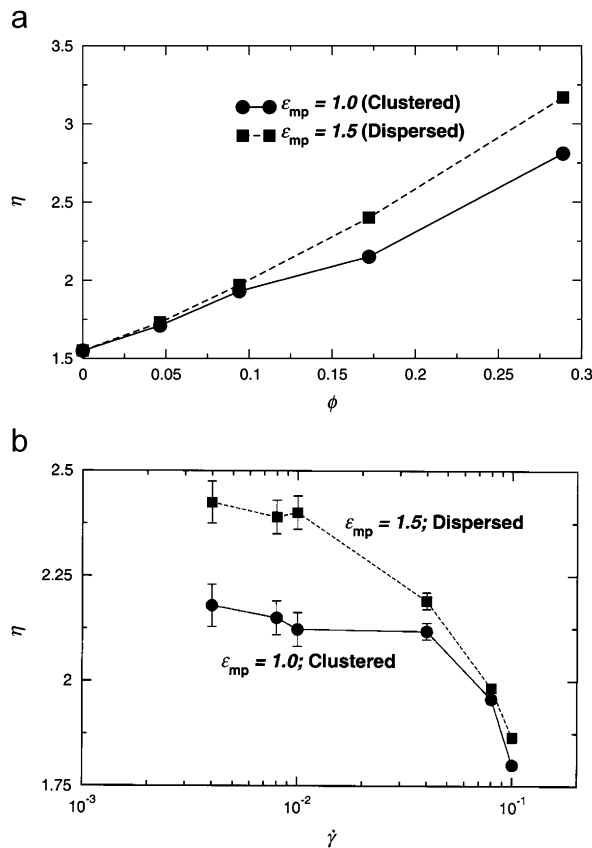


Fig. 45. Viscosity η as a function of (a) nanoparticle loading ϕ for a fixed shear rate $\dot{\gamma} = 0.01$, (b) shear rate $\dot{\gamma}$ for $\phi = 0.172$ [210]. Reproduced from Starr, Douglas and Glotzer by permission of American Institute of Physics.

vicinity of the nanoparticles. Meanwhile, the shear tends to disperse clustered nanoparticle configuration in this system, which is important for improving processing. Pryamitsyn and Ganesan [211] used coarse-grained computer simulation to study the mechanisms governing the steady-shear rheology of nanoparticle–polymer composites. They found that the shear rheology of the composites is similar to that of colloidal suspensions in a simple fluid. At dilute and semidilute particle concentrations, the composite shear rheology is dominated by the shear thinning of the polymer chains. At higher particle concentrations, the shear rheology is dominated by the particles stresses while polymer contribution becomes less important.

Other approaches have also been attempted. For example, using a theoretical network model, Sarvestani and Picu [212] investigated the viscoelastic behavior of polymer nanocomposites with a low filler volume fraction and strong polymer–filler

interactions. Their results demonstrated that to a large extent the overall material viscoelasticity can be controlled by the lifetime of filler–polymer junctions. Besides, the model exhibited the transition to rubber-like behavior at low frequencies and constant viscosity at low strain rates and shear thinning response in fast flows. However, this model has some limitations, including the pure additive of stress production and no stress transfer in the two networks, neglection of the hydrodynamic interactions and the conversion between different segments. In another study, Song and Youn [213] examined the effect of dispersion state of CNTs on rheological properties of nanocomposites by BD simulation based on a bi-mode finitely extensible nonlinear elastic (FENE) dumbbell model. Pyrz [214] proposed a new atomic strain concept which allows the calculation of continuum quantities directly within a discrete molecular system. The concept is based on the Voronoi tessellation of the molecular system and calculation of atomic site strains. The obtained stomatic strain tensor is applied to investigate interfacial stress distribution of nanotube–polymer nanocomposites. Wang et al. [215] studied the shear rheology and morphology of carbon nanofiber-polystyrene composites formed by melt-blended and solvent-cast processes. They developed a nanostructurally based model for carbon nanofiber–polystyrene composites which captured the dependence of nanofiber orientation on strain rate observed in their experiments. When applied to shear flows, the model predicted steady-state viscosities and normal stress differences of the composites as a function of shear rate, polymer matrix properties, fiber length and mass concentration.

3.6. Nanocomposite mechanical properties

Fillers added to polymer matrix can change the mechanical properties of the matrix in several ways. First, a filler itself can impart additional strength and toughness through its own mechanical properties. Second, a filler can inhibit failure by blocking the propagation of cracks. Third, the structural changes of polymer layer near the filler surface can alter mechanical properties. It is generally accepted that the mechanical property improvement is related to the filler properties (i.e., particle size, shape, aspect ratio), filler dispersion in the polymer matrix and the interaction between filler and polymer [216,217]. With particle size reduced from

micrometer to nanometer (e.g., silicates and clay platelets, nanotubes), a dramatic improvement in mechanical behavior of the polymer composites can be achieved. Clay platelets are thought to possess better reinforcement effects than those of spherical and rod-like particles [218]. For example, the complete exfoliation is considered much advantageous to the strength and stiffness of the composite [219] whereas the partial exfoliation results in the reduction of reinforcement efficiency [220,221]. Understanding the structural origins of the exceptional mechanical properties exhibited in polymer nanocomposites is of significance in the design and development of nanocomposites for engineering applications.

Mechanical properties of polymer nanocomposites can be calculated by using computer modeling and simulation methods at a wide range of length and time scales, for example, from molecular scale (e.g., MD), microscale (e.g., Halpin–Tsai) to macroscale (e.g., FEM), and their combination or the so-called multiscale methods. The use of MD simulations is inevitable for the analysis of such nanocomposites in order to study the local load transfers, interface properties, or failure modes at the nanoscale. Meanwhile, continuum models based on micromechanics are also shown to be useful in the global analysis for characterizing such nanocomposites at the microscale or macroscale. Here we discuss some significant progress in the fundamental understanding of the mechanical properties of polymer nanocomposites, in connection with a few recent reviews [222–224].

3.6.1. Molecular models

Molecular modeling is a powerful tool in the study of atomic structure and interactions at the nanometer length scale, and thus in the prediction of materials properties like elastic response, vibrational frequencies, heat of reaction, electric permittivity and binding energies. Among various molecular modeling methods, MD is one of the widely used techniques for the simulation of nanomaterials and nanosystems. For example, MD allows us to investigate the mechanical reinforcement and examine the effect of mechanical loading on specific regions of nanoparticle–polymer composites. Recent MD simulations [225] have predicted that the nanotube–polymer interface can be reinforced by covalently bonding between nanotube and polymer matrix. The shear strength of nanotube–polymer interface was found to be

increased by over an order of magnitude with the introduction of a relatively low density of chemical bonds between nanotube and polymer matrix. Meanwhile, the load transfer and hence modulus of nanotube–polymer composites can be effectively increased by deliberately adding chemical cross-linking. Gersappe [226] employed a MD simulation to probe the molecular mechanisms by which nanofillers reinforce polymer matrix. They found that the ability of the nanofiller to increase the toughness of the material results from the equivalence of time scales of motion for the polymer and the filler, since that filler is of the same size as the polymer chain. As seen from Fig. 46, the normalized work to failure (W^*), i.e., the work to failure of the nanocomposite after cavitation divided by the work to failure with no filler, increases with the increase in surface area of fillers (which results from using smaller size of filler particles, σ_f) and the increase in the attraction (ε_{fp}) between the filler and the polymer. This means the toughness is improved in nanocomposites.

Efforts have recently been made to assess the ability of stress transfer through the nanoparticle–polymer interface by using molecular modeling and simulation [225,227–229]. For example, Liao and Li [227] and Wong et al. [230] used MM to quantify CNT–polymer interfacial shear stress. The interfacial shear stress was found to be about one order

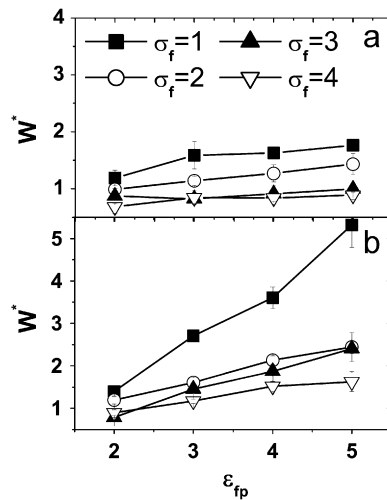


Fig. 46. The normalized work to failure W^* as a function of the size of the filler particle σ when the pulling velocity is $v = 0.03\sigma/v_T$. (a) The temperature is fixed at $T = 0.3e/kT$. (b) The temperature is fixed at $T = 1.1e/kT$. Similar trends are observed for the other pulling velocities [226]. Reproduced from Gersappe by permission of American Physical Society.

of magnitude higher than microfiber-reinforced composites. By using MM and MD, Qian et al. [231] studied the load transfer of a SWCNT bundle (i.e., closest-packed nanotubes) instead of individual and separated nanotubes. They found that the surface tension and the inter-tube corrugation contributed to load transfer in the parallel bundle and the twisting of nanotubes in the bundle could significantly enhance the load transfer. The deformation of the rope upon twisting is shown in Fig. 47.

Gou et al. [232,233] used MM and MD simulations to study the molecular interaction and load transfer in the presence of SWCNT and nanotube rope by pulling out a single nanotube from the rope or a nanotube/rope from the epoxy matrix as shown in Fig. 48. The interfacial shear strength between the nanotube and the epoxy resin was calculated to be up to 75 MPa, which indicates an effective stress transfer from the epoxy resin to the nanotube. It was also showed that the molecular interaction and

load transfer are dependent on not only the physical interactions between the nanotubes and epoxy matrix but also the internal interactions within the nanotube rope system. Moreover, the simulation results showed that individual nanotubes have stronger interactions with the epoxy resins and hence provide better load transfer than the nanotube rope. In another study, Frankland et al. [228] used MD simulations to explore the nanostructural effects of CNTs on the overall mechanical properties of polymer nanocomposites. Their simulations showed that when subjected to longitudinally loading, the long nanotube composites (Fig. 49a) have the most significant enhancement in the stiffness (i.e., stress-strain curve) relative to the polymer whereas the short nanotube composites (Fig. 49b) have no enhancement relative to the polymer. When subjected to transverse loading (Fig. 50), both the long and short nanotube composites exhibit similar behavior relative to that of the polymer, thus, there seems to be no

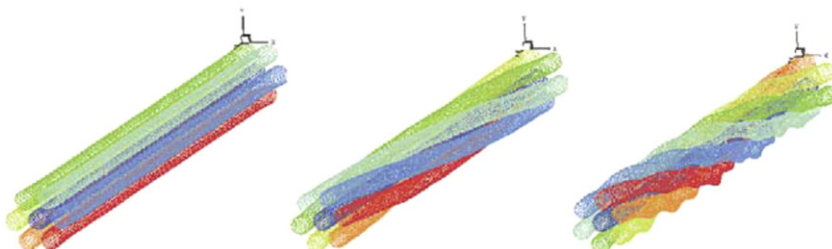


Fig. 47. Snapshots of the twist of the single-walled carbon nanotube [231]. Reproduced from Qian, Liu and Ruoff by permission of Elsevier Science Ltd.

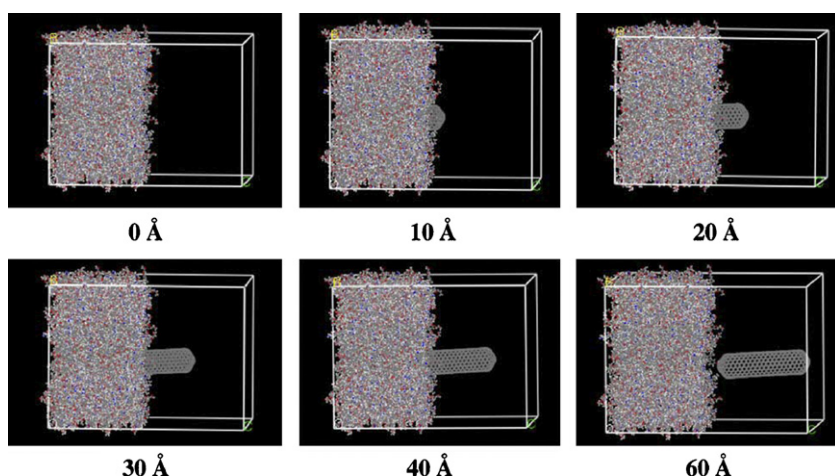


Fig. 48. Snapshots of the pullout simulations of a single tube from the composite [233]. Reproduced from Gou, Liang, Zhang and Wang by permission of Elsevier Science Ltd.

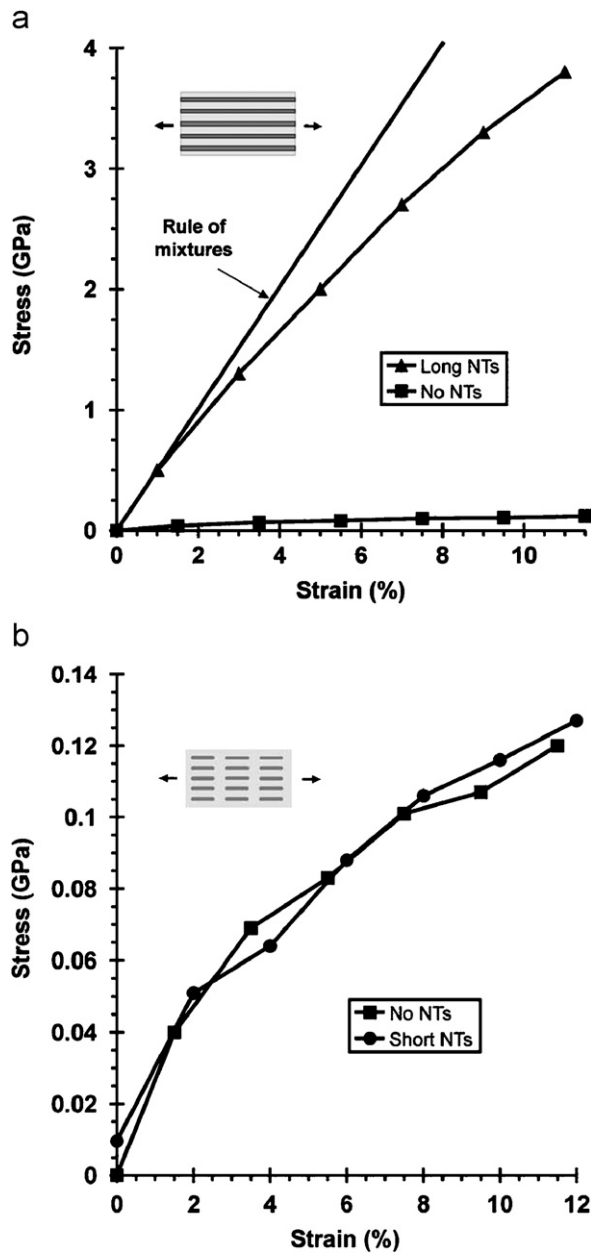


Fig. 49. Longitudinal stress-strain relations of long-nanotube (a) and short-nanotube (b) composites and the results from the rule of mixtures [228]. Reproduced from Frankland, Harik, Odegard, Brenner and Gates by permission of Elsevier Science Ltd.

appreciable load transfer from the polymer to the nanotube. However, a high anisotropic stress after loading is indicated in long nanotube composites since its stress after loading to the same strain level in the transverse direction is about 30 times lower than that in longitudinal direction. Similar results were reported by Zhu et al. [234] for Epon 862

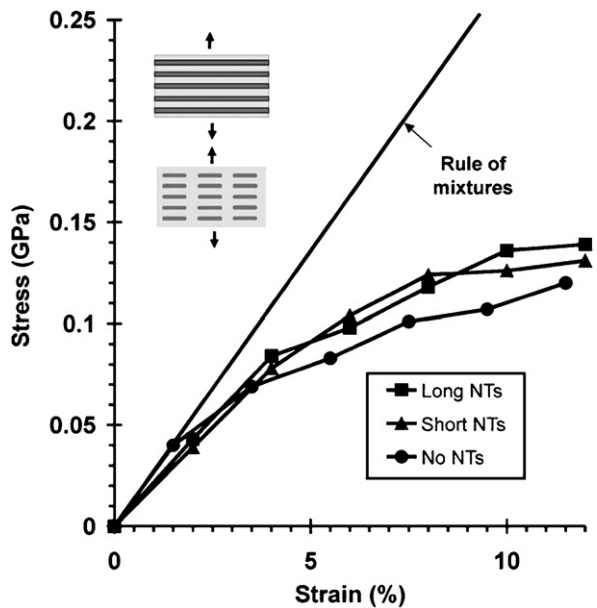


Fig. 50. Transverse stress-strain curves of both long- and short-nanotube composites compared with polymer matrix without nanotubes and the results from the transverse rule of mixtures for the long NT-filled composite [228]. Reproduced from Frankland, Harik, Odegard, Brenner and Gates by permission of Elsevier Science Ltd.

composites reinforced with long and short CNTs. They used the MD method to simulate the stress-strain curves of the composites from which the corresponding elastic Young's moduli were predicted. They found that a long CNT can greatly improve the Young's modulus of the Epon 862 composite, about 10 times stiffer than that of the Epon 862 matrix. However, a short CNT can only improve the Young's modulus by about 20% as compared to that of the Epon 862 matrix. Moreover, at a low strain level, the MD predicted that the modulus for long CNT-reinforced Epon 862 composites is consistent with the prediction based on the rule-of-mixture. However, in CNT-polyethylene composites, Mokashi et al. [235] reported different results of mechanical behaviors. By using MM simulations, they found that the length of CNT and the configuration of polyethylene play an important role in the tensile response and fracture of the nanocomposites. In particular, when reinforced with long through CNTs, crystalline polyethylene demonstrated moderate improvements in the tensile strength and elastic stiffness while amorphous polyethylene demonstrated significant increase in the overall tensile properties. On the other hand, when reinforced with embedded short CNTs,

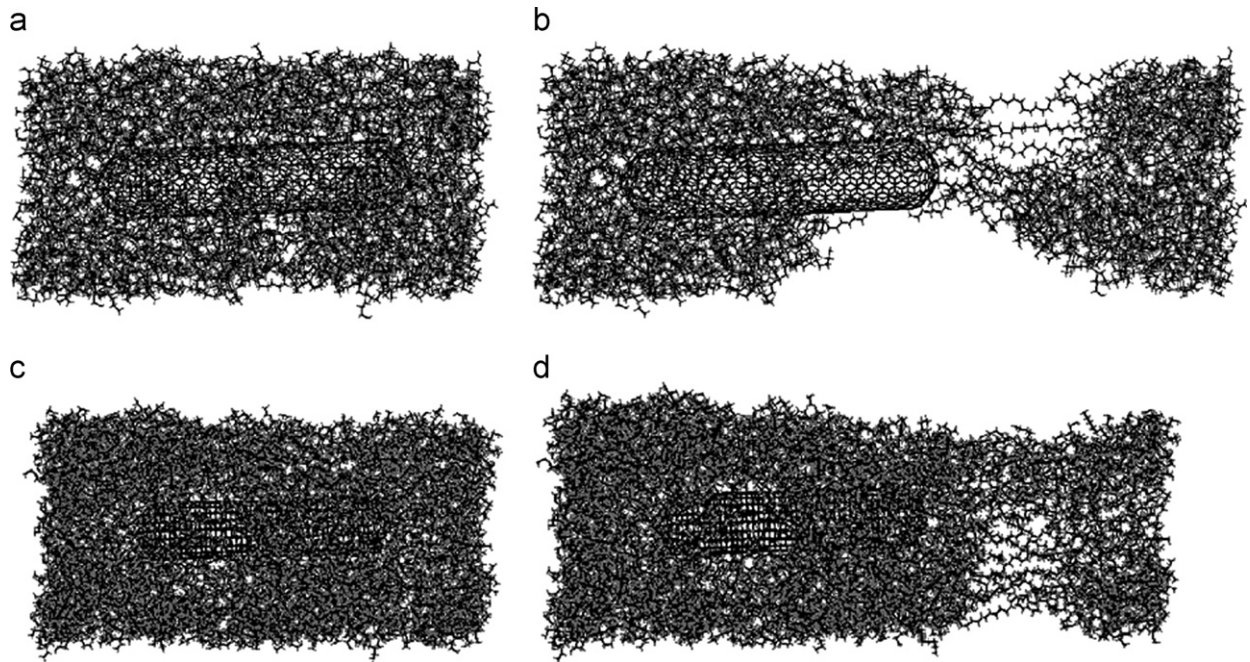


Fig. 51. Tensile loading of embedded short nanotube–amorphous PE composites: (a) equilibrium structure (6.25% volume fraction), (b) corresponding structure (a) at 45% strain, (c) equilibrium structure (3.59% volume fraction), (d) corresponding structure (c) at 26% strain [235]. Reproduced from Mokashi, Qian and Liu by permission of Elsevier Science Ltd.

amorphous polyethylene showed a significant decrease in Young's modulus and tensile strength, indicating from the poor load transfer from the matrix to nanotubes. Figs. 51 and 52 show the tensile loading and stress–strain curves of embedded short nanotube–amorphous polyethylenene composites at different volume fraction, respectively.

Recently, Lordi and Yao [229] have studied the interfacial adhesion mechanisms of nanotube composites by using MM to determine the binding energy and sliding frictional stress between CNTs and a range of polymer matrix (Fig. 53). The energy of the bound configuration was minimized during their calculation and the difference in energy ΔU , is twice the interface binding energy γ_i , scaled by the area of interaction A_i :

$$\gamma_i = \frac{\Delta U}{2A_i}. \quad (70)$$

Frictional stresses were calculated from the energy gradient of dragging the polymer along the nanotube surface in the direction of the tube axis:

$$\rho_{\max} = \frac{\max|\partial U/\partial s|}{A_i}, \quad (71)$$

where ρ_{\max} is the maximum stress along the tube axis, $\partial U/\partial s$ is the gradient of the potential energy

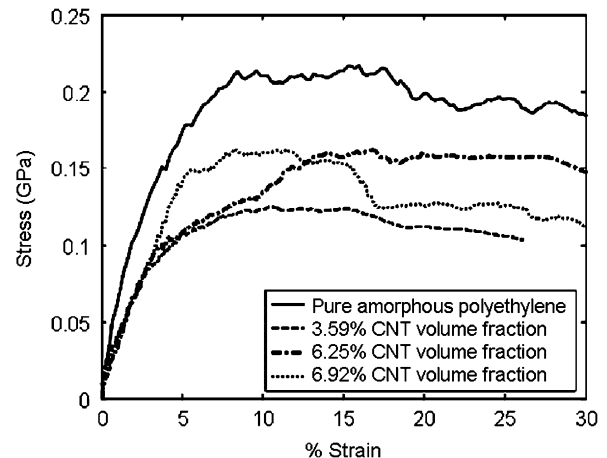


Fig. 52. Engineering stress versus strain plots for amorphous polyethylene and embedded short nanotube composites [235]. Reproduced from Mokashi, Qian and Liu by permission of Elsevier Science Ltd.

during the dragging. They found that the binding energies and frictional forces play only a minor role in determining the strength of the interface, but that helical polymer conformations are essential. Thus, it was believed that polymer conformation, due to molecular-level entanglement of the two phases and forced long-range ordering of the polymer, may

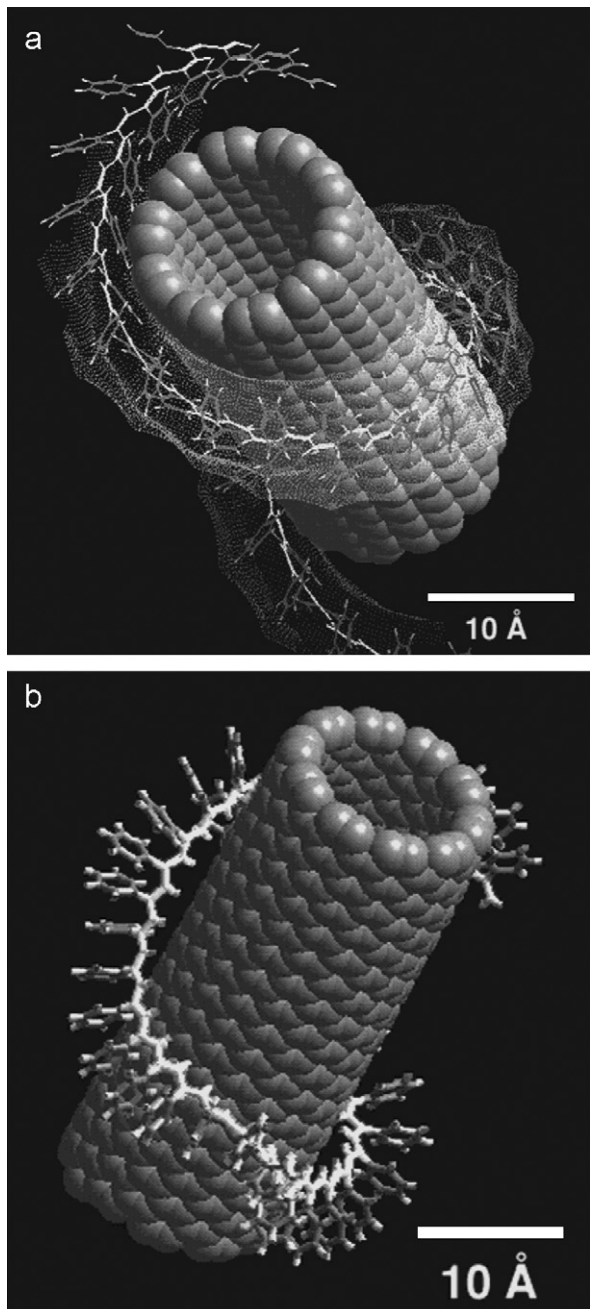


Fig. 53. (a) Cisoidal poly (phenylacetylene) (PPA) wraps perfectly around a (10,10) single-walled carbon nanotube, shown as a space-filling model with ball radius equal to the van der Waals radius. The dotted surface shows accessible surface area of the polymer to the nanotube. (b) Transoidal PPA, which has a slightly smaller helical diameter than the cisoidal version, distorts around the nanotube and wraps more tightly. Backbone atoms are shown in white [229]. Reproduced from Lordi and Yao by permission of Materials Research Society.

play a very important role in determining the interface strength between nanotube and polymer. By using MD simulation, Zheng et al. [236] investigated the molecular interactions between SWCNT and various polymers (i.e., polyethylene, polypropylene, polystyrene and polyaniline). They simulated two typical interactive process modes: polymer wrapping onto the surface of CNT, and polymer filling into CNT. They found that the interaction depends strongly on the specific monomer structure (e.g., aromatic rings) and the nanotube chirality and diameter. Fig. 54 shows the interaction energy during the wrapping and filling processes which initially increases for all the polymers. During wrapping process, polystyrene and polyaniline have a stronger interaction which can be attributed to the groups of aromatic rings. During the filling process, polyethylene, polypropylene and polystyrene shows stronger interaction and can fill into a (10,10) nanotube cavity due to the attractive van der Waals interactions. Prathab et al. [237] reported a MD study on molecular interactions between polymer and various metal oxides (i.e., Al₂O₃, Fe₂O₃, SiO₂ and TiO₂).

The MD simulations on ethylene–vinyl alcohol copolymer organoclay nanocomposites by Aleperstein et al. [238] revealed that the presence of octadecylamine upon the clay modification leads to the formation of hydrogen bonding between the amine hydrogen of octadecylamine and hydroxyl oxygen of the copolymer. Such bonding was believed to contribute to the improved storage modulus observed. However, for nanoparticle-reinforced polymer nanocomposites, the estimation of their elastic properties requires accurate knowledge of the elastic moduli of each component. To this end, Suter et al. [239] have attempted to determine the mechanical properties of individual clay platelet by large-scale MD simulations. Their simulations showed that there is a collective thermal motion of atoms consisting of clay platelet. This motion produces low-amplitude, long-wavelength undulations of the the clay platelets containing 1 055 000 atoms as shown in Fig. 55 by the height function $h(x, y, 1)$. The clay platelet remains a predominantly flat phase after 300 ps. However, the longest wavelength undulations are visible in the x direction after 500 ps while only smaller wavelength undulation is seen in the y direction even after 2 ns. From such thermal bending fluctuatin, they estimated the bending modulus of clay platelet to be 1.6×10^{-17} J, corresponding to an in-plane

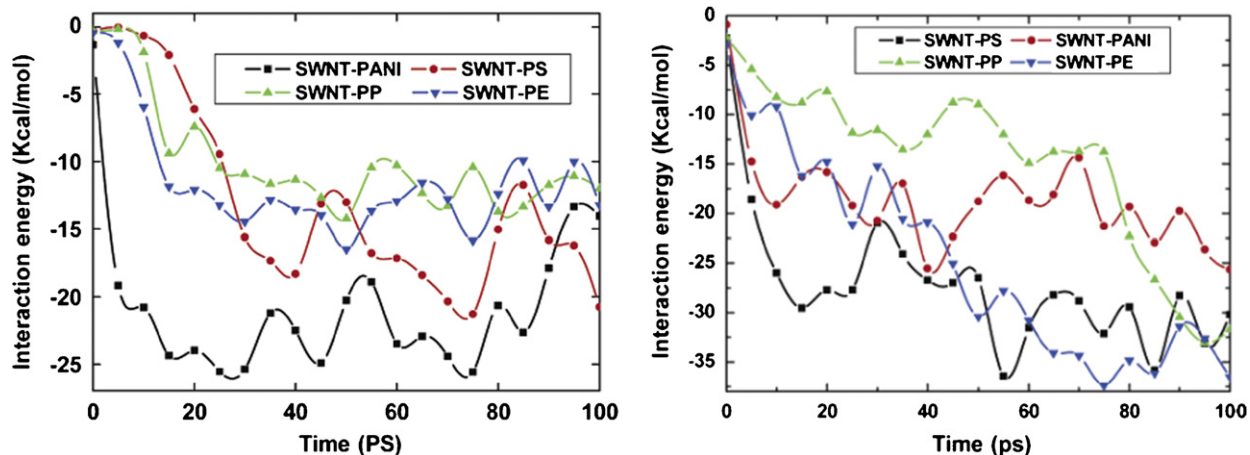


Fig. 54. Interaction energy evolution for single-walled carbon nanotube–polymer composites during 100 ps of wrapping (left) and filling (right) simulations [236]. Reproduced from Zheng et al. by permission of the American Chemical Society.

Young's modulus of 230 GPa. Capaldi et al. [240] used molecular simulation to determine the mechanical properties (i.e., elastic constant) of crystalline silsesquioxane. Their results showed that the moduli of crystalline octacyclopentyl polyhedral oligomeric silsesquioxane are anisotropic, with a Reuss-averaged bulk modulus of 7.5 GPa, an isotropic averaged Young's modulus of 11.78 GPa, and an isotropic averaged shear modulus of 4.75 GPa. These isotropic averages can be used in micromechanical models to calculate the effective elastic properties of polymer nanocomposites containing crystalline aggregates of silsesquioxane. A similar MD study has also been done by Patel et al. [241] who analyzed silsesquioxane packing around the polymer backbone and its effect on polymer motion, and predicted the elastic moduli by the static deformation method. On the other hand, Bizet et al. [242] studied the influence of introducing polyhedral oligomeric silsesquioxanes as pendant groups onto the poly (methyl methacrylate) backbone, on the intermolecular interaction and on the mobility at a molecular level. They found that the incorporation of these silsesquioxanes reduces the intensity of the intermolecular interactions between neighboring macromolecules. Moreover, the silsesquioxane has a very low mobility and hence can be regarded as anchoring points linked to the macromolecules.

The molecular origins of mechanical reinforcement of polymer nanocomposites have been studied by various modeling and simulation methods, which led to two different opinions: one attributes exclusively the reinforcement to nanoparticle aggregation

or clustering while the other attributes to the formation of the interphase (i.e., a transient polymer network) between nanoparticle and bulk polymer. For example, at high particle loadings Pryamitsyn and Ganesan [243] demonstrated that reinforcement occurs due to particle jamming. On the other hand, at low particle loadings, they found that polymer–particle reinforcing network is important in mechanical reinforcement. Similarly, Salaniwal et al. [244] reported that a strong polymer–particle interaction results in the formation of a solid like network, with an almost infinite relaxation time. Adnan et al. [245] investigated the elastic properties of amorphous polyethylene reinforced with different size of fullerene bucky-ball nanoparticles. They found that the elastic properties of nanocomposites are significantly enhanced with the reduction of particle size, which is attributed to the densification of polymer matrix near the nanoparticles and the particle–polymer interface attractive energy. To clarify these two reinforcement mechanisms, Sen et al. [246] conducted an extensive MD study on amorphous polymers filled with solid nanoparticles. They concluded that the mechanical reinforcement observed experimentally can result from either particle agglomeration or a polymer-based network. Their relative contribution depends strongly on the particle–polymer interaction energy and range, particle volume fraction and the state of particle dispersion.

By using MD, Chauve et al. [247] examined the reinforcing effects of cellulose whisker ethylene–vinyl acetate (EVA) copolymer nanocomposites. They evaluated the work of adhesion necessary to

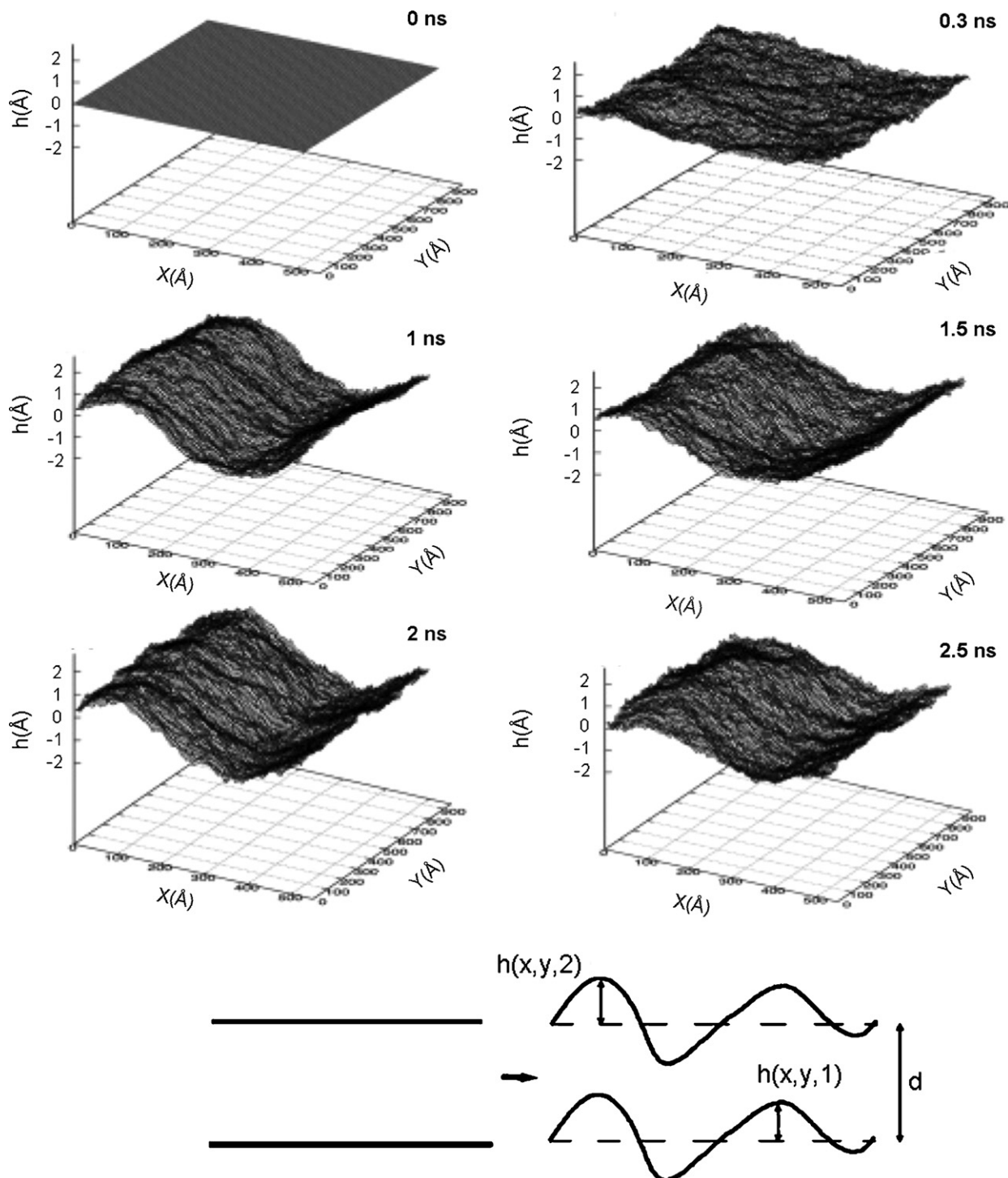


Fig. 55. Evolution of long-wavelength undulatory modes illustrated by the height function $h(x,y,1)$ for a single clay platelet, containing 1,055,000 atoms. The height function $h(x,y,n)$ defines the height of the clay platlet above a flat reference plane [239]. Reproduced from Suter, Coveney, Greenwell and Thyveetil by permission of American Chemical Society.

separate two interacting cellulose surface from the calculated interaction energy. More specifically, adhesion work is the difference between the energy of the total system with the interacting surfaces and those of the two separated polymers (i.e., cellulose and polymer). It was shown that a larger energy is needed to separate polar EVA copolymers from cellulose than that of the non-polar ethylene homopolymer. Meanwhile, the electrostatic interaction depends strongly on the polymer polarity and strong hydrogen bonding is observed between cellulose and polar EVA copolymers. Therefore, they concluded that strong filler–polymer affinity would lead to greater reinforcing effects. In another study, Minisini and Tsobnang [248] studied the graft effect on the interaction energy between functionalized polypropylene and an organomodified clay surface. It is shown in Fig. 56 that the interaction energy is more negative for the three functionalized polypropylenes than for pure polypropylene, which indicates an improved interaction between the polymer and the inorganic surface in the presence of functional groups (i.e., maleic anhydride). Nevertheless, the improvement for the system with PPMS (30 kcal/mol) is within the standard deviation of 36 kcal/mol. By using MD simulation, Song and Chen [249] investigated the fracture behavior of exfoliated clay–polymer nanocomposites. Their results showed that the interfacial interactions and the difference of relaxation time between clay and polymer chains have significant influences on the fracture strength of polymers. In particular, for polymers with glass transition temperature below (e.g., polyurethane) or near room temperature (e.g.,

nylon), the addition of clay nanoplatelets can significantly enhance the mechanical properties of these polymers. However, for polymers with glass transition temperature above room temperature (e.g., epoxy resins and polystyrene), the addition of nanoplatelets does not improve the toughness of the materials. If the nanoplates added are to toughen these polymers, it is necessary to reduce the difference of relaxation time between clay and polymer chains to create a stress relaxation interface through the surface modification of clay platelets.

Recently, Sen et al. [250] used MC simulations to investigate the elastomeric properties of polypropylene in the presence of spherical nanoparticles. They found that increasing the chain length or decreasing the temperature would lead to an increase in the end-to-end distance of polymer chains, and shrink the elastic region during deformation. Thus, the presence of the nanofillers, due to their effect on chain conformation, would affect significantly the elastomeric properties of nanocomposites. Kalfus and Jancar [251] used the reptation model and the percolation concept to interpret the modulus recovery times observed in poly(vinylacetate)-hydroxyapatite nanocomposite. The nanocomposite was considered as a two-component system consisting of bulk polymer matrix and effective particles, with the latter composed of adsorbed polymer shell and particle core. They found that the storage modulus recovery time was governed by the chain relaxation processes of polymer matrix adsorbed on the particle surface other than the particle network and its rearrangement. The retarded reptation motion in the interphase region was identified as the slowest relaxation process controlling the terminal recovery time.

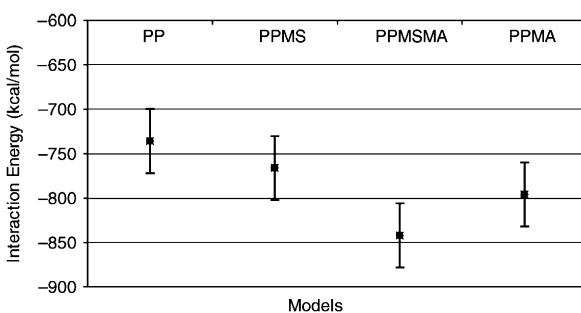


Fig. 56. Computed interaction energies between organoclay surface and polypropylene (PP) as a function of the functional groups. Here PPMS, PPMSMA and PPMA are polypropylenes grafted with functional groups of paramethylphenyl, paramethylphenyl maleic anhydride and maleic anhydride, respectively [248]. Reproduced from Minisini and Tsobnang by permission of Elsevier Science Ltd.

3.6.2. Continuum models

The mechanical properties of conventional particle–polymer composites have been successfully predicted by different continuum models. These models generally assume simplified geometries for each component and perfect load transfer between the components by, e.g., neglecting interfacial phenomena. They provide a rapid assessment of the key factors (e.g., particle volume fraction, particle geometry and orientation, and the property ratios of particle and matrix) in controlling the reinforcement and mechanical properties. Recently, some of these models (e.g., Halpin–Tsai, Mori–Tanaka, lattice spring model and FEM) have been applied to estimate the thermal-mechanical

properties [252,253], Young's modulus [254], and reinforcement efficiency [252] of polymer nanocomposites and the dependence of materials modulus on the individual factor of fillers (e.g., aspect ratio, shape, orientation, clustering), and the modulus ratio of filler to polymer matrix. For instance, Paul and co-workers investigated the nylon 6 filled with layered clays and glass fibers by using the composite theories of Chow [252], and Halpin-Tsai and Mori-Tanaka [43]. Based on the calculation, they attributed the superior reinforcement in exfoliated nylon 6 nanocomposites to the high modulus and high aspect ratio of clay platelets and their ability to reinforce in two directions. Moreover, they found there is a dramatic decrease in reinforcing efficiency when increasing the number of platelets per stack and the gallery spacing between platelets, which is attributed to the reduction in both the aspect ratio and effective modulus of clay clusters (i.e., the stack of a number of clay platelets). Considering the large distribution of filler shape, size and aspect ratio, it is thus very important to determine quantitatively the morphology and the structure-mechanical properties of polymer nanocomposites. Furthermore, the superior reinforcement (Fig. 57) and improved heat distortion temperatures of clay-based nylon 6 nanocomposites are found to result primarily from the combination of high modulus and high aspect ratio of clay platelets, rather than the changes in polymer matrix induced by the clay platelets [252]. This conclusion may be arguable as the polymer-filler interphase is often considered as a critical factor in the property enhancement in polymer nanocomposites.

Luo and Daniel [255] have developed a three-phase model (i.e., epoxy matrix, exfoliated clay platelet and clay cluster) to account for partial exfoliation and intercalation of clay. The Mori-Tanaka method was applied to calculate the modulus of the nanocomposite as a function of various parameters. With appropriate parameters obtained from experiments, the predicted results as shown in Fig. 58 are in good agreement with experimental measurements. It was also found (Fig. 59) that: (i) a higher degree of filler dispersion produces a higher composite modulus; (ii) the exfoliation ratio is the most effective parameter in enhancing composite stiffness; (ii) the aspect ratio of clay platelet has a distinct effect on stiffness enhancement; (iv) a large intercalation basal spacing is preferred but its effect on composite modulus is marginal unless it is accompanied by a high cluster aspect ratio.

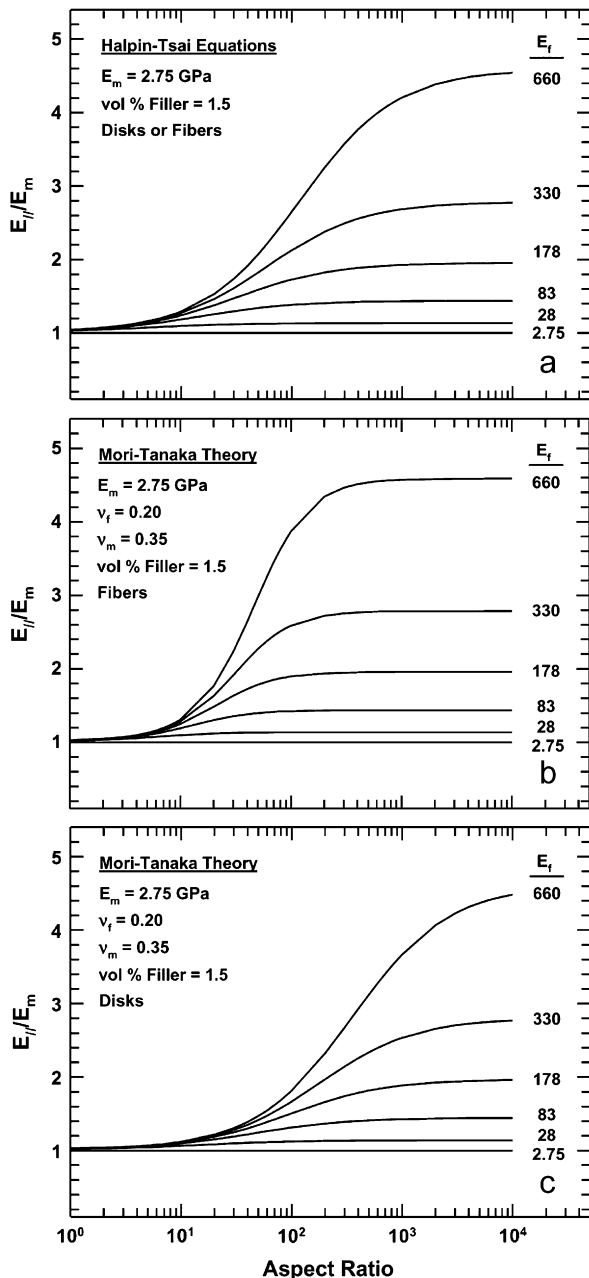


Fig. 57. The effect of filler aspect ratio and modulus on the longitudinal reinforcement of composites based on fiber and disk-like fillers as determined by (a) Halpin-Tsai equations (fiber or disks) and Mori-Tanaka theory for (b) fiber and (c) disk reinforcement [43]. Reproduced from Fornes and Paul by permission of Elsevier Science Ltd.

Jo et al. [256] developed a constitutive model to study the effect of intercalated and agglomerated nanoclays on elastic modulus of poly(methylmethacrylate) nanocomposite foams. The predicted stress-strain curves were in agreement with their experimental

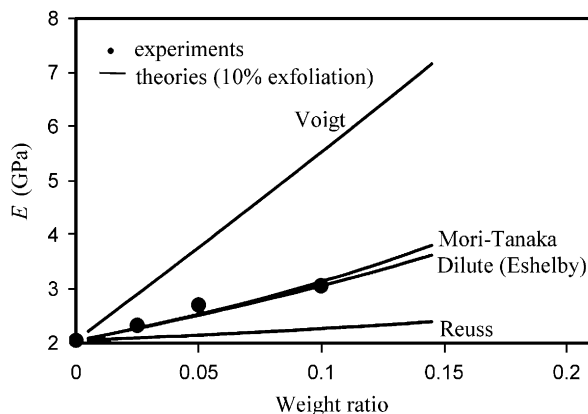


Fig. 58. Predicted and experimental Young's moduli of epoxy/clay nanocomposite as a function of clay concentration [255]. Reproduced from Luo and Daniel by permission of Elsevier Science Ltd.

measurements. In addition, with properly determined material parameters, this model can predict the tensile behavior of the intercalated and aggregated clay–poly(methylmethacrylate) nanocomposites. In another study, Zheng et al. [254] developed a model to predict the effective elastic properties of stationary and flow-induced phases of nanorod–polymer composites. This model combined the micromechanics-based Mori–Tanaka model with the probability distribution functions of the Doi–Hess hydrodynamic theory for nanorod dispersions. They examined the effects of nanoparticle volume fraction, flow type and flow rate on nanocomposite elasticity tensors. de Villoria and Miravete [118] developed a new micromechanical model called as dilute suspension of clusters to estimate the influence of the dispersion of nanofillers in nanocomposite Young's modulus. Compared to other models (e.g., Voigt–Reuss, Halpin–Tsai, modified mixture law and Cox), this new model improved significantly the theoretical-experimental correlation for epoxy composites reinforced with the clusters of CNTs. Moreover, it provides an easy way to evaluate the effect of the inhomogeneous dispersion of the nanofillers on the mechanical properties of the composites.

Based on Halpin–Tsai model, Brune and Bicerano [253] developed analytical solutions for elasticity equations and addressed some important aspects of the micromechanics of clay-based polymer nanocomposites, such as the buckling of clay platelets, partial clay exfoliation and imperfect platelet alignment on the reinforcement efficiency. Their model predicted a critical strain above which

the clay platelet would buckle and thus reduce the compressive modulus relative to the tensile modulus. It was also shown (Fig. 60) that both partial exfoliation and imperfect would significantly decrease the reinforcement efficiency (e.g., Young's modulus).

Wu et al. [257] examined the modulus reinforcement of rubber-clay nanocomposites using composite theories based on Guth, Halpin–Tsai and the modified Halpin–Tsai equations. By introducing a modulus reduction factor for the platelet-like fillers, the predicted moduli are closer to the experimental measurements (Fig. 61). Moreover, it was shown the Guth and the modified Halpin–Tsai equations are able to predict the modulus of rubber-clay nanocomposites over a wide range of clay volume fractions while the Halpin–Tsai equation is suitable for those with low clay volume fractions. Li et al. [258] studied the reinforcing mechanisms of SWCNT–epoxy composites by Halpin–Tsai and Mori–Tanaka models. Their results are in good agreement with the experiment results. Moreover, they found that the covalent nanotube–polymer bonding, matrix crystallinity, tensile properties of reinforcement and matrix, bundle curvature and alignment, play a dominant role in mechanical reinforcement.

In order to understand the effects of filler loading and filler–filler interaction strength on the viscoelastic behavior, Chabert et al. [259] proposed two micromechanical models (i.e., a self-consistent scheme and a discrete model) to account for the short range interactions between fillers, which leads to a good agreement with the experimental results. In addition, the discrete model highlighted the importance of filler–filler interactions on the reinforcement above the percolation threshold. The effect of the filler–filler interactions on the viscoelasticity of filled cross-linked polymer (i.e., rubber) was studied by Raos et al. [260] via DPD simulation. They examined such effect through four systems with dispersed (D), moderately aggregated (M2 and M5), and fully aggregated (A) filler particles as shown in Fig. 62. Their simulations indicated that filler–filler interactions have a clear effect on the dynamics shear modulus. For a given morphology, increasing filler–filler interactions always results in a certain increase of the modulus. Buxton and Balazs [261] used lattice spring model to examine the effects of filler geometry (e.g., platelet, spheres and rods), intercalation–exfoliation of clay platelets on the mechanical behavior of

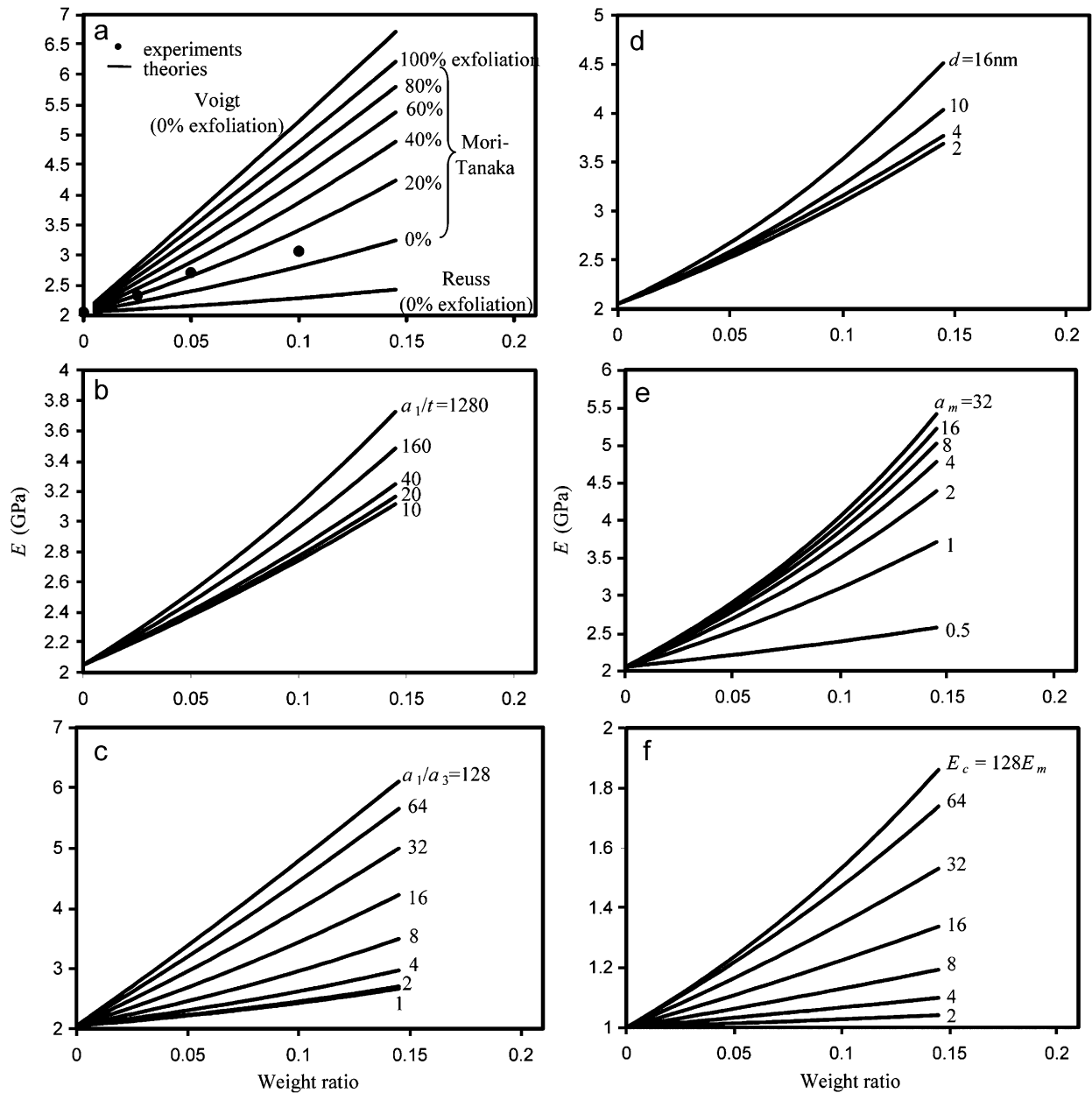


Fig. 59. Young's moduli of epoxy/clay nanocomposite as a function of clay concentration for different: (a) exfoliation ratios; (b) exfoliated clay layer aspect ratios; (c) intercalated clay cluster aspect ratios; (d) layer spacings; (e) intragallery stiffness factors; and (f) clay/matrix stiffness ratios [255]. Reproduced from Luo and Daniel by permission of Elsevier Science Ltd.

particle-reinforced polymers. It was found that polymers filled with platelets experience the most significant increase in reinforcement efficiency while those filled with spheres have the lowest reinforcement efficiency. Their simulations also showed that the incomplete exfoliation of clay platelets would lead to a less effective reinforcement of polymer matrix, which is in agreement with the experimental

observations [220,221]. They attributed the reinforcement efficiency to the volume of polymer matrix constrained in the proximity of the particles. In other words, a more homogeneous dispersion of clay platelets in polymer matrix leads to a greater volume of polymer being constrained by the platelet particles and thus the increases of the reinforcement efficiency. Liu and Brinson [262] developed a hybrid

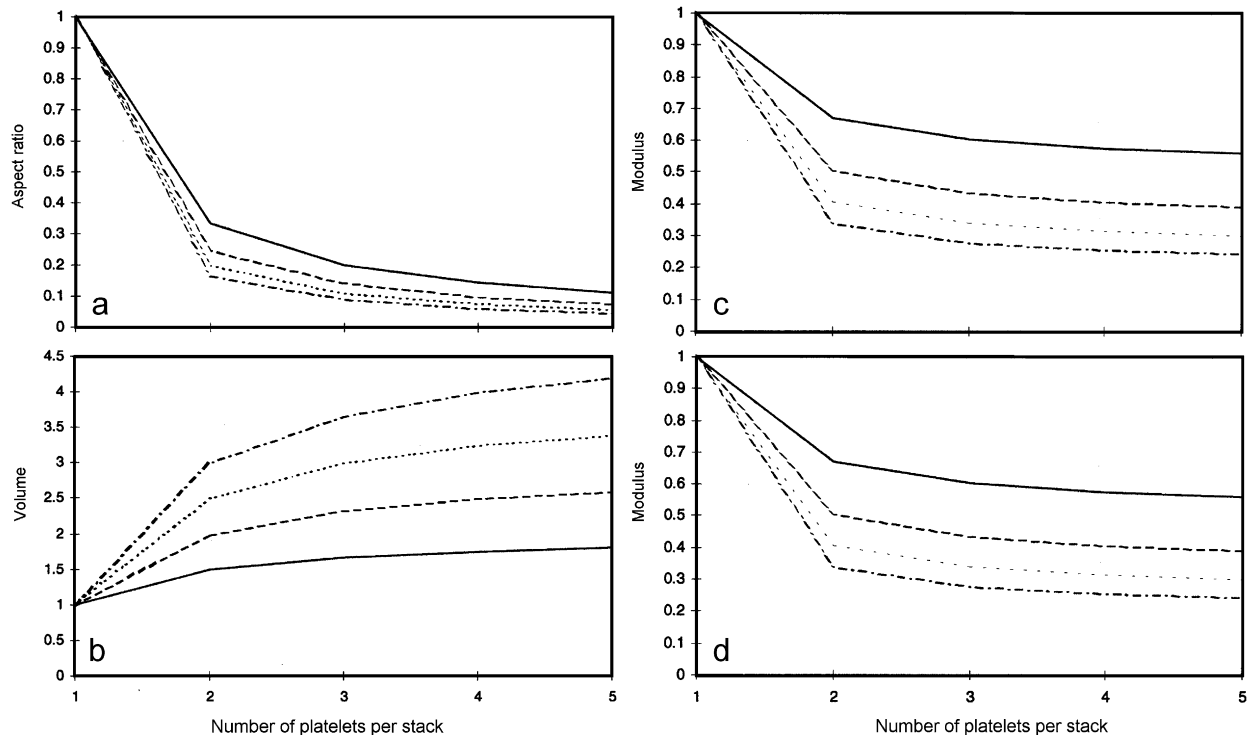


Fig. 60. Effect of the number of platelets per stack (N) and ratio of platelet spacing to platelet thickness in a stack (s/t) on: (a) the ratio of the aspect ratio of the stacks to that of individual platelets; (b) the ratio of the volume fraction of platelet stacks to that of individual platelets; and (c) and (d) the ratio of the stack modulus to the platelet modulus ratio (E_r) of 100 and 100,000, respectively [253]. Reproduced from Brune and Bicerano by permission of Elsevier Science Ltd.

numerical-analytical modeling technique to predict the viscoelastic response of polymer nanocomposites. This method uses a finite element unit cell analysis to determine the strain concentration tensors of nanoparticle, and then couples the numerical result with the micromechanical Mori-Tanaka model to predict the overall nanocomposite response. The predicted pattern of the interphase influence of the nanocomposites is in agreement with the experimental observation. In addition, it is believed that this method can also be used to predict the thermal and electrical properties of polymer nanocomposites, the behaviors of other types of nanocomposites such as metal and ceramic matrix nanocomposites.

The use of continuum-based models may overcome such problems as expensive cost and configuration/material specific of molecular modeling and simulation [263–265]. Recently, Wagner [266] used a continuum-based method (i.e., modified Kelly-Tyson approach) to estimate the interfacial shear strength in polymer composites reinforced by SWCNTs in which uniform interfacial shear and

axial normal stresses are assumed. More recently, Li and Chou [267] developed a continuum-based computational model for interfacial stress transfer in nanotube-reinforced polymer composites in which they employed molecular structural mechanics to characterize the nanotube and FEM to model the polymer matrix. In another study, by using a multiscale approach, Gao and Li [268] developed a shear-lag model to predict the interfacial stress of CNT-polymer composite in which the volume element is represented by a composite cylinder embedded with a capped nanotube. The atomistic structure of the capped nanotube is incorporated in the model by using the molecular structural mechanics. The continuum-based shear-lag analysis is performed using elasticity theory for axisymmetric problems. Their predictions agree qualitatively with those by the computational model. In addition, it was shown that nanotube aspect ratio plays a critical role in designing the nanotube-reinforced polymer composites. These studies thus shed new light on the understanding of the load transfer across the nanotube-matrix

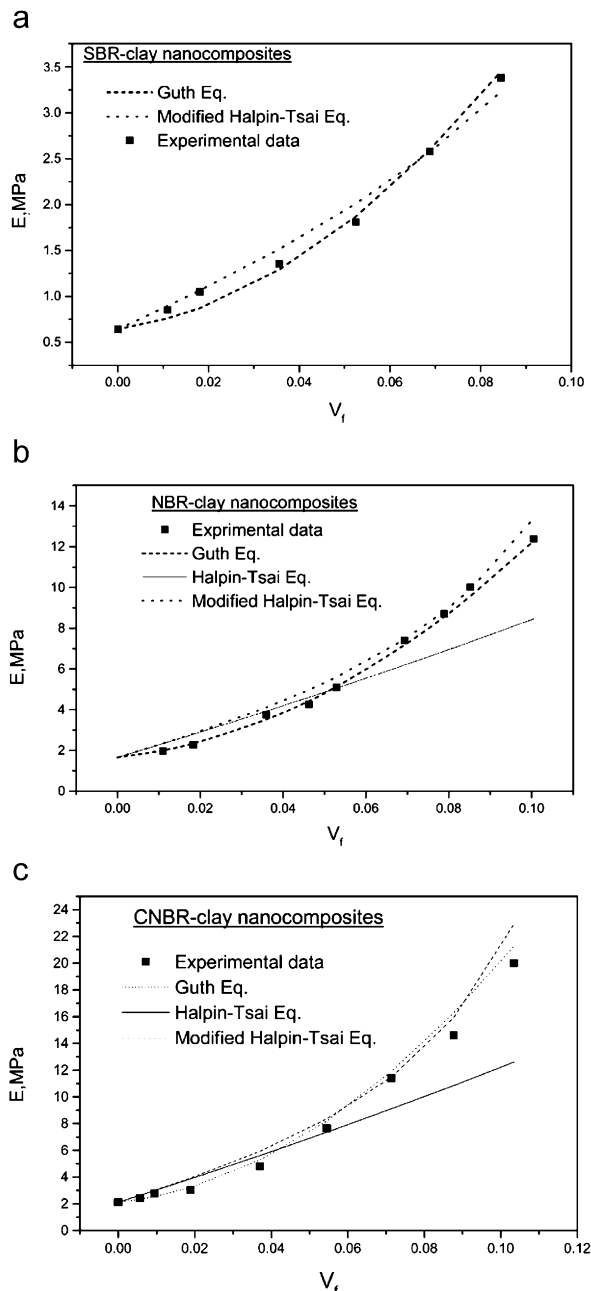


Fig. 61. Experimentally measured modulus and theoretical predictions by three different models after introducing modulus reduction factor 0.66 in the: Guth, Halpin-Tsai, and modified Halpin-Tsai equations for: (a) SBR-clay nanocomposites; (b) NBR-clay nanocomposites; and (c) CNBR-clay nanocomposites [257]. Reproduced from Wu, Jia, Yu and Zhang by permission of Elsevier Science Ltd.

interface and provide some guidance for the development of analytical models as well as novel composite materials. Tsai and Sun [269] used a shear lag model to investigate the load transfer

efficiency of nanoclay platelets in a polymer matrix. They showed that well-dispersed clay platelets in the polymer matrix, due to their high aspect ratio, can significantly enhance the load transfer efficiency. For tactoid nanocomposites in which clay platelets are held together as clusters, the load transfer efficiency is much lower and depends on the number of platelets per cluster.

FEM has also been used to predict the mechanical properties of polymer nanocomposites. Fisher et al. [270] developed a model that combines FEM with micromechanical method (i.e., Mori-Tanaka model) to determine the effective reinforcing modulus of a wavy embedded nanotube. This model is then used to predict the effective modulus of a polymer reinforced with a distribution of wavy nanotubes. The effective reinforcement was reduced significantly even with slight nanotube curvature, which indicated that nanotube waviness may be an additional mechanism limiting the modulus enhancement of nanotube-reinforced polymers. Bradshaw et al. [271] used a three-dimensional FEM of a single infinitely long sinusoidal fiber within an infinite matrix to calculate the dilute strain concentration tensor. This tensor was then utilized in a Mori-Tanaka model to predict the effective modulus of the material with aligned or randomly oriented inclusions. It is believed that this hybrid FEM-micromechanical method can also be applied to any composite microstructure containing non-ellipsoidal inclusions. Ashrafi and Hubert [272] predicted the elastic properties of nanoarrays consisting of SWCNT through a finite element analysis. The predicted properties were then used to examine the properties of carbon nanoarray-polymer composites and the effects of nanoarray volume fraction and aspect ratio using conventional micromechanics. Song and Youn [273] reported a study on the effective elastic properties of CNT composites by using the asymptotic expansion homogenization method. This method is able to transform a heterogeneous medium to an equivalent homogeneous medium and hence perform both localization and homogenization for heterogeneous medium. In their study, the control volume FEM was adopted to implement such homogenization process. They found that the numerically calculated elastic modulus is in good agreement with that obtained by analytical model. Moreover, it is believed that this homogenization method has great potential for predicting elastic modulus and thermal conductivity of heterogeneous composites because it can easily handle the complex geometry and material anisotropy.

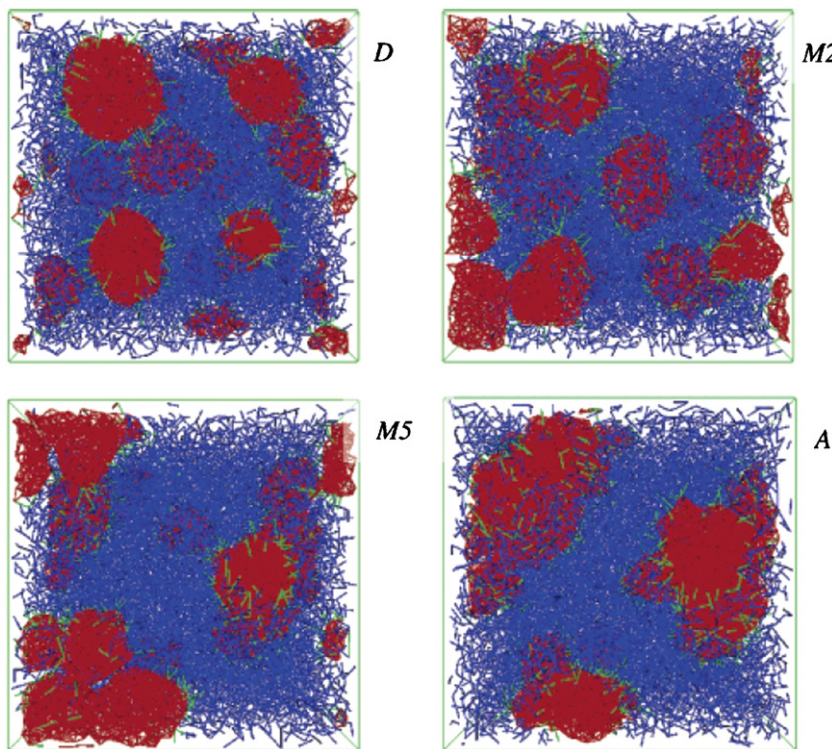


Fig. 62. Snapshots of the systems with dispersed (*D*), moderately aggregated (*M*2 and *M*5), and fully aggregated (*A*) filler particles. The filler–filler bonds are drawn in red, the polymer–polymer bonds in blue, and the polymer–filler bonds in green [260]. Reproduced from Raos, Moreno and Elli by permission of American Chemical Society.

In addition to nanotube–polymer nanocomposites, FEM has also been used to estimate the mechanical properties of polymer nanocomposites reinforced with other nanoparticles. For example, the effective elastic properties of silica nanoparticle-reinforced polymer nanocomposites were predicted by means of various FEM-based computational models [274–276]. These models reasonably reproduced the nanocomposite microstructure, i.e., particle size, amount and spacial arrangement. These studies highlighted the importance of including an interphase layer around particles as a third constituent material in the prediction of mechanical properties. To account for the contribution of the interphase to the elastic modulus of polymer nanocomposites, Saber-Samandari and Khatibi [277] developed a 3D unit cell model to represent the three constituent phases including particle, interphase and matrix. The elastic modulus of the interphase at any point, r , is calculated by

$$E_i(r) = E_m(r_i/r) + [(r_i - r)/(r_i - r_f)]^{n/2} [E_f - E(r_i/r_f)], \quad (72)$$

where E_m and E_f are matric and nanoparticle elastic moduli, respectively, r_f and r_i are the filler and interphase radii, and n is the intragallery enhancement factor which depends on the chemistry and surface treatment of the particles considered. They investigated the effects of matrix and filler stiffness as well as interphase thickness on Young's modulus of clay-based polymer nanocomposites.

Work has recently been done to compare the predicted mechanical properties from both micromechanical models and FEM. Hbaieb et al. [278] recently assessed the accuracy of Mori–Tanaka model against FEM in determining the stiffness of clay–polymer nanocomposites. Comparing to 3D models, 2D FEM models do not predict accurately the elastic modulus of real clay–polymer nanocomposites. The Mori–Tanaka model predicts accurately the stiffness of intercalated clay–polymer nanocomposites with clay volume fraction up to about 5% but underestimates the stiffness at higher volume fractions. Moreover, the Mori–Tanaka model overestimates the stiffness of exfoliated clay–polymer nanocomposites. Lagoudas and co-workers [279,280] employed both micromechanics

techniques and FEM to estimate the effective elastic properties of CNT-reinforced composites. In their analysis, they first calculated the effective properties of CNTs by composite cylinders micromechanics. These effective properties were then used in the self-consistent and Mori–Tanaka methods to obtain effective elastic properties of polymer composites reinforced with single or multiwalled CNTs. The effects of nanotube clustering and polymer–nanotube interphase were investigated. They found that composite cylinders method provides satisfactory representations for obtaining the effective elastic constants for a continuous range of volume fractions below a critical value. Near and above the critical volume fraction, FEM has more advantageous in handling the complicated fiber–polymer interactions. Liu and Chen [281–283] recently used the finite element and boundary element methods (FEM/BEM) to study CNT–composite models, where RVEs containing one or multiple CNTs are modeled as thin elastic layer in the shape of a capsule (for short CNT) or an open cylinder (for long CNT). Effective elastic properties of the CNT composites are evaluated and compared with the rules of mixtures. It was shown that the stress gradient across the interface of the CNT and matrix is very high and the number of elements can become prohibitively large for the FEM in large-scale modeling of CNT composites. These investigators also developed a continuum model of nanotube-based composites for large-scale analysis at the microscale. The nanotubes are treated as rigid fibers in the elastic matrix, due to its high stiffness compared with most polymer matrix materials. A recently developed fast multipole BEM is employed to solve the boundary integral equations governing this rigid-inclusion problem. The estimated effective Young's moduli using this rigid-fiber model and the BEM are found to be very close to those obtained using an MD-based multiscale approach reported in the literature. Moreover, it is expected that the elasticity of the CNT fibers and more realistic interface conditions based on MD simulation results of CNT composites can be incorporated readily in this fast multipole BEM. Later, Huang et al. [284] extended the above method by introducing an equivalent length coefficient to consider the 3D end effects of SWCNs in matrix to develop a modified mixture model for the prediction of Young's modulus. They concluded that the extended model can be applied to CNT loading between 0% and 5% while the Liu and Chen's

model is suitable for a nanotube loading close to 5%.

Tseng and Wang [285] recently reported a constitutive modeling framework to predict the mechanical properties of nanoparticle-reinforced composites. They showed that the effects of interparticle interaction are significant and cannot be neglected especially in the case of high particle loading. Their constitutive model may potentially be applied for FEM-based numerical simulation to solve practical engineering problems of nanoparticle-reinforced composites. On the other hand, Miyagawa et al. [286] used a pseudoinclusion model to estimate the aspect ratio and the number of platelets of clay cluster epoxy nanocomposites from Tando–Weng and Halpin–Tsai equation. Their study showed that the conventional equations, Tando–Weng and Halpin–Tsai, are useful, with the pseudoinclusion model for intercalated clay nanocomposites, to predict the elastic modulus as well as coefficient of thermal expansion. Guz et al. [287] addressed a compressive failure theory for polymer nanocomposites developed based on the microbuckling mechanism and the three-dimensional linear theory of stability of deformable bodies. Two approaches are employed in their work: the first approach uses a homogenous anisotropic model while the second uses a piecewise-homogenous model. This compressive failure theory is then applied to laminated and fibrous nanocomposites with different microstructures. Yang et al. [288] investigated the tensile creep resistance of polyamide 66 nanocomposites reinforced with either TiO₂ or clay nanoparticles by using the constitutive Burgers creep model and the empirical Findley power law. The simulated results from both models agree quite well with the experimental data and also confirm the enhanced creep resistance of nanofillers even at extended long time scale.

3.6.3. Equivalent-continuum and self-similar models

Continuum models normally assume that each phase (e.g., polymer matrix and filler) in polymer composites has the same properties as if the other phase is not there. Although they have been used to examine some factors on materials mechanical reinforcement, as pointed out by Brune and Bicerano [253], the well-defined concepts in conventional two-phase composites can no longer be directly applied to polymer nanocomposites due to the hierarchical morphology of the filler structure and surrounding polymer matrix at nanometer length scale. Moreover, in polymer nanocomposites,

the polymer molecules and nanofillers have the equivalent size and the polymer–filler interactions are highly dependent on the local molecular structure and bonding at the interface. Therefore, the structures of nanofillers and polymer chains cannot be considered as continuous phase at these small length scales, and the bulk mechanical properties can no longer be determined through traditional continuum-based micromechanical approaches. In order to understand the dependence of composite properties on nanofiller content and structure, the mechanical behavior of nanofillers should be described properly and the conversion of filler weight fraction to filler volume fraction should be treated carefully. Recently, two methods, equivalent-continuum model and self-similar model, have been proposed for modeling the mechanical properties of polymer nanocomposites in which the molecular structure and interactions are incorporated into the continuum mechanics-based models.

In the equivalent-continuum model, Odegard and coworkers [45,86,224,263] utilized MM to model a specific polymer–filler interaction and to construct a homogeneous, equivalent-continuum reinforcing element (i.e effective nanofiller) consisting of a nanofiller and its surrounding polymer as shown in Fig. 63. The micromechanics method is then used

to determine the effective bulk mechanical properties of the equivalent-continuum reinforcing elements embedded in a continuous polymer. Thus, this method represents the nanoscale interactions between polymer and nanofiller and at the same time provides a consistent and rigorous scheme to determine continuum properties for the polymer nanocomposites. Fig. 64 shows the Young's and shear moduli of four composite systems determined by using the concept of effective nanofillers. It is clear that when the effective particle size is less than 1000 Å, both Young's and shear moduli predicted are increased with the particle size but their values are less than those predicted from the Mori–Tanaka model. However, with the particle size larger than 1000 Å, the moduli predicted from both models are consistent. The independence of the predicted moduli from the Mori–Tanaka model on effective particle size is attributed to the neglect of the effective interface. In nanotube polymer nanocomposites, the nanotube, the local polymer near the nanotube, and the nanotube–polymer interface are modeled as an effective continuum fiber which retains the local molecular structure and bonding information, as defined by MD, and serves as a means for linking the equivalent-continuum and micromechanics models. The latter is then used to predict bulk mechanical properties of nanotube

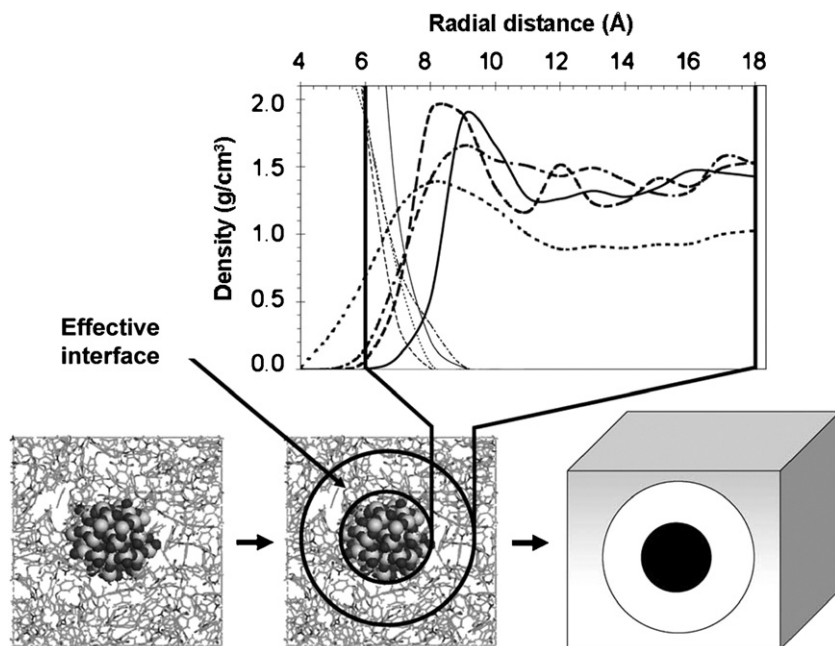


Fig. 63. Schematic of the process used to determine effective interface [86]. Reproduced from Odegard, Clancy and Gates by permission of Elsevier Science Ltd.

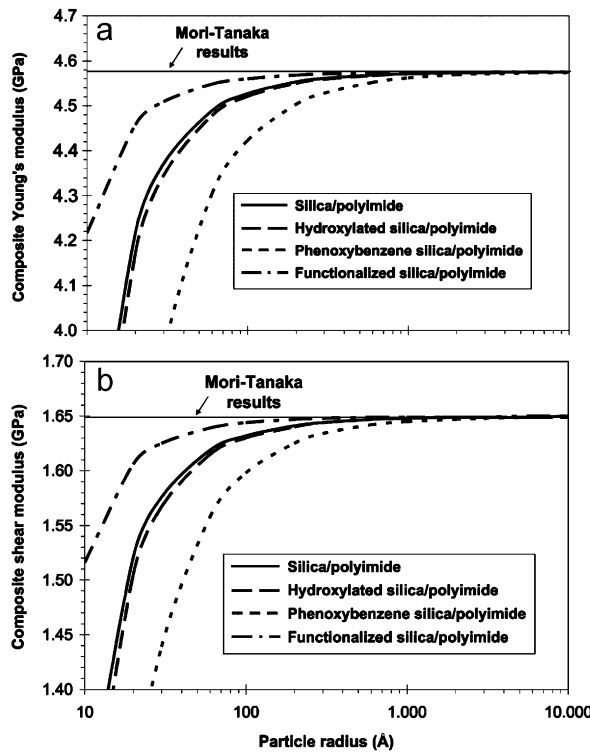


Fig. 64. Young's (a) and shear (b) moduli of four composite systems versus effective particle radius [86]. Reproduced from Odegard, Clancy and Gates by permission of Elsevier Science Ltd.

polymer composites as a function of nanotube size, orientation, and volume fraction.

In the self-similar approach, Pipes and coworkers [46,289–291] used lattice dynamics to model an array of nanotubes and then constructed the composite model by embedding the nanotube arrays into a polymer matrix. This composite model is subsequently used in a series of self-similar concentric-cylinder models to build an overall model of a microfiber as shown in Fig. 3. Thus, the self-similar approach spans three orders of magnitude in scale with interconnected models that relate performance of a single nanotube to nanoarray, nanowire, and microfiber. They estimated the translation of properties from the nanoscale to the microscale, and the scale transfer efficiencies. Moreover, they predicted the mechanical properties of the helical nanoarray, the nanowire, and the microfiber, such as the axial Young's modulus, shearing modulus, and Poisson's ratio as shown in Fig. 65. In another study, Odegard et al. [44] used both equivalent-continuum model and the self-similar approach to predict the elastic properties of single-wall nanotube polymer composites. It

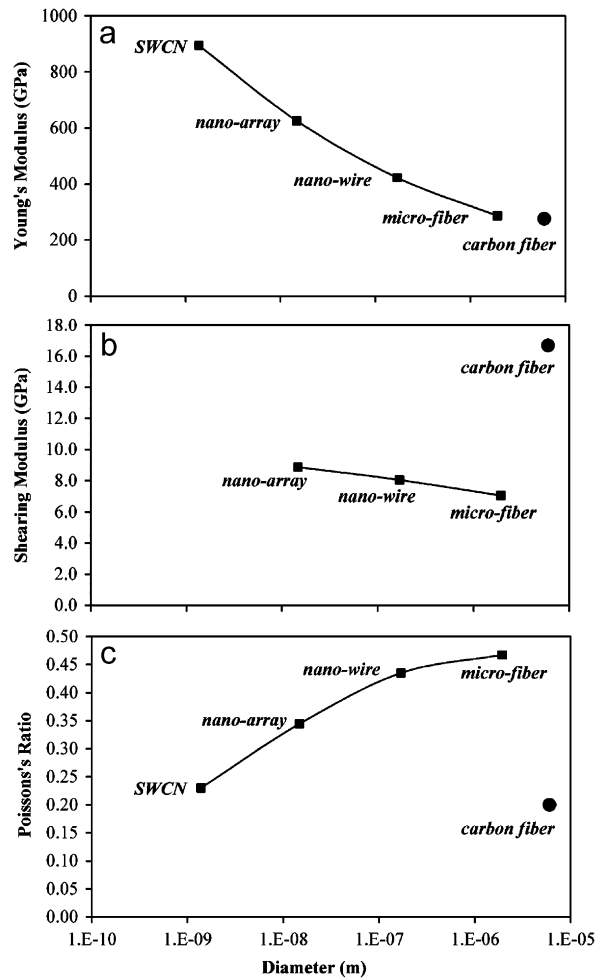


Fig. 65. The axial Young's modulus (a), shearing modulus (b), and Poisson's ratio (c) estimated for single-walled carbon nanotube, nano-array, nano-wire and the microfiber [289]. Reproduced from Pipes and Hubert by permission of American Chemical Society.

was shown that both of them can predict elastic properties of single-wall polymer composites in a combined range spanning from dilute to hyper-concentrated volume fractions of single-wall nanotubes. The predicted consistent Young's moduli for a single-wall polymer composite determined using both approaches are shown to be consistent.

4. Multiscale strategies for modeling polymer nanocomposites

4.1. Challenges

A main goal of computational materials science is the rapid and accurate prediction of new materials

and their new properties and features, which is very difficult to achieve with traditional modeling and simulation methods at a single length and time scale with the current computer power [292–297]. Therefore, it is expected to use the multiscale simulation strategies to bridge the models and simulation techniques across a broad range of length and time scales to address the macroscopic or mesoscopic behaviors of materials from a detailed molecular description. The challenge for multiscale simulations is to move, as seamlessly as possible, from one scale to another so that the calculated parameters, properties and numerical information can be efficiently transferred across scales. In particular, the challenge for polymer nanocomposites is to predict accurately their hierarchical structures and behaviors and to capture the phenomena on length scales that span typically 5–6 orders of magnitude and time scales that can span a dozen orders of magnitude. For example, a clay particle with a diameter of 0.5 μm and 100 layers would have about 85 million atoms. If such a particle is dispersed into polymer matrix to form polymer nanocomposites containing 5% of clay in weight, the system would then have about 3 billions of atoms. Thus, it is too large for classical MD and enormously too large for QM. Moreover, the observable properties of the

materials depend on a hierarchy of structure including: chemical detail at the atomistic level, individual chains, microscopic features involving aggregates of chains and clusters of clay platelets, up to continuum phenomena at the macroscale. As a result, the complete description of a polymer nanocomposite typically requires a wide range of length scales from the chemical bond, at around one Angstrom in length, up to chain aggregates extending for many hundreds of Angstroms and beyond. There is also a wide range of time scales, with chemical bond vibrations occurring over tens of femtoseconds and, at the other extreme, collective motions of many chains taking seconds or much longer. From this point of view, new strategies for multiscale modeling and simulation are essential to predict accurately the physical/chemical properties and material behavior which links the methods from microscale to mesoscale and macroscale levels as shown in Fig. 66 [11,12,14,16,29,168,255,298].

4.2. Sequential and concurrent approaches

In general, there are two types of multiscale methods as shown in Fig. 67: sequential [299,300] and concurrent multiscale approaches [47,301,302]. In sequential approaches such as the most cases

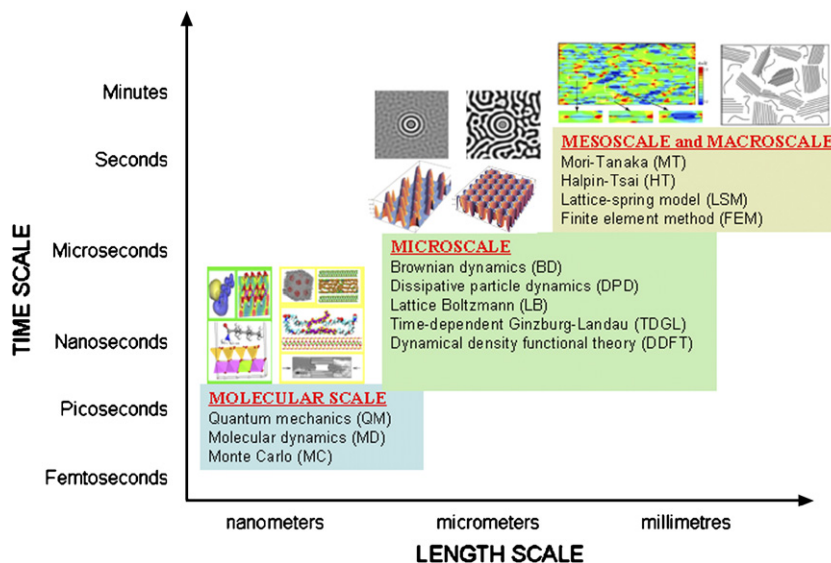


Fig. 66. Computer modeling and simulation methods for nanoparticle–polymer nanocomposites [11,12,14,16,29,168,255,298]. Reproduced from (i) Lee, Baljon and Loring by permission of American Institute of Physics; (ii) Smith, Bedrov, Li and Byutner by permission of American Institute of Physics; (iii) Zeng, Yu, Lu and Standish by permission of American Chemical Society; (iv) Zeng, Yu and Lu by permission of Institute of Physics; (v) Sheng, Boyce, Parks, Rutledge, Abes and Cohen by permission of Elsevier Science Ltd; (vi) Luo and Daniel by permission of Elsevier Science Ltd; (vii) Thompson, Ginzburg, Matsen and Balazs by permission of American Chemical Society; and (viii) Lee, Douglas and Glotzer by permission of American Physical Society.

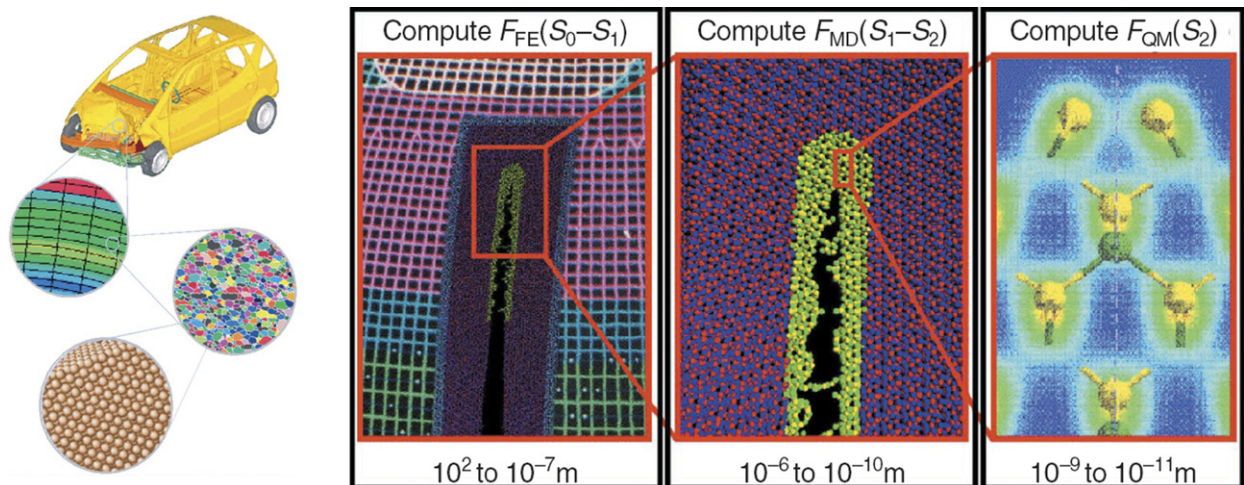


Fig. 67. Multiscale modeling and simulation strategies: sequential (left) [300]. Reproduced from Raabe by permission of Wiley-VCH, and concurrent approaches (right) [301]. Reproduced from Nakano, Bachlechner, Kalia, Lidorikis, Vashishta, Voyatzis, Campbell, Ogata and Shimojo by permission of IEEE.

discussed in the previous sections, a series of hierarchical computational methods are linked in such a way that the calculated quantities from a computational simulation at one scale are used to define the parameters of the model operative on the adjoining larger scale. Such parameter-passing, sequential approaches have proven effective, especially when material behavior can be parsed into several scales, each with its own distinct characteristics. Kremer and Müller-Plathe [299] described a sequential approach which spans from atomistic or molecular scale (atoms) to microscale (monomers) and then to macroscale (chains), and adopts the parameter-passing strategy in which the effective free-energy terms for the coarse-grained model are obtained by statistical averaging of fast degrees of freedom within the more detailed model. Recently, Doi [303] has developed a suite of state-of-the-art simulation tools (i.e., OCTA) to model polymers at the molecular and mesoscale method. Although each tool performs calculations using only one method, the output from one method can be used directly as input for another, allowing an off-line bridging of length and time scales.

In concurrent approaches, several computational methods are linked together in a combined model in which different scales of material behavior are considered concurrently and communicate using some sort of handshaking procedure [180,304–306]. Such approaches resemble the multigrid techniques used for partial differential equations or the general renormalization-group idea of statistical physics.

While intellectually most appealing, these approaches have not yet been developed into a general scheme. Ortiz et al. [307] described a new concurrent multiscale approach which is based on an atomistic-continuum handshake arranged in such a way that atomic details of material microstructure are resolved only where necessary. The rest of the material is treated as a continuum within a finite element framework. Through the use of adaptive mesh refinement, the interaction between the atomistic and continuum descriptions is organized in an entirely seamless fashion.

4.3. Current research status

The development of polymer nanocomposites relies largely on our understanding of the structure–property relationship of the materials which requires a multiscale model to predict the material properties from the information of particle properties, molecular structure, molecular interaction, mesoscale morphology. The current research in modeling and simulation of polymer nanocomposites are largely limited to individual length and time scale. However, it should be noted that some efforts have recently been made to develop multiscale strategies for predicting the multiscale level of structure, properties, and processing performance of polymer nanocomposites based on nanoparticle reinforcement (e.g., nanosphere, nanotube, nanorod and clay platelet). We will describe some of these work and interesting readers are recommended to

the two reviews by Lau et al. [308] and Valavalala and Odegard [224].

Balazs and co-workers [35,169–171,177,185,309] recently combined DFT with SCF to calculate the phase behavior of clay-based polymer nanocomposites and other polymer–nanoparticle mixtures. In this combined model, the thermodynamic behavior and interaction information among various components are obtained from the SCF model which served as an input to a DFT to calculate the phase behavior. Similar multiscale modeling strategies have also been implemented at Dow to predict the thermodynamic equilibrium morphologies and many properties of nanocomposites from the chemical structures and the relative amounts of the formulation ingredients and to help product development [309].

On the other hand, Glotzer and co-workers [48,49] proposed a multiscale approach for nanoparticle-filled polymers which combines the coarse-grained MD, mesoscopic TDGL, and macroscopic continuum finite element techniques. This approach bridges the length scales necessary to link molecular phenomena to macroscopic properties. The link between mesoscale structure and macroscale mechanical properties was accomplished by using the output of the TDGL/CHC simulations as input for the finite element analysis. The link between the MD simulations and the TDGL/CHC simulations was less direct, and made only qualitatively through incorporation of filler–polymer interaction terms in the CHC free-energy function.

Porter [310] proposed a multiscale model, representing bone as a natural hybrid nanocomposite of high aspect ratio hydroxyapatite mineral particles in a polymer matrix of oriented tropocollagen, to predict the mechanical properties and structure–property relationship. The physical properties such as elastic modulus, energy dissipation, phase transition temperatures and failure initiation conditions are calculated by a self-consistent mean-field method from their molecular structure. These model parameters quantify the ensemble average energy components of a material at an atomistic level, and can be calculated by atomistic simulations or simple empirical methods. The resultant individual material properties are then used in a conventional Halpin–Tsai model at a larger scale to predict the anisotropic mechanical properties of lamellar bone. The model successfully explains and predicts the effects of mineral volume fraction and particle aspect ratio on the elastic modulus of bone.

Buxton and Balazs [311] investigated the effects of the spatial distribution of spherical nanoparticles on the mechanical behavior of nanoparticle-filled diblock copolymer composites by coupling CHC–BD–LSM models. In particular, the morphology of nanoparticle–diblock copolymer mixture was conducted through the combination of a CHC theory for the diblock copolymers and a BD for the nanoparticles. The output of this CHC–BD model serves as the input to the LSM, which consists of a three-dimensional network of springs. Their simulation results are showed in Figs. 68–70. It was found that the confinement of nanoparticles within a given domain of a bicontinuous diblock mesophase causes the nanoparticles to percolate and form essentially a rigid backbone throughout the material. This continuous nanoparticle distribution significantly increases the reinforcement efficiency of the nanoparticles and dramatically increases the Young's modulus of the material. They also found that increasing volume fraction of nanoparticles causes geometric percolation of the particles and the formation of a rigid particle network throughout the system. In a further work, Shou et al. [120] investigated the effects of aspect ratio of rod-like particles on the mechanical properties of diblock copolymers by coupling the SCF–DFT model with the LSM simulation. Their results showed that high

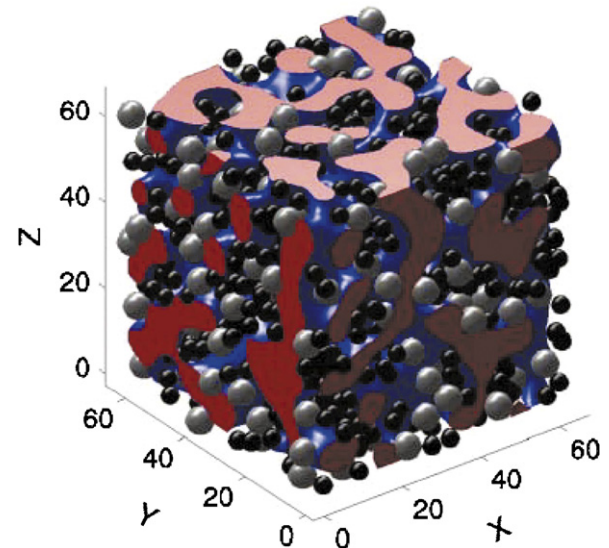


Fig. 68. Three-dimensional morphology of a filled diblock copolymeric system. The isosurface between A and B components is blue, isocaps are red, and the small and large particles are black and gray, respectively [311]. Reproduced from Buxton and Balazs by permission of American Physical Society.

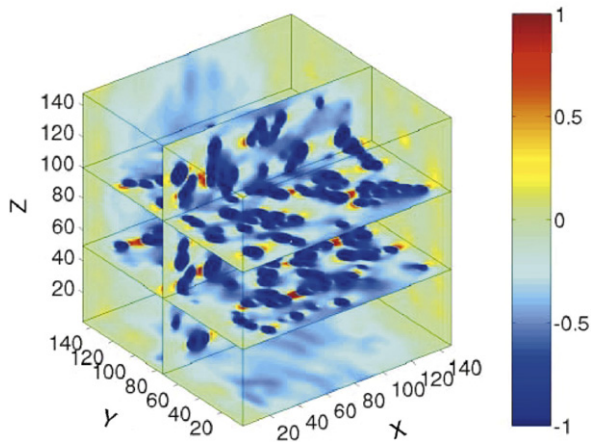


Fig. 69. The relative strain fields for a system containing a 10% volume fraction of small and a 10% volume fraction of large particles, confined within the domains of a diblock copolymer [311]. Reproduced from Buxton and Balazs by permission of American Physical Society.

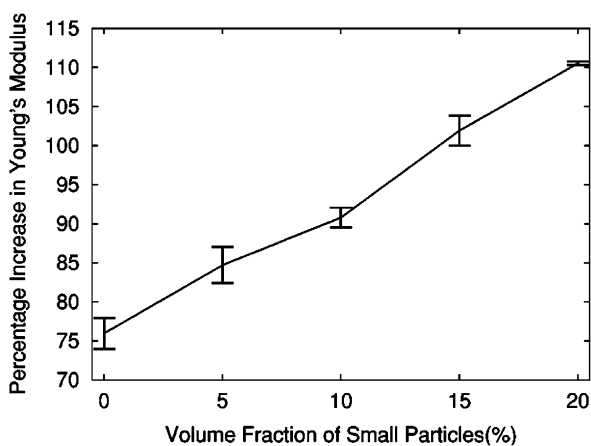


Fig. 70. The percentage increase in Young's modulus as a function of small particle volume fraction. The overall volume fraction of small and large particles is maintained at 20% [311]. Reproduced from Buxton and Balazs by permission of American Physical Society.

aspect ratio rods can dramatically increase the Young's modulus of the material.

By integrating a CHC-BD morphological model with a LSM micromechanical simulation, Buxton and Balazs [186] investigated the mechanical and electrical properties of nanocomposites composed of nanorods and a binary polymer blend. In their study, a bicontinuous morphology, isolated from the hybrid model of a CHC theory for binary mixtures and a BD for nanorods, served as the input to the LSM to determine the mechanical properties,

and a finite difference model to calculate the electrical conductance of the material. It was found that the reinforcement efficiency of this bicontinuous network is significantly increased as compared to that of composites where the nanorods are randomly dispersed in a homogeneous matrix.

Recently, Sheng et al. [298] used the combined MD and continuum models (e.g., FEM, Mori-Tanaka, Halpin-Tsai) to predict the dependence of the stiffness of clay-based polymer nanocomposite on clay content. Their results in Fig. 71 demonstrated the negative effects of particle interaction on load transfer, i.e., particles with high aspect ratio shield the matrix from straining, and thus reduce the efficiency of load transfer to neighboring particles. Increase in particle volume fraction and aspect ratio leads to an increase in such deleterious particle interactions. In their models, the concept of effective particle, representing multilayer stack with a certain number of silicate platelets and interlayer galleries as shown in Fig. 72, has been introduced and particle stiffness is estimated from MD simulations. Based on the concept of effective particle, they employed various continuum models to calculate the overall elastic modulus of polymer-clay nanocomposites and their dependence on the polymer matrix and clay properties as well as internal clay structural parameters. This combined model can capture the strong modulus enhancements observed in clay-based elastomer nanocomposites. In fact, the predicted elastic moduli as shown in Fig. 73 are in good agreement with experimental data. However, when the nanocomposite experiences a morphological transition from intercalated to completely exfoliated, these models predicted only a moderate modulus increase other than a dramatic increase usually observed experimentally. Prichard and co-workers [312,313] reported a hierarchical procedure which bridges the atomistic and mesoscopic simulations for clay-polymer nanocomposites, nanotube-polymer composites and polymer blends. They estimated the interaction parameters of the mesoscopic DPD model by mapping the corresponding energy values obtained from MD simulations. Fig. 74 shows the scheme of the surfactant mapping in which each alkylammonium molecule is described by five DPD beads, one for the head and two for each tail. Fig. 75 shows the morphology of clay-nylon 6 nanocomposites obtained from DPD simulation which is in good agreement with previous experimental and atomistic simulation results. As can be seen, a fixed wall of nanoclay is

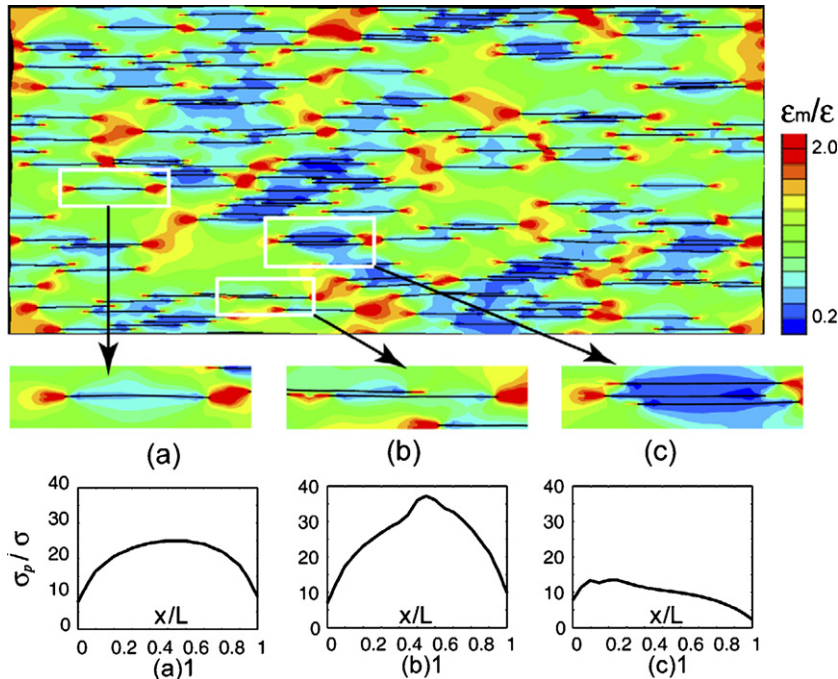


Fig. 71. Effect of strain shielding on load transfer efficiency: (a) isolated particle; (b) partly overlapped particle; (c) completely overlapped particle: (a) 1, (b) 1 and (c) 1 are normalized stress distributions in particle (a), (b) and (c), respectively; σ_p is the axial stress in the particle, σ is the macroscopic axial stress, $x = L$ is the fractional distance along the particle, from left to right [298]. Reproduced from Sheng, Boyce, Parks, Rutledge, Abes and Cohen by permission of Elsevier Science Ltd.

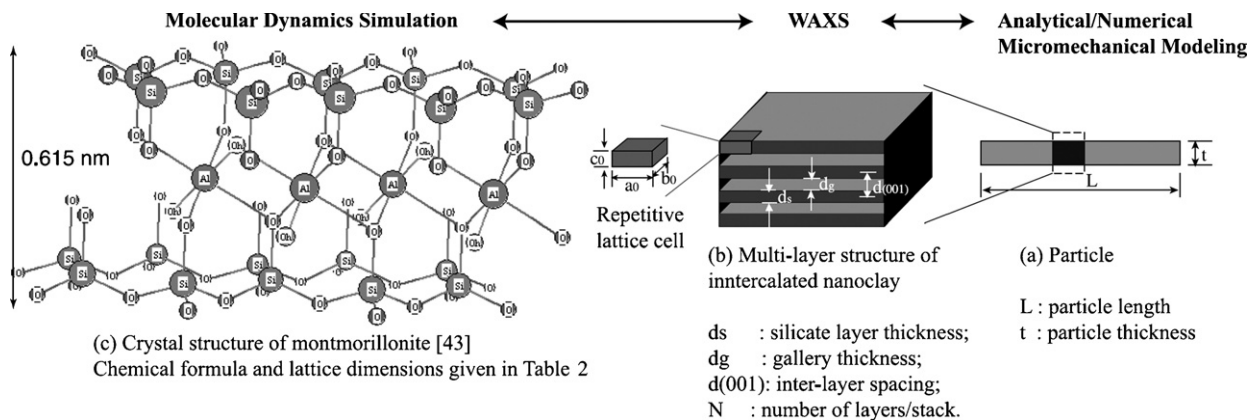


Fig. 72. Hierarchical structure of the nanoclay, WAXS represents wide angle X-ray scattering [298]. Reproduced from Sheng, Boyce, Parks, Rutledge, Abes and Cohen by permission of Elsevier Science Ltd.

obtained and the polar heads of the surfactants are attracted to it while the long apolar hydrocarbonic surfactant tails are flattened.

The exceptional viscoelastic properties of polymer nanocomposites cannot be predicted by the well-developed theoretical and modeling methods of conventional polymer composites. To overcome such deficiency, a third component (i.e., interfacial

polymer) has been introduced to the theoretical estimates. However, it is unclear how to determine the thickness of such interfacial layer and its time-dependent properties and their dependence on nanofiller concentration. To solve this problem, Borodin et al. [314] have recently proposed a multiscale modeling method (Fig. 76) which links MD simulation with stress-relaxation simulations

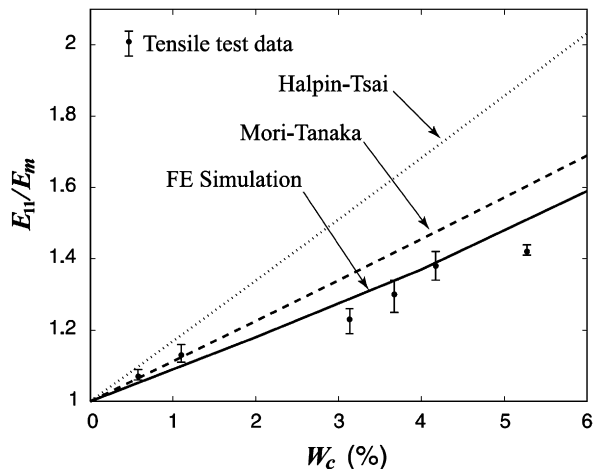


Fig. 73. Predictions of the effective longitudinal modulus for nylon 6/clay nanocomposites as a function of clay weight fraction (W_c) [298]. Reproduced from Sheng, Boyce, Parks, Rutledge, Abes and Cohen by permission of Elsevier Science Ltd.

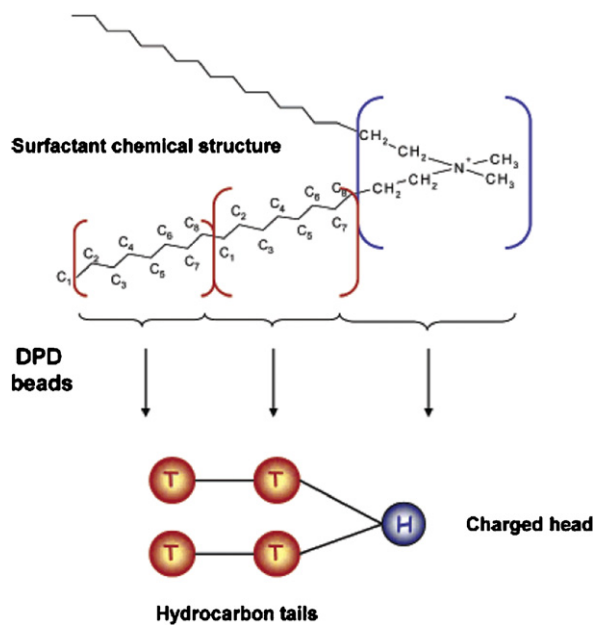


Fig. 74. Scheme showing the surfactant mapping from atomistic representation to DPD beads [312]. Reproduced from Scocchi, Posocco, Fermeglia and Prich by permission of American Chemical Society.

and material point method simulations. This method consists of three steps: (i) obtain the viscoelastic properties of bulk polymer from MD simulations and then estimate the position-dependent shear modulus of the interfacial polymer through the polymer-bead mean-square displacement; (ii) perform

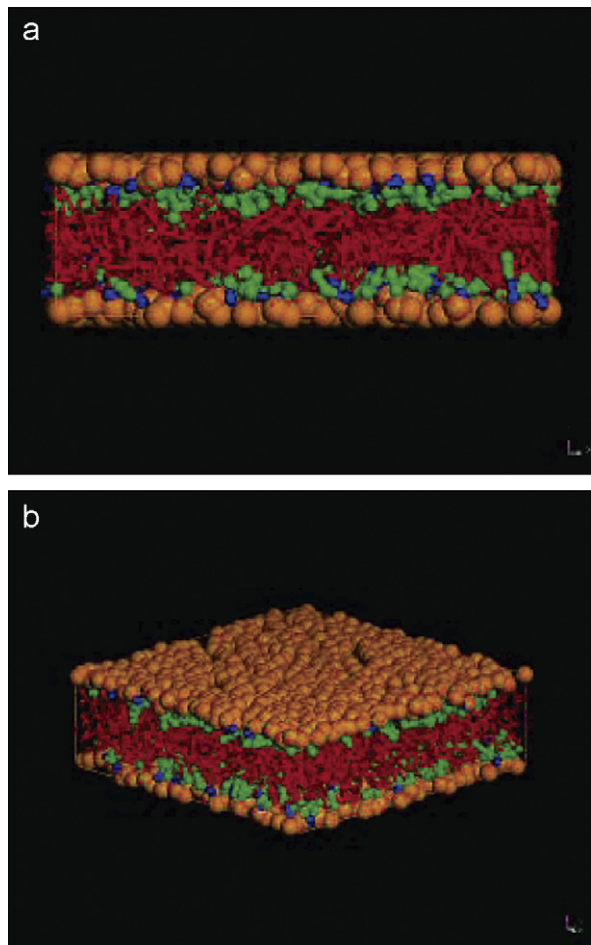


Fig. 75. Morphology of the clay–nylon 6 nanocomposite system obtained via DPD simulation: (a) perspective view and (b) frontal view. Color code: orange, clay; blue, surfactant head; green, surfactant tails; red, polymer [312]. Reproduced from Scocchi, Posocco, Fermeglia and Prich by permission of American Chemical Society.

stress-relaxation simulation of the polymer nanocomposites with material-point-method to extract the viscoelastic properties of the nanocomposites; and (iii) validate the average composite viscoelastic properties obtained from material point method simulation with those from MD simulations. The simulations of polymer–cylinder particle nanocomposites indicated that an increase in polymer–particle attractive interaction can lead to an increase in the time-dependent shear modulus by a few orders of magnitude. In another study, Clancy and Gates [315] presented a multiscale modeling approach in which MD simulation is used to calculate the interfacial thermal resistance values of nanotube–polymer composites. Then, these values are used in an analytical model to

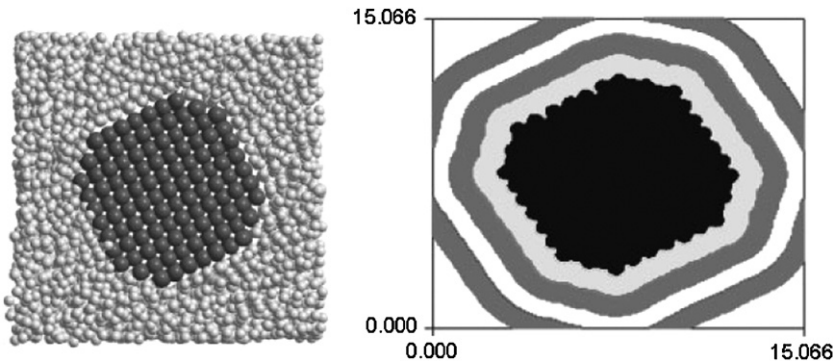


Fig. 76. Snapshots of MD simulations of a cylinder embedded in a polymer matrix and an equivalent system used in material point method simulations, where four interfacial polymer layers and bulk polymer are shown in different colors [314]. Reproduced from Borodin, Bedrov, Smith, Naim and Bardenhagen by permission of Wiley Periodicals, Inc.

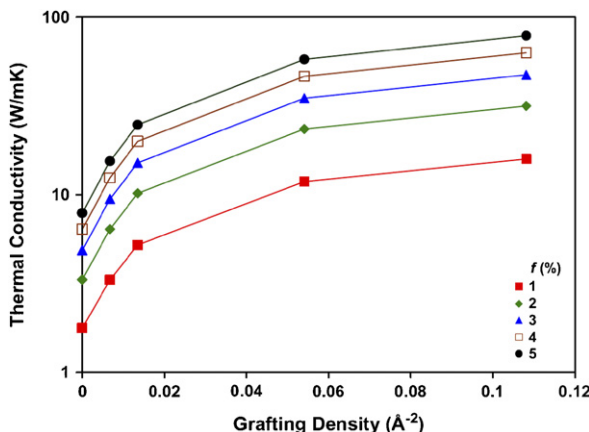


Fig. 77. The dependence of thermal conductivity of the composite to the matrix on the grafting density and volume fractions (in the range of 1–5%) of carbon nanotubes [315]. Reproduced from Clancy and Gates by permission of Elsevier Science Ltd.

predict the bulk thermal conductivity of the composites. They found that the interfacial thermal resistance values are strongly influenced by the grafting density and chain length of linear hydrocarbon chains covalently bonded to the nanotube surface. Moreover, the thermal conductivity of the composites (Fig. 77) was found to depend strongly on nanotube length, volume fraction, thermal conductivity, and the interfacial thermal resistance.

5. Concluding remarks

The development of polymer nanocomposites necessitates a comprehensive understanding of the phenomena at different time and length scales. In the past decade or so, this need has significantly

stimulated the development of computer modeling and simulation, either as a complementary or alternative technique to experimentation. In this connection, many traditional simulation techniques (e.g., MC, MD, BD, LB, Ginzburg–Landau theory, micromechanics and FEM) have been employed, and some novel simulation techniques (e.g., DPD, equivalent-continuum and self-similar approaches) have been developed to study polymer nanocomposites. These techniques indeed represent approaches at various time and length scales from molecular scale (e.g., atoms), to microscale (e.g., coarse-grains, particles, monomers) and then to macroscale (e.g., domains), and have shown success to various degrees in addressing many aspects of polymer nanocomposites.

The simulation techniques developed thus far have different strengths and weaknesses, depending on the need of research. For example, molecular simulations can be used to investigate molecular interactions and structure on the scale of 0.1–10 nm. The resulting information is very useful to understanding the interaction strength at nanoparticle–polymer interfaces and the molecular origin of mechanical improvement. However, molecular simulations are computationally very demanding, thus not so applicable to the prediction of mesoscopic structure and properties defined on the scale of 0.1–10 μm , for example, the dispersion of nanoparticles in polymer matrix and the morphology of polymer nanocomposites. To explore the morphology on these scales, mesoscopic simulations such as coarse-grained methods, DPD and dynamic mean field theory are more effective. On the other hand, the macroscopic properties of materials are usually studied by the use of mesoscale or macroscale techniques such as

micromechanics and FEM. But these techniques may have limitations when applied to polymer nanocomposites because of the difficulty to deal with the interfacial nanoparticle–polymer interaction and the morphology, which are considered crucial to the mechanical improvement of nanoparticle-filled polymer nanocomposites.

Therefore, despite the progress over the past years, there are a number of challenges in computer modeling and simulation. In general, these challenges represent the work in two directions. First, there is a need to develop new and improved simulation techniques at individual time and length scales. Secondly, it is important to integrate the developed methods at wider range of time and length scales, spanning from quantum mechanical domain (a few atoms) to molecular domain (many atoms), to mesoscopic domain (many monomers or chains), and finally to macroscopic domain (many domains or structures), to form a useful tool for exploring the structural, dynamic, and mechanical properties, as well as optimizing design and processing control of polymer nanocomposites. The need for the second development is obvious. For example, the morphology is usually determined from the mesoscale techniques whose implementation requires information about the interactions between various components (e.g., nanoparticle–nanoparticle and nanoparticle–polymer) that should be derived from molecular simulations. Developing such a multiscale method is very challenging but indeed represents the future of computer simulation and modeling, not only in polymer nanocomposites but also other fields. New concepts, theories and computational tools should be developed in the future to make truly seamless multiscale modeling a reality. Such development is crucial in order to achieve the longstanding goal of predicting particle–structure–property relationships in material design and optimization.

Acknowledgment

The authors would like to thank Australian Research Council (ARC) for the financial support through the ARC Centre of Excellence for Functional Nanomaterials.

References

- [1] Komarneni S. Nanocomposites. *J Mater Chem* 1992;2: 1219–30.
- [2] Giannelis EP. Polymer layered silicate nanocomposites. *Adv Mater* 1996;8:29–35.
- [3] Pinnavaia TJ, Lan T. Nanolayer reinforcement in polymer–clay nanocomposites. In: Johnson WS, editor. Proceedings of the American Society for Composites, 11th technical conference. Atlanta: American Society for Composites, 1996. p. 558–65.
- [4] Krishnamoorti R, Vaia RA. Polymer nanocomposites: synthesis, characterization, and modeling. Washington, DC: American Chemical Society; 2001.
- [5] Alexandre M, Dubois P. Polymer–layered silicate nanocomposites: preparation, properties and uses of a new class of materials. *Mater Sci Eng R* 2000;28:1–63.
- [6] Ray SS, Okamoto M. Polymer/layered silicate nanocomposites: a review from preparation to processing. *Prog Polym Sci* 2003;28:1539–641.
- [7] Zeng QH, Yu AB, Lu GQ, Paul DR. Clay-based polymer nanocomposites: research and commercial development. *J Nanosci Nanotechnol* 2005;5:1574–92.
- [8] Komarneni S. Nanophase and nanocomposite materials IV. Warrendale: Materials Research Society; 2002.
- [9] Tjong SC. Structural and mechanical properties of polymer nanocomposites. *Mater Sci Eng R* 2006;53:73–197.
- [10] Okada A, Usuki A. Twenty years of polymer–clay nanocomposites. *Macromol Mater Eng* 2006;291: 1449–76.
- [11] Lee JY, Baljon ARC, Loring RF, Panagiotopoulos AZ. Simulation of polymer melt intercalation in layered nanocomposites. *J Chem Phys* 1998;109:10321–30.
- [12] Smith GD, Bedrov D, Li LW, Byutner O. A molecular dynamics simulation study of the viscoelastic properties of polymer nanocomposites. *J Chem Phys* 2002;117:9478–89.
- [13] Smith JS, Bedrov D, Smith GD. A molecular dynamics simulation study of nanoparticle interactions in a model polymer–nanoparticle composite. *Compos Sci Technol* 2003;63:1599–605.
- [14] Zeng QH, Yu AB, Lu GQ, Standish RK. Molecular dynamics simulation of organic-inorganic nanocomposites: layering behavior and interlayer structure of organoclays. *Chem Mater* 2003;15:4732–8.
- [15] Vacatello M. Predicting the molecular arrangements in polymer-based nanocomposites. *Macromol Theory Simul* 2003;12:86–91.
- [16] Zeng QH, Yu AB, Lu GQ. Interfacial interactions and structure of polyurethane intercalated nanocomposite. *Nanotechnology* 2005;16:2757–63.
- [17] Allen MP, Tildesley DJ. Computer simulation of liquids. Oxford: Clarendon Press; 1989.
- [18] Frenkel D, Smit B. Understanding molecular simulation: from algorithms to applications. 2nd ed. San Diego: Academic Press; 2002.
- [19] Metropolis N, Rosenbluth AW, Marshall N, Rosenbluth MN, Teller AT. Equation of state calculations by fast computing machines. *J Chem Phys* 1953;21:1087–92.
- [20] Carmesin I, Kremer K. The bond fluctuation method: a new effective algorithm for the dynamics of polymers in all spatial dimensions. *Macromolecules* 1988;21:2819–23.
- [21] Hoogerbrugge PJ, Koelman JMVA. Simulating microscopic hydrodynamic phenomena with dissipative particle dynamics. *Europhys Lett* 1992;19:155–60.
- [22] Gibson JB, Chen K, Chynoweth S. Simulation of particle adsorption onto a polymer-coated surface using the

- dissipative particle dynamics method. *J Colloid Interface Sci* 1998;206:464–74.
- [23] Dzwinel V, Yuen DA. A two-level, discrete particle approach for large-scale simulation of colloidal aggregates. *Int J Mod Phys C* 2000;11:1037–61.
- [24] Dzwinel W, Yuen DA. A two-level, discrete-particle approach for simulating ordered colloidal structures. *J Colloid Interface Sci* 2000;225:179–90.
- [25] Chen S, Doolen GD. Lattice Boltzmann method for fluid flows. *Annu Rev Fluid Mech* 1998;30:329–64.
- [26] Cahn JW. On spinodal decomposition. *Acta Metall* 1961;9:795–801.
- [27] Cahn JW, Hilliard JE. Spinodal decomposition: a reprise. *Acta Metall* 1971;19:151–61.
- [28] Cahn JW. Free energy of a nonuniform system. II. Thermodynamic basis. *J Chem Phys* 1959;30:1121–4.
- [29] Lee BP, Douglas JF, Glotzer SC. Filler-induced composition waves in phase-separating polymer blends. *Phys Rev E* 1999;60:5812–22.
- [30] Oono Y, Puri S. Study of phase-separation dynamics by use of cell dynamical-systems. I. Modeling. *Phys Rev A* 1988; 38:434–53.
- [31] Bahiana M, Oono Y. Cell dynamic system approach to block copolymers. *Phys Rev A* 1990;41:6763–71.
- [32] Ginzburg VV, Qiu F, Paniconi M, Peng GW, Jasnow D, Balazs AC. Simulation of hard particles in a phase-separating binary mixture. *Phys Rev Lett* 1999;82:4026–9.
- [33] Qiu F, Ginzburg VV, Paniconi M, Peng GW, Jasnow D, Balazs AC. Phase separation under shear of binary mixtures containing hard particles. *Langmuir* 1999;15: 4952–6.
- [34] Ginzburg VV, Gibbons C, Qiu F, Peng GW, Balazs AC. Modeling the dynamic behavior of diblock copolymer/particle composites. *Macromolecules* 2000;33:6140–7.
- [35] Ginzburg VV, Qiu F, Balazs AC. Three-dimensional simulations of diblock copolymer/particle composites. *Polymer* 2002;43:461–6.
- [36] He G, Balazs AC. Modeling the dynamic behavior of mixtures of diblock copolymers and dipolar nanoparticles. *J Comput Theor Nanosci* 2005;2:99–107.
- [37] Altevogt P, Ever OA, Fraaije JGEM, Maurits NM, van Vlimmeren BAC. The MesoDyn project: software for mesoscale chemical engineering. *J Mol Struct* 1999;463: 139–43.
- [38] Kawakatsu T, Doi M, Hasegawa A. Dynamic density functional approach to phase separation dynamics of polymer systems. *Int J Mod Phys C* 1999;10:1531–40.
- [39] Morita H, Kawakatsu T, Doi M. Dynamic density functional study on the structure of thin polymer blend films with a free surface. *Macromolecules* 2001;34:8777–83.
- [40] Doi M. OCTA-a free and open platform and softwares of multiscale simulation for soft materials <<http://octa.jp/>>. 2002.
- [41] Tucker III CL, Liang E. Stiffness predictions for unidirectional short-fiber composites: review and evaluation. *Compos Sci Technol* 1999;59:655–71.
- [42] Tandon GP, Weng GJ. The effect of aspect ratio of inclusions on the elastic properties of unidirectionally aligned composites. *Polym Compos* 1984;5:327–33.
- [43] Fornes TD, Paul DR. Modeling properties of nylon 6/clay nanocomposites using composite theories. *Polymer* 2003; 44:4993–5013.
- [44] Odegard GM, Pipes RB, Hubert P. Comparison of two models of SWCN polymer composites. *Compos Sci Technol* 2004;64:1011–20.
- [45] Odegard GM, Gates TS, Wise KE, Park C, Siochi EJ. Constitutive modeling of nanotube-reinforced polymer composites. *Compos Sci Technol* 2003;63:1671–87.
- [46] Pipes RB, Hubert P. Helical carbon nanotube arrays: mechanical properties. *Compos Sci Technol* 2002;62: 419–28.
- [47] Rudd RE, Broughton JQ. Concurrent coupling of length scales in solid state systems. *Phys Stat Sol B* 2000;217: 251–91.
- [48] Starr FW, Glotzer SC. Simulations of filled polymers on multiple length scales, In: Nakatani AI, Hjelm RP, Gerspacher M, Krishnamoorti R, editors. *Filled and nanocomposite polymer materials*, Materials research symposium proceedings. Warrendale: Materials Research Society, 2001. p. KK4.1.1–KK4.1.13.
- [49] Glotzer SC, Starr FW. Towards multiscale simulations of filled and nanofilled polymers, In: Cummings PT, Westmoreland PR, Carnahan B, editors. *Foundations of molecular modeling and simulation: Proceedings of the 1st international conference on molecular modeling and simulation*. Keystone: American Institute of Chemical Engineers, 2001. p. 44–53.
- [50] Vaia RA, Giannelis EP. Polymer melt intercalation in organically-modified layered silicates: model predictions and experiment. *Macromolecules* 1997;30:8000–9.
- [51] Vaia RA, Giannelis EP. Lattice model of polymer melt intercalation in organically-modified layered silicates. *Macromolecules* 1997;30:7990–9.
- [52] Balazs AC, Singh C, Zhulina E. Modeling the interactions between polymers and clay surfaces through self-consistent field theory. *Macromolecules* 1998;31:8370–81.
- [53] Tanaka G, Goettler LA. Predicting the binding energy for nylon 6,6/clay nanocomposites by molecular modeling. *Polymer* 2002;43:541–53.
- [54] Fermeglia M, Ferrone M, Prich S. Computer simulation of nylon-6/organoclay nanocomposites: prediction of the binding energy. *Fluid Phase Equilib* 2003;212:315–29.
- [55] Scheutjens J, Fleer GJ. Statistical-theory of the adsorption of interacting chain molecules. 1. Partition-function, segment density distribution, and adsorption-isotherms. *J Phys Chem* 1979;83:1619–35.
- [56] Scheutjens J, Fleer GJ. Statistical-theory of the adsorption of interacting chain molecules. 2. Train, loop, and tail size distribution. *J Phys Chem* 1980;84:178–90.
- [57] Carignano MA, Szleifer I. Statistical thermodynamic theory of grafted polymeric layers. *J Chem Phys* 1993;98: 5006–18.
- [58] Balazs AC, Singh C, Zhulina E, Lyatskaya Y. Modeling the phase behavior of polymer/clay nanocomposites. *Acc Chem Res* 1999;32:651–7.
- [59] Zhulina E, Singh C, Balazs AC. Attraction between surfaces in a polymer melt containing telechelic chains: guidelines for controlling the surface separation in intercalated polymer-clay composites. *Langmuir* 1999;15: 3935–43.
- [60] Huh J, Balazs AC. Behavior of confined telechelic chains under shear. *J Chem Phys* 2000;113:2025–31.
- [61] Kuznetsov DV, Balazs AC. Scaling theory for end-functionalized polymers confined between two surfaces:

- predictions for fabricating polymer/clay nanocomposites. *J Chem Phys* 2000;112:4365–75.
- [62] Kuznetsov DV, Balazs AC. Phase behavior of end-functionalized polymers confined between two surfaces. *J Chem Phys* 2000;113:2479–83.
- [63] Groenewold J, Fredrickson GH. Elastic interactions and stability of clay-filled lamellar phases. *Eur Phys J E* 2001;5:171–82.
- [64] Kudryavtsev YV, Govorun EN, Litmanovich AD, Fischer HR. Polymer melt intercalation in clay modified by diblock copolymers. *Macromol Theory Simul* 2004;13:392–9.
- [65] Reister E, Fredrickson GH. Nanoparticles in a diblock copolymer background: the potential of mean force. *Macromolecules* 2004;37:4718–30.
- [66] Kim Y, White JL. Modeling of polymer/clay nanocomposite formation. *J Appl Polym Sci* 2006;101:1657–63.
- [67] Toth R, Ferrone M, Miertus S, Chiellini E, Fermeglia M, Pricl S. Structure and energetics of biocompatible polymer nanocomposite systems: a molecular dynamics study. *Biomacromolecules* 2006;7:1714–9.
- [68] Bedrov D, Smith GD, Smith JS. Matrix-induced nanoparticle interactions in a polymer melt: a molecular dynamics simulation study. *J Chem Phys* 2003;119:10438–47.
- [69] Baljon ARC, Lee JY, Loring RF. Molecular view of polymer flow into a strongly attractive slit. *J Chem Phys* 1999;111:9068–72.
- [70] Balazs AC, Ginzburg VV, Qiu F, Peng GW, Jasnow D. Multi-scale model for binary mixtures containing nanoscopic particles. *J Phys Chem B* 2000;104:3411–22.
- [71] Ginzburg VV, Peng G, Qiu F, Jasnow D, Balazs AC. Kinetic model of phase separation in binary mixtures with hard mobile impurities. *Phys Rev E* 1999;60:4352–9.
- [72] Gendelman OV, Manevitch LI, Manevitch OL. Solitonic mechanism of structural transition in polymer-clay nanocomposites. *J Chem Phys* 2003;119:1066–9.
- [73] Ginzburg VV, Gendelman OV, Manevitch LI. Simple “kink” model of melt intercalation in polymer-clay nanocomposites. *Phys Rev Lett* 2001;86:5073–5.
- [74] Vaia RA, Jandt KD, Kramer EJ, Giannelis EP. Kinetics of polymer melt intercalation. *Macromolecules* 1995;28:8080–5.
- [75] Lee JY, Baljon ARC, Loring RF. Spontaneous swelling of layered nanostructures by a polymer melt. *J Chem Phys* 1999;111:9754–60.
- [76] Lee JY, Baljon ARC, Sogah DY, Loring RF. Molecular dynamics study of the intercalation of diblock copolymers into layered silicates. *J Chem Phys* 2000;112:9112–9.
- [77] Cheng MH, Balazs AC, Yeung C, Ginzburg VV. Modeling reactive compatibilization of a binary blend with interacting particles. *J Chem Phys* 2003;118:9044–52.
- [78] Anderson KL, Sinsawat A, Vaia RA, Farmer BL. Control of silicate nanocomposite morphology in binary fluids: Coarse-grained molecular dynamics simulations. *J Polym Sci Part B: Polym Phys* 2005;43:1014–24.
- [79] Pinnavaia TJ, Beall GW. Polymer-clay nanocomposites. London: Wiley; 2000.
- [80] Sharaf MA, Mark JE. Monte Carlo simulations on the effects of nanoparticles on chain deformations and reinforcement in amorphous polyethylene networks. *Polymer* 2004;45:3943–52.
- [81] Kloczkowski A, Sharaf MA, Mark JE. Computer-simulations on filled elastomeric materials. *Chem Eng Sci* 1994;49:2889–97.
- [82] Yuan QW, Kloczkowski A, Mark JE, Sharaf MA. Simulations on the reinforcement of poly(dimethylsiloxane) elastomers by randomly distributed filler particles. *J Polym Sci Part B: Polym Phys* 1996;34:1647–57.
- [83] Vacatello M. Monte Carlo simulations of polymer melts filled with solid nanoparticles. *Macromolecules* 2001;34:1946–52.
- [84] Starr FW, Schroder TB, Glotzer SC. Molecular dynamics simulation of a polymer melt with a nanoscopic particle. *Macromolecules* 2002;35:4481–92.
- [85] Starr FW, Schroder TB, Glotzer SC. Effects of a nanoscopic filler on the structure and dynamics of a simulated polymer melt and the relationship to ultrathin films. *Phys Rev E* 2001;6402.
- [86] Odegard GM, Clancy TC, Gates TS. Modeling of the mechanical properties of nanoparticle/polymer composites. *Polymer* 2005;46:553–62.
- [87] Hackett E, Manias E, Giannelis EP. Computer simulation studies of PEO/layer silicate nanocomposites. *Chem Mater* 2000;12:2161–7.
- [88] Vacatello M. Chain dimensions in filled polymers: an intriguing problem. *Macromolecules* 2002;35:8191–3.
- [89] Ozmusul MS, Picu RC. Structure of polymers in the vicinity of convex impenetrable surfaces: the athermal case. *Polymer* 2002;43:4657–65.
- [90] Picu RC, Ozmusul MS. Structure of linear polymeric chains confined between impenetrable spherical walls. *J Chem Phys* 2003;118:11239–48.
- [91] Ozmusul MS, Picu CR, Sternstein SS, Kumar SK. Lattice Monte Carlo simulations of chain conformations in polymer nanocomposites. *Macromolecules* 2005;38:4495–500.
- [92] Vacatello M. Monte Carlo simulations of the interface between polymer melts and solids. Effects of chain stiffness. *Macromol Theory Simul* 2001;10:187–95.
- [93] Vacatello M. Phantom chain simulations of polymer-nanofiller systems. *Macromolecules* 2003;36:3411–6.
- [94] Vacatello M. Phantom chain simulations of realistically sized polymer-based nanocomposites. *Macromol Theory Simul* 2006;15:303–10.
- [95] Breu J, Raj N, Catlow CRA. Chiral recognition among trisdiimine-metal complexes, Part 4. Atomistic computer modeling of $[\text{Ru}(\text{bpy})_3]^{2+}$ and $[\text{Ru}(\text{phen})_3]^{2+}$ intercalated into low charged smectites. *J Chem Soc, Dalton Trans* 1999;835–45.
- [96] Kuppa V, Menakanit S, Krishnamoorti R, Manias E. Simulation insights on the structure of nanoscopically confined poly(ethylene oxide). *J Polym Sci Part B: Polym Phys* 2003;41:3285–98.
- [97] Manias E, Kuppa V, Yang DK, Zax DB. Relaxation of polymers in 2 nm slit-pores: confinement induced segmental dynamics and suppression of the glass transition. *Colloids Surf, A* 2001;187:509–21.
- [98] Boulet P, Covency PV, Stackhouse S. Simulation of hydrated Li^{+} , Na^{+} - and K^{+} -montmorillonite/polymer nanocomposites using large-scale molecular dynamics. *Chem Phys Lett* 2004;389:261–7.
- [99] Yang DK, Zax DB. Li^{+} dynamics in a polymer nanocomposite: an analysis of dynamic line shapes in nuclear magnetic resonance. *J Chem Phys* 1999;110:5325–36.

- [100] Gaudel-Siri A, Brocorens P, Siri D, Gardeben F, Bredas JL, Lazzaroni R. Molecular dynamics study of epsilon-caprolactone intercalated in Wyoming sodium montmorillonite. *Langmuir* 2003;19:8287–91.
- [101] Gardeben F, Bredas JL, Lazzaroni R. Molecular dynamics simulations of nanocomposites based on poly(epsilon-caprolactone) grafted on montmorillonite clay. *J Phys Chem B* 2005;109:12287–96.
- [102] Sikdar D, Katti DR, Katti KS. A molecular model for epsilon-caprolactam-based intercalated polymer clay nanocomposite: integrating modeling and experiments. *Langmuir* 2006;22:7738–47.
- [103] Katti KS, Sikdar D, Katti DR, Ghosh P, Verma D. Molecular interactions in intercalated organically modified clay and clay–polycaprolactam nanocomposites: experiments and modeling. *Polymer* 2006;47:403–14.
- [104] Zeng QH, Yu AB, Lu GQ, Standish RK. Molecular dynamics simulation of the structural and dynamic properties of dioctadecyltrimethyl ammonium in organoclays. *J Phys Chem B* 2004;108:10025–33.
- [105] Paul DR, Zeng QH, Yu AB, Lu GQ. The interlayer swelling and molecular packing in organoclays. *J Colloid Interface Sci* 2005;292:462–8.
- [106] Zeng QH, Yu AB, Lu GQ, Standish RK. Interfacial interactions and structure of organic-inorganic nanohybrids. *J Mater Sci Technol* 2005;21:114–8.
- [107] Greenwell HC, Harvey MJ, Boulet P, Bowden AA, Coveney PV, Whiting A. Interlayer structure and bonding in nonswelling primary amine intercalated clays. *Macromolecules* 2005;38:6189–200.
- [108] Heinz H, Vaia RA, Krishnamoorti R, Farmer BL. Self-assembly of alkylammonium chains on montmorillonite: effect of chain length, head group structure, and cation exchange capacity. *Chem Mater* 2007;19:59–68.
- [109] Krishnamoorti R, Vaia RA, Giannelis EP. Structure and dynamics of polymer-layered silicate nanocomposites. *Chem Mater* 1996;8:1728–34.
- [110] Manias E, Subbotin A, Hadzioannou G, Tenbrinke G. Adsorption–desorption kinetics in nanoscopically confined oligomer films under shear. *Mol Phys* 1995;85:1017–32.
- [111] Bitsanis IA, Pan CM. The origin of glassy dynamics at solid oligomer interfaces. *J Chem Phys* 1993;99:5520–7.
- [112] Manias E, Hadzioannou G, tenBrinke G. Inhomogeneities in sheared ultrathin lubricating films. *Langmuir* 1996;12:4587–93.
- [113] He HP, Galy J, Gerard JF. Molecular simulation of the interlayer structure and the mobility of alkyl chains in HDTMA⁺/montmorillonite hybrids. *J Phys Chem B* 2005;109:13301–6.
- [114] Picu RC, Rakshit A. Dynamics of free chains in polymer nanocomposites. *J Chem Phys* 2007;126:144909.
- [115] Desai T, Kebinski P, Kumar S. Molecular dynamics simulations of polymer transport in nanocomposites. *J Chem Phys* 2005;122:134910.
- [116] Huang JH, Mao ZF, Qian CJ. Dynamic Monte Carlo study on the polymer chain in random media filled with nanoparticles. *Polymer* 2006;47:2928–32.
- [117] Crosby AJ, Lee JY. Polymer nanocomposites: the “nano” effect on mechanical properties. *Polym Rev* 2007;47:217–29.
- [118] de Villoria RG, Miravete A. Mechanical model to evaluate the effect of the dispersion in nanocomposites. *Acta Mater* 2007;55:3025–31.
- [119] Travasso RDM, Buxton GA, Kuksenok O, Good K, Balazs AC. Modeling the morphology and mechanical properties of sheared ternary mixtures. *J Chem Phys* 2005;122:194906.
- [120] Shou ZY, Buxton GA, Balazs AC. Predicting the self-assembled morphology and mechanical properties of mixtures of diblocks and rod-like nanoparticles. *Compos Interfaces* 2003;10:343–68.
- [121] Yung KC, Wang J, Yue TM. Modeling Young’s modulus of polymer–layered silicate nanocomposites using a modified Halpin–Tsai micromechanical model. *J Rein Plast Compos* 2006;25:847–61.
- [122] Zhou JH, Zhu RX, Zhou JM, Chen MB. Molecular dynamics simulation of diffusion of gases in pure and silica-filled poly(1-trimethylsilyl-1-propyne) [PTMSP]. *Polymer* 2006;47:5206–12.
- [123] Xue LP, Borodin O, Smith GD. Modeling of enhanced penetrant diffusion in nanoparticle–polymer composite membranes. *J Membr Sci* 2006;286:293–300.
- [124] Sorrentino A, Tortora M, Vittoria V. Diffusion behavior in polymer–clay nanocomposites. *J Polym Sci Part B: Polym Phys* 2006;44:265–74.
- [125] Lu CS, Mai YW. Influence of aspect ratio on barrier properties of polymer–clay nanocomposites. *Phys Rev Lett* 2005;95:088303.
- [126] Dalmas F, Dendievel R, Chazeau L, Cavaille JY, Gauthier C. Carbon nanotube-filled polymer of electrical conductivity in composites. Numerical simulation three-dimensional entangled fibrous networks. *Acta Mater* 2006;54:2923–31.
- [127] Asakura S, Oosawa F. On interaction between 2 bodies immersed in a solution of macromolecules. *J Chem Phys* 1954;22:1255–6.
- [128] Vrij A. Polymers at interfaces and interactions in colloidal dispersions. *Pure Appl Chem* 1976;48:471–83.
- [129] Poon WCK, Selje JS, Robertson MB, Ilett SM, Pirie AD, Pusey PN. An experimental-study of a model colloid–polymer mixture. *J Phys II* 1993;3:1075–86.
- [130] Meijer EJ, Frenkel D. Computer-simulation of polymer-induced clustering of colloids. *Phys Rev Lett* 1991;67:1110–3.
- [131] Lekkerkerker HNW, Poon WCK, Pusey PN, Stroobants A, Warren PB. Phase-behavior of colloid plus polymer mixtures. *Europhys Lett* 1992;20:559–64.
- [132] Meijer EJ, Frenkel D. Colloids dispersed in polymer solutions—a computer simulation study. *J Chem Phys* 1994;100:6873–87.
- [133] Dijkstra M, vanRoij R. Entropy-drive demixing in binary hard-core mixtures: from hard spherocylinders towards hard spheres. *Phys Rev E* 1997;56:5594–602.
- [134] Adams M, Dogic Z, Keller SL, Fraden S. Entropically driven microphase transitions in mixtures of colloidal rods and spheres. *Nature* 1998;393:349–52.
- [135] Bolhuis PG, Stroobants A, Frenkel D, Lekkerkerker HNW. Numerical study of the phase behavior of rodlike colloids with attractive interactions. *J Chem Phys* 1997;107:1551–64.
- [136] Ginzburg VV, Singh C, Balazs AC. Theoretical phase diagrams of polymer/clay composites: the role of grafted organic modifiers. *Macromolecules* 2000;33:1089–99.
- [137] Lyatskaya Y, Balazs AC. Modeling the phase behavior of polymer–clay composites. *Macromolecules* 1998;31:6676–80.

- [138] Onsager L. The effects of shape on the interaction of colloidal particles. *Ann NY Acad Sci* 1949;51:627–59.
- [139] Ginzburg VV, Balazs AC. Calculating phase diagrams of polymer–platelet mixtures using density functional theory: implications for polymer/clay composites. *Macromolecules* 1999;32:5681–8.
- [140] Ginzburg VV, Balazs AC. Calculating phase diagrams for nanocomposites: the effect of adding end-functionalized chains to polymer/clay mixtures. *Adv Mater* 2000;12:1805–9.
- [141] Schweizer KS, Yethiraj A. Polymer reference interaction site model theory: new molecular closures for phase separating fluids and alloys. *J Chem Phys* 1993;98:9053–79.
- [142] Hooper JB, Schweizer KS, Desai TG, Koshy R, Kebinski P. Structure, surface excess and effective interactions in polymer nanocomposite melts and concentrated solutions. *J Chem Phys* 2004;121:6986–97.
- [143] Hooper JB, Schweizer KS. Contact aggregation, bridging, and steric stabilization in dense polymer–particle mixtures. *Macromolecules* 2005;38:8858–69.
- [144] Hooper JB, Schweizer KS. Theory of phase separation in polymer nanocomposites. *Macromolecules* 2006;39:5133–42.
- [145] Zhao L, Li YG, Zhong CL. Integral equation theory study on the structure and effective interactions in star polymer nanocomposite melts. *J Chem Phys* 2007;126:014906.
- [146] Zhao L, Li YG, Zhong C, Mi J. Structure and effective interactions in polymer nanocomposite melts: an integral equation theory study. *J Chem Phys* 2006;124:144913.
- [147] Zhao L, Li YG, Mi JG, Zhong CL. Integral equation theory for atactic polystyrene melt with a coarse-grained model. *J Chem Phys* 2005;123:124905.
- [148] Tanaka H, Lovinger AJ, Davis DD. Pattern evolution caused by dynamic coupling between wetting and phase separation in binary liquid mixture containing glass particles. *Phys Rev Lett* 1994;72:2581.
- [149] Qiu F, Peng G, Ginzburg VV, Balazs AC, Chen HY, Jasnow D. Spinodal decomposition of a binary fluid with fixed impurities. *J Chem Phys* 2001;115:3779–84.
- [150] Suppa D, Kuksenok O, Balazs AC, Yeomans JM. Phase separation of a binary fluid in the presence of immobile particles: a lattice Boltzmann approach. *J Chem Phys* 2002;116:6305–10.
- [151] Karim A, Douglas JF, Nisato G, Liu DW, Amis EJ. Transient target patterns in phase separating filled polymer blends. *Macromolecules* 1999;32:5917–24.
- [152] Dennis HR, Hunter DL, Chang D, Kim S, White JL, Cho JW, et al. Effect of melt processing conditions on the extent of exfoliation in organoclay-based nanocomposites. *Polymer* 2001;42:9513–22.
- [153] Forner TD, Yoon PJ, Keskkula H, Paul DR. Nylon 6 nanocomposites: the effect of matrix molecular weight. *Polymer* 2001;42:9929–40.
- [154] Forner TD, Yoon PJ, Hunter DL, Keskkula H, Paul DR. Effect of organoclay structure on nylon 6 nanocomposite morphology and properties. *Polymer* 2002;43:5915–33.
- [155] Dijkstra M, Hansen JP, Madden PA. Statistical model for the structure and gelation of smectite clay suspensions. *Phys Rev E* 1997;55:3044–53.
- [156] Maiti A, Wescott J, Kung P. Nanotube–polymer composites: insights from Flory–Huggins theory and mesoscale simulations. *Mol Simul* 2005;31:143–9.
- [157] Soo PP, Huang BY, Jang YI, Chiang YM, Sadoway DR, Mayes AM. Rubbery block copolymer electrolytes for solid-state rechargeable lithium batteries. *J Electrochem Soc* 1999;146:32–7.
- [158] Hasegawa N, Okamoto H, Kawasumi M, Usuki A. Preparation and mechanical properties of polystyrene–clay hybrids. *J Appl Polym Sci* 1999;74:3359–64.
- [159] Lin BH, Morkved TL, Meron M, Huang ZQ, Viccaro PJ, Jaeger HM, et al. X-ray studies of polymer/gold nanocomposites. *J Appl Phys* 1999;85:3180–4.
- [160] Cole DH, Shull KR, Baldo P, Rehn L. Dynamic properties of a model polymer/metal nanocomposite: gold particles in poly(tert-butyl acrylate). *Macromolecules* 1999;32:771–9.
- [161] Morkved TL, Wiltzius P, Jaeger HM, Grier DG, Witten TA. Mesoscopic self-assembly of gold islands in diblock-copolymer films. *Appl Phys Lett* 1994;64:422–4.
- [162] Zehner RW, Lopes WA, Morkved TL, Jaeger H, Sita LR. Selective decoration of a phase-separated diblock copolymer with thiol-passivated gold nanocrystals. *Langmuir* 1998;14:241–4.
- [163] Lauter-Pasyuk V, Lauter HJ, Ausserer D, Gallot Y, Cabuil V, Kornilov EI, et al. Effect of nanoparticle size on the internal structure of copolymer–nanoparticles composite thin films studied by neutron reflection. *Physica B* 1997;241:1092–4.
- [164] Sevink GJA, Zvelindovsky AV, van Vlimmeren BAC, Maurits NM, Fraaije JGEM. Dynamics of surface directed mesophase formation in block copolymer melts. *J Chem Phys* 1999;110:2250–6.
- [165] Huh J, Ginzburg VV, Balazs AC. Thermodynamic behavior of particle/diblock copolymer mixtures: Simulation and theory. *Macromolecules* 2000;33:8085–96.
- [166] Oberdisse J, Hine P, Pyckhout-Hintzen W. Structure of interacting aggregates of silica nanoparticles in a polymer matrix: small-angle scattering and reverse Monte Carlo simulations. *Soft Matter* 2007;3:476–85.
- [167] Zhang X, Zhang ZL, Glotzer SC. Simulation study of cyclic-tethered nanocube self-assemblies: effect of tethered nanocube architectures. *Nanotechnology* 2007;18:115706.
- [168] Thompson RB, Ginzburg VV, Matsen MW, Balazs AC. Block copolymer-directed assembly of nanoparticles: forming mesoscopically ordered hybrid materials. *Macromolecules* 2002;35:1060–71.
- [169] Lee JY, Thompson RB, Jasnow D, Balazs AC. Entropically driven formation of hierarchically ordered nanocomposites. *Phys Rev Lett* 2002;89:155503.
- [170] Thompson RB, Lee JY, Jasnow D, Balazs AC. Binary hard sphere mixtures in block copolymer melts. *Phys Rev E* 2002;66:031801.
- [171] Lee JY, Thompson RB, Jasnow D, Balazs AC. Effect of nanoscopic particles on the mesophase structure of diblock copolymers. *Macromolecules* 2002;35:4855–8.
- [172] Sides SW, Kim BJ, Kramer EJ, Fredrickson GH. Hybrid particle-field simulations of polymer nanocomposites. *Phys Rev Lett* 2006;96:250601.
- [173] Fraaije J, van Vlimmeren BAC, Maurits NM, Postma M, Evers OA, Hoffmann C, et al. The dynamic mean-field density functional method and its application to the mesoscopic dynamics of quenched block copolymer melts. *J Chem Phys* 1997;106:4260–9.
- [174] Zvelindovsky AVM, van Vlimmeren BAC, Sevink GJA, Maurits NM, Fraaije J. Three-dimensional simulation of

- hexagonal phase of a specific polymer system under shear: the dynamic density functional approach. *J Chem Phys* 1998;109:8751–4.
- [175] Zvelindovsky AV, Sevink GJA, van Vlimmeren BAC, Maurits NM, Fraaije J. Three-dimensional mesoscale dynamics of block copolymers under shear: the dynamic density-functional approach. *Phys Rev E* 1998;57: R4879–82.
- [176] Hamdoun B, Ausserre D, Joly S, Gallot Y, Cabuil V, Clinard C. New nanocomposite materials. *J Phys II* 1996;6:493–501.
- [177] Thompson RB, Ginzburg VV, Matsen MW, Balazs AC. Predicting the mesophases of copolymer–nanoparticle composites. *Science* 2001;292:2469–72.
- [178] Buxton GA, Lee JY, Balazs AC. Computer simulation of morphologies and optical properties of filled diblock copolymers. *Macromolecules* 2003;36:9631–7.
- [179] Sumita M, Sakata K, Asai S, Miyasaka K, Nakagawa H. Dispersion of fillers and the electrical-conductivity of polymer blends filled with carbon-black. *Polym Bull* 1991; 25:265–71.
- [180] Sumita M, Sakata K, Hayakawa Y, Asai S, Miyasaka K, Tanemura M. Double percolation effect on the electrical-conductivity of conductive particles filled polymer blends. *Colloid Polym Sci* 1992;270:134–9.
- [181] Lux F. Models proposed to explain the electrical-conductivity of mixtures made of conductive and insulating materials. *J Mater Sci* 1993;28:285–301.
- [182] Wescott JT, Kung P, Maiti A. Conductivity of carbon nanotube polymer composites. *Appl Phys Lett* 2007;90: 033116.
- [183] Lee JY, Thompson RB, Jasnow D, Balazs AC. Self-assembly of a binary mixture of particles and diblock copolymers. *Faraday Discuss* 2003;123:121–31.
- [184] Liu DH, Zhong CL. Cooperative self-assembly of nanoparticle mixtures in lamellar diblock copolymers: a dissipative particle dynamics study. *Macromol Rapid Commun* 2006;27:458–62.
- [185] Peng GW, Qiu F, Ginzburg VV, Jasnow D, Balazs AC. Forming supramolecular networks from nanoscale rods in binary, phase-separating mixtures. *Science* 2000;288: 1802–4.
- [186] Buxton GA, Balazs AC. Predicting the mechanical and electrical properties of nanocomposites formed from polymer blends and nanorods. *Mol Simul* 2004;30:249–57.
- [187] He G, Ginzburg VV, Balazs AC. Determining the phase behavior of nanoparticle-filled binary blends. *J Polym Sci Part B: Polym Phys* 2006;44:2389–403.
- [188] Chervanyov AI, Balazs AC. Effect of particle size and shape on the order–disorder phase transition in diblock copolymers. *J Chem Phys* 2003;119:3529–34.
- [189] Jain A, Gutmann JS, Garcia CBW, Zhang YM, Tate MW, Gruner SM, et al. Effect of filler dimensionality on the order–disorder transition of a model block copolymer nanocomposite. *Macromolecules* 2002;35:4862–5.
- [190] Kotov NA. Ordered layered assemblies of nanoparticles. *MRS Bull* 2001;26:992–7.
- [191] Decher G. Fuzzy nanoassemblies: toward layered polymeric multicomposites. *Science* 1997;277:1232–7.
- [192] Fasolka MJ, Mayes AM. Block copolymer thin films: physics and applications. *Annu Rev Mater Res* 2001;31: 323–55.
- [193] Lee JY, Shou Z, Balazs AC. Modeling the self-assembly of copolymer–nanoparticle mixtures confined between solid surfaces. *Phys Rev Lett* 2003;91:136103.
- [194] Lee JY, Shou ZY, Balazs AC. Predicting the morphologies of confined copolymer/nanoparticle mixtures. *Macromolecules* 2003;36:7730–9.
- [195] Subbotin A, Semenov A, Hadzioannou G, Tenbrinke G. Rheology of confined polymer melts under shear flow-weak adsorption limit. *Macromolecules* 1995;28:3901–3.
- [196] Subbotin A, Semenov A, Manias E, Hadzioannou G, Tenbrinke G. Rheology of confined polymer melts under shear flow-strong adsorption limit. *Macromolecules* 1995; 28:1511–5.
- [197] Homola AM, Nguyen HV, Hadzioannou G. Influence of monomer architecture on the shear properties of molecularly thin polymer melts. *J Chem Phys* 1991;94: 2346–51.
- [198] Hu HW, Carson GA, Granick S. Relaxation-time of confined liquids under shear. *Phys Rev Lett* 1991;66: 2758–61.
- [199] Thompson PA, Grest GS, Robbins MO. Phase-transitions and universal dynamics in confined films. *Phys Rev Lett* 1992;68:3448–51.
- [200] Israelachvili J, McGuigan P, Gee M, Homola A, Robbins M, Thompson P. Liquid dynamics in molecularly thin-films. *J Phys: Condens Matter* 1990;2:SA89–98.
- [201] van Alsten J, Granick S. Shear rheology in a confined geometry—polysiloxane melts. *Macromolecules* 1990;23: 4856–62.
- [202] Bitsanis I, Hadzioannou G. Molecular dynamics simulations of the structure and dynamics of confined polymer melts. *J Chem Phys* 1990;92:3827–47.
- [203] Subbotin A, Semenov A, Hadzioannou G, tenBrinke G. Nonlinear rheology of confined polymer melts under oscillatory flow. *Macromolecules* 1996;29:1296–304.
- [204] Boek ES, Coveney PV, Lekkerkerker HNW, van der Schoot P. Simulating the rheology of dense colloidal suspensions using dissipative particle dynamics. *Phys Rev E* 1997;55:3124–33.
- [205] Ruths M, Granick S. Tribology of confined Fomblin-Z perfluoropolyalkyl ethers: role of chain-end chemical functionality. *J Phys Chem B* 1999;103:8711–21.
- [206] Ruths M, Granick S. Tribology of confined Fomblin-Z perfluoropolyalkylethers: molecular weight dependence and comparison between unfunctionalized and telechelic chains. *Tribol Lett* 1999;7:161–72.
- [207] Krishnamoorti R, Ren JX, Silva AS. Shear response of layered silicate nanocomposites. *J Chem Phys* 2001;114: 4968–73.
- [208] Havet G, Isayev AI. A thermodynamic approach to the rheology of highly interactive filler–polymer mixtures: Part I—theory. *Rheol Acta* 2001;40:570–81.
- [209] Havet G, Isayev AI. A thermodynamic approach to the rheology of highly interactive filler–polymer mixtures. Part II. Comparison with polystyrene/nanosilica mixtures. *Rheol Acta* 2003;42:47–55.
- [210] Starr FW, Douglas JF, Glotzer SC. Origin of particle clustering in a simulated polymer nanocomposite and its impact on rheology. *J Chem Phys* 2003;119:1777–88.
- [211] Pyramidsyn V, Ganesan V. Mechanisms of steady-shear rheology in polymer-nanoparticle composites. *J Rheol* 2006;50:655–83.

- [212] Sarvestani AS, Picu CR. Network model for the viscoelastic behavior of polymer nanocomposites. *Polymer* 2004;45:7779–90.
- [213] Song YS, Youn JR. Modeling of rheological behavior of nanocomposites by Brownian dynamics simulation. *Korea—Aust Rheol J* 2004;16:201–12.
- [214] Pyrz R. Atomistic/continuum transition—the concept of atomic strain tensor. In: Liu HY, Hu XZ, Hoffman M, editors. *Fracture of materials: moving forwards*. Switzerland: Trans Tech Publications; 2006. p. 193–8.
- [215] Wang YR, Xu JH, Bechtel SE, Koelling KW. Melt shear rheology of carbon nanofiber/polystyrene composites. *Rheol Acta* 2006;45:919–41.
- [216] Ghoniem NM, Busso EP, Kioussis N, Huang HC. Multi-scale modelling of nanomechanics and micromechanics: an overview. *Philos Mag* 2003;83:3475–528.
- [217] Brechet Y, Cavaille JYY, Chabert E, Chazeau L, Dendievel R, Flandin L, et al. Polymer based nanocomposites: effect of filler–filler and filler–matrix interactions. *Adv Eng Mater* 2001;3:571–7.
- [218] Carrado KA, Xu L. In situ synthesis of polymer–clay nanocomposites from silicate gels. *Chem Mater* 1998;10:1440–5.
- [219] Lan T, Kaviratna PD, Pinnavaia TJ. Mechanism of clay tactoid exfoliation in epoxy–clay nanocomposites. *Chem Mater* 1995;7:2144–50.
- [220] Kojima Y, Usuki A, Kawasumi M, Okada A, Kurauchi T, Kamigaito O. Synthesis of nylon 6-clay hybrid by montmorillonite intercalated with ϵ -caprolactam. *J Polym Sci, Part A: Polym Chem* 1993;31:983–6.
- [221] Kojima Y, Usuki A, Kawasumi M, Okada A, Kurauchi T, Kamigaito O. One-pot synthesis of nylon 6-clay hybrid. *J Polym Sci, Part A: Polym Chem* 1993;31:1755–8.
- [222] Salvetat JP, Bhattacharyya S, Pipes RB. Progress on mechanics of carbon nanotubes and derived materials. *J Nanosci Nanotechnol* 2006;6:1857–82.
- [223] Lau KT, Gu C, Hui D. A critical review on nanotube and nanotube/nanoclay related polymer composite materials. *Compos Part B: Eng* 2006;37:425–36.
- [224] Valavalas PK, Odegard GM. Modeling techniques for determination of mechanical properties of polymer nanocomposites. *Rev Adv Mater Sci* 2005;9:34–44.
- [225] Frankland SJV, Caglar A, Brenner DW, Griebel M. Molecular simulation of the influence of chemical cross-links on the shear strength of carbon nanotube–polymer interfaces. *J Phys Chem B* 2002;106:3046–8.
- [226] Gersappe D. Molecular mechanisms of failure in polymer nanocomposites. *Phys Rev Lett* 2002;89:058301.
- [227] Liao K, Li S. Interfacial characteristics of a carbon nanotube-polystyrene composite system. *Appl Phys Lett* 2001;79:4225–7.
- [228] Frankland SJV, Harik VM, Odegard GM, Brenner DW, Gates TS. The stress–strain behavior of polymer–nanotube composites from molecular dynamics simulation. *Compos Sci Technol* 2003;63:1655–61.
- [229] Lordi V, Yao N. Molecular mechanics of binding in carbon-nanotube–polymer composites. *J Mater Res* 2000;15:2770–9.
- [230] Wong M, Paramsothy M, Xu XJ, Ren Y, Li S, Liao K. Physical interactions at carbon nanotube–polymer interface. *Polymer* 2003;44:7757–64.
- [231] Qian D, Liu WK, Ruoff RS. Load transfer mechanism in carbon nanotube ropes. *Compos Sci Technol* 2003;63:1561–9.
- [232] Gou JH, Minaie B, Wang B, Liang ZY, Zhang C. Computational and experimental study of interfacial bonding of single-walled nanotube reinforced composites. *Comput Mater Sci* 2004;31:225–36.
- [233] Gou JH, Liang ZY, Zhang C, Wang B. Computational analysis of effect of single-walled carbon nanotube rope on molecular interaction and load transfer of nanocomposites. *Compos Part B: Eng* 2005;36:524–33.
- [234] Zhu R, Pan E, Roy AK. Molecular dynamics study of the stress–strain behavior of carbon-nanotube reinforced Epon 862 composites. *Mater Sci Eng, A* 2007;447:51–7.
- [235] Mokashi VV, Qian D, Liu YJ. A study on the tensile response and fracture in carbon nanotube-based composites using molecular mechanics. *Compos Sci Technol* 2007;67:530–40.
- [236] Zheng QB, Xue QZ, Yan KO, Hao LZ, Li Q, Gao XL. Investigation of molecular interactions between SWNT and polyethylene/polypropylene/polystyrene/polyaniline molecules. *J Phys Chem C* 2007;111:4628–35.
- [237] Prathab B, Subramanian V, Aminabhavi TM. Molecular dynamics simulations to investigate polymer–polymer and polymer–metal oxide interactions. *Polymer* 2007;48:409–16.
- [238] Aleperstein D, Artzi N, Siegmann A, Narkis M. Experimental and computational investigation of EVOH/clay nanocomposites. *J Appl Polym Sci* 2005;97:2060–6.
- [239] Suter JL, Coveney PV, Greenwell HC, Thyveetil MA. Large-scale molecular dynamics study of montmorillonite clay: emergence of undulatory fluctuations and determination of material properties. *J Phys Chem C* 2007;111:8248–59.
- [240] Capaldi FM, Boyce MC, Rutledge GC. The mechanical properties of crystalline cyclopentyl polyhedral oligomeric silsesquioxane. *J Chem Phys* 2006;124.
- [241] Patel RR, Mohanraj R, Pittman CU. Properties of polystyrene and polymethyl methacrylate copolymers of polyhedral oligomeric silsesquioxanes: a molecular dynamics study. *J Polym Sci Part B: Polym Phys* 2006;44:234–48.
- [242] Bizet S, Galy J, Gerard JF. Molecular dynamics simulation of organic–inorganic copolymers based on methacryl-POSS and methyl methacrylate. *Polymer* 2006;47:8219–27.
- [243] Pryamitsyn V, Ganesan V. Origins of linear viscoelastic behavior of polymer–nanoparticle composites. *Macromolecules* 2006;39:844–56.
- [244] Salaniwal S, Kumar SK, Douglas JF. Amorphous solidification in polymer–platelet nanocomposites. *Phys Rev Lett* 2002;89:258301.
- [245] Adnan A, Sun CT, Mahfuz H. A molecular dynamics simulation study to investigate the effect of filler size on elastic properties of polymer nanocomposites. *Compos Sci Technol* 2007;67:348–56.
- [246] Sen S, Thomin JD, Kumar SK, Kebinski P. Molecular underpinnings of the mechanical reinforcement in polymer nanocomposites. *Macromolecules* 2007;40:4059–67.
- [247] Chauve G, Heux L, Arouini R, Mazeau K. Cellulose poly(ethylene-co-vinyl acetate) nanocomposites studied by molecular modeling and mechanical spectroscopy. *Biomacromolecules* 2005;6:2025–31.

- [248] Minisini B, Tsobnang F. Molecular dynamics study of specific interactions in grafted polypropylene organomodified clay nanocomposite. *Compos Part A: Appl Sci Manuf* 2005;36:539–44.
- [249] Song M, Chen L. Molecular dynamics simulation of the fracture in polymer-exfoliated layered silicate nanocomposites. *Macromol Theory Simul* 2006;15:238–45.
- [250] Sen TZ, Sharaf MA, Mark JE, Kloczkowski A. Modeling the elastomeric properties of stereoregular polypropylenes in nanocomposites with spherical fillers. *Polymer* 2005;46:7301–8.
- [251] Kalfus J, Jancar J. Relaxation processes in PVAc-HA nanocomposites. *J Polym Sci Part B: Polym Phys* 2007;45: 1380–8.
- [252] Yoon PJ, Fornes TD, Paul DR. Thermal expansion behavior of nylon 6 nanocomposites. *Polymer* 2002;43: 6727–41.
- [253] Brune DA, Bicerano J. Micromechanics of nanocomposites: comparison of tensile and compressive elastic moduli, and prediction of effects of incomplete exfoliation and imperfect alignment on modulus. *Polymer* 2002;43:369–87.
- [254] Zheng XY, Forest MG, Lipton R, Zhou RH. Nematic polymer mechanics: flow-induced anisotropy. *Continuum Mech Therm* 2007;18:377–94.
- [255] Luo JJ, Daniel IM. Characterization and modeling of mechanical behavior of polymer/clay nanocomposites. *Compos Sci Technol* 2003;63:1607–16.
- [256] Jo C, Fu J, Naguib HE. Constitutive modeling for intercalated PMMA/clay nanocomposite foams. *Polym Eng Sci* 2006;46:1787–96.
- [257] Wu YP, Jia QX, Yu DS, Zhang LQ. Modeling Young's modulus of rubber-clay nanocomposites using composite theories. *Polym Test* 2004;23:903–9.
- [258] Li XD, Gao HS, Scrivens WA, Fei DL, Xu XY, Sutton MA, et al. Reinforcing mechanisms of single-walled carbon nanotube-reinforced polymer composites. *J Nanosci Nanotechnol* 2007;7:2309–17.
- [259] Chabert E, Dendievel R, Gauthier C, Cavaille JY. Prediction of the elastic response of polymer based nanocomposites: a mean field approach and a discrete simulation. *Compos Sci Technol* 2004;64:309–16.
- [260] Raos G, Moreno M, Elli S. Computational experiments on filled rubber viscoelasticity: what is the role of particle-particle interactions. *Macromolecules* 2006;39: 6744–51.
- [261] Buxton GA, Balazs AC. Lattice spring model of filled polymers and nanocomposites. *J Chem Phys* 2002;117: 7649–58.
- [262] Liu H, Brinson LC. A hybrid numerical-analytical method for modeling the viscoelastic properties of polymer nanocomposites. *J Appl Mech* 2006;73:758–68.
- [263] Odegard GM, Gates TS, Nicholson LM, Wise KE. Equivalent-continuum modeling of nano-structured materials. *Compos Sci Technol* 2002;62:1869–80.
- [264] Wang CY, Ru CQ, Mioduchowski A. Axially compressed buckling of pressured multiwall carbon nanotubes. *Int J Solids Struct* 2003;40:3893–911.
- [265] Pantano A, Parks DM, Boyce MC. Mechanics of deformation of single- and multi-wall carbon nanotubes. *J Mech Phys Solids* 2004;52:789–821.
- [266] Wagner HD. Nanotube–polymer adhesion: a mechanics approach. *Chem Phys Lett* 2002;361:57–61.
- [267] Li CY, Chou TW. Multiscale modeling of carbon nanotube reinforced polymer composites. *J Nanosci Nanotechnol* 2003;3:423–30.
- [268] Gao XL, Li K. A shear-lag model for carbon nanotube-reinforced polymer composites. *Int J Solids Struct* 2005;42:1649–67.
- [269] Tsai J, Sun CT. Effect of platelet dispersion on the load transfer efficiency in nanoclay composites. *J Compos Mater* 2004;38:567–79.
- [270] Fisher FT, Bradshaw RD, Brinson LC. Fiber waviness in nanotube-reinforced polymer composites-I: modulus predictions using effective nanotube properties. *Compos Sci Technol* 2003;63:1689–703.
- [271] Bradshaw RD, Fisher FT, Brinson LC. Fiber waviness in nanotube-reinforced polymer composites-II: modeling via numerical approximation of the dilute strain concentration tensor. *Compos Sci Technol* 2003;63:1705–22.
- [272] Ashrafi B, Hubert P. Modeling the elastic properties of carbon nanotube array/polymer composites. *Compos Sci Technol* 2006;66:387–96.
- [273] Song YS, Youn JR. Modeling of effective elastic properties for polymer based carbon nanotube composites. *Polymer* 2006;47:1741–8.
- [274] Avella M, Bondioli F, Cannillo V, Errico ME, Ferrari AM, Focher B, et al. Preparation, characterisation and computational study of poly(epsilon-caprolactone) based nanocomposites. *Mater Sci Technol* 2004;20:1340–4.
- [275] Bondioli F, Cannillo V, Fabbri E, Messori M. Epoxy-silica nanocomposites: preparation, experimental characterization, and modeling. *J Appl Polym Sci* 2005;97:2382–6.
- [276] Cannillo V, Bondioli F, Lusvarghi L, Montorsi M, Avella M, Errico ME, et al. Modeling of ceramic particles filled polymer–matrix nanocomposites. *Compos Sci Technol* 2006;66:1030–7.
- [277] Saber-Samandari S, Khatibi AA. The effect of interphase on the elastic modulus of polymer based nanocomposites. In: Liu HY, Hu XZ, Hoffman M, editors. Fracture of materials: moving forwards. Switzerland: Tans Tech Publications; 2006. p. 199–204.
- [278] Hbaieb K, Wang QX, Chia YHJ, Cotterell B. Modelling stiffness of polymer/clay nanocomposites. *Polymer* 2007; 48:901–9.
- [279] Seidel GD, Lagoudas DC. Micromechanical analysis of the effective elastic properties of carbon nanotube reinforced composites. *Mech Mater* 2006;38:884–907.
- [280] Hammerand DC, Seidel GD, Lagoudas DC. Computational micromechanics of clustering and interphase effects in carbon nanotube composites. *Mech Adv Mater Struct* 2007;14:277–94.
- [281] Liu YJ, Chen XL. Continuum models of carbon nanotube-based composites using the boundary element method. *Electron J Bound Elem* 2003;1:316–35.
- [282] Liu YJ, Chen XL. Evaluations of the effective material properties of carbon nanotube-based composites using a nanoscale representative volume element. *Mech Mater* 2003;35:69–81.
- [283] Chen XL, Liu YJ. Square representative volume elements for evaluating the effective material properties of carbon nanotube-based composites. *Comput Mater Sci* 2004;29: 1–11.
- [284] Huang G, Wang B, Lu HB, Mamedov A, Gupta S. Material characterization and modeling of single-wall

- carbon nanotube/polyelectrolyte multilayer nanocomposites. *J Appl Mech* 2006;73:737–44.
- [285] Tseng KK, Wang LS. Modeling and simulation of mechanical properties of nano-particle filled materials. *J Nanopart Res* 2004;6:489–94.
- [286] Miyagawa H, Rich MJ, Drzal LT. Amine-cured epoxy/clay nanocomposites. II. The effect of the nanoclay aspect ratio. *J Polym Sci Part B: Polym Phys* 2004;42:4391–400.
- [287] Guz AN, Rodger AA, Guz IA. Developing a compressive failure theory for nanocomposites. *Int Appl Mech* 2005;41: 233–55.
- [288] Yang JL, Zhang Z, Schlarb AK, Friedrich K. On the characterization of tensile creep resistance of polyamide 66 nanocomposites. Part II: modeling and prediction of long-term performance. *Polymer* 2006;47:6745–58.
- [289] Pipes RB, Hubert P. Scale effects in carbon nanostructures: self-similar analysis. *Nano Lett* 2003;3:239–43.
- [290] Pipes RB, Frankland SJV, Hubert P, Saether E. Self-consistent properties of carbon nanotubes and hexagonal arrays as composite reinforcements. *Compos Sci Technol* 2003;63:1349–58.
- [291] Pipes RB, Hubert P. Helical carbon nanotube arrays: thermal expansion. *Compos Sci Technol* 2003;63:1571–9.
- [292] Cagin T, Che J, Qi Y, Zhou Y, Demiralp E, Gao G, et al. Computational materials chemistry at the nanoscale. *J Nanopart Res* 1999;1:51–69.
- [293] Goddard III WA, Cagin T, Blanco M, Vaidehi N, Dasgupta S, Floriano W, et al. Strategies for multiscale modeling and simulation of organic materials: polymers and biopolymers. *Comput Theor Polym Sci* 2001;11: 329–43.
- [294] Muller M. Mesoscopic and continuum models. In: Moore JH, Spencer ND, editors. *Encyclopedia of physical chemistry and chemical physics*. Bristol: Institute of Physics; 2001. p. 2087–110.
- [295] Müller-Plathe F. Coarse-graining in polymer simulation: from the atomistic to the mesoscopic scale and back. *Chem Phys Chem* 2002;3:754–69.
- [296] Crawshaw J, Windle AH. Multiscale modelling in polymer science. *Fibre Diffr Rev* 2003;11:52–67.
- [297] Nieminen RM. From atomistic simulation towards multiscale modelling of materials. *J Phys: Condens Matter* 2002; 14:2859–76.
- [298] Sheng N, Boyce MC, Parks DM, Rutledge GC, Abes JI, Cohen RE. Multiscale micromechanical modeling of polymer/clay nanocomposites and the effective clay particle. *Polymer* 2004;45:487–506.
- [299] Kremer K, Müller-Plathe F. Multiscale problems in polymer science: simulation approaches. *MRS Bull* 2001; 26:205–10.
- [300] Raabe D. Challenges in computational materials science. *Adv Mater* 2002;14:639–50.
- [301] Nakano A, Bachlechner ME, Kalia RK, Lidorikis E, Vashishta P, Voyatzis GZ, et al. Multiscale simulation of nanosystems. *Comput Sci Eng* 2001;3:56–66.
- [302] Curtin WA, Miller RE. Atomistic/continuum coupling in computational materials science. *Modell Simul Mater Sci Eng* 2003;11:R33–68.
- [303] Doi M. OCTA (open computational tool for advanced material technology). *Macromol Symp* 2003;195:101–7.
- [304] Broughton JQ, Abraham FF, Bernstein N, Kaxiras E. Concurrent coupling of length scales: methodology and application. *Phys Rev B* 1999;60:2391–403.
- [305] Ogata S, Lidorikis E, Shimojo F, Nakano A, Vashishta P, Kalia RK. Hybrid finite-element/molecular-dynamics/electronic-density-functional approach to materials simulations on parallel computers. *Comput Phys Commun* 2001;138: 143–54.
- [306] Shenoy VB, Miller R, Tadmor EB, Phillips R, Ortiz M. Quasicontinuum models of interfacial structure and deformation. *Phys Rev Lett* 1998;80:742–5.
- [307] Ortiz M, Cuitino AM, Knap J, Koslowski M. Mixed atomistic/continuum models of material behavior: the art of transcending atomistics and informing continua. *MRS Bull* 2001;26:216–21.
- [308] Lau KT, Chipara M, Ling HY, Hui D. On the effective elastic moduli of carbon nanotubes for nanocomposite structures. *Compos Part B: Eng* 2004;35:95–101.
- [309] Bicerano J, Balijepalli S, Doufas A, Ginzburg V, Moore J, Somasi M, et al. Polymer modeling at the Dow Chemical Company. *J Macromol Sci, Polym Rev* 2004;C44:53–85.
- [310] Porter D. Pragmatic multiscale modelling of bone as a natural hybrid nanocomposite. *Mater Sci Eng, A* 2004; 365:38–45.
- [311] Buxton GA, Balazs AC. Simulating the morphology and mechanical properties of filled diblock copolymers. *Phys Rev E* 2003;67:031802.
- [312] Scocchi G, Posocco P, Fermeglia M, Prich S. Polymer-clay nanocomposites: a multiscale molecular modeling approach. *J Phys Chem B* 2007;111:2143–51.
- [313] Fermeglia M, Prich S. Multiscale modeling for polymer systems of industrial interest. *Prog Org Coat* 2007;58: 187–99.
- [314] Borodin O, Bedrov D, Smith GD, Nairn J, Bardenhagen S. Multiscale modeling of viscoelastic properties of polymer nanocomposites. *J Polym Sci Part B: Polym Phys* 2005; 43:1005–13.
- [315] Clancy TC, Gates TS. Modeling of interfacial modification effects on thermal conductivity of carbon nanotube composites. *Polymer* 2006;47:5990–6.